

CHALMERS



Shock absorber modelling

Master's Thesis in the Master's programme Automotive Engineering

HENRIK SKAGERSTRAND

Department of Applied Mechanics

Division of Vehicle Engineering and Autonomous Systems

Vehicle Dynamics Group

CHALMERS UNIVERSITY OF TECHNOLOGY

Göteborg, Sweden 2014

Master's thesis 2015:01

MASTER'S THESIS IN AUTOMOTIVE ENGINEERING

Shock absorber modelling

HENRIK SKAGERSTRAND

Department of Applied Mechanics
Division of Vehicle Dynamics

CHALMERS UNIVERSITY OF TECHNOLOGY

Göteborg, Sweden 2014

Shock absorber modelling
HENRIK SKAGERSTRAND

© Henrik Skagerstrand, 2014

Master's Thesis 2015:01
ISSN 1652-8557
Department of Applied Mechanics
Division of Vehicle Dynamics

Chalmers University of Technology
SE-412 96 Göteborg
Sweden
Telephone: + 46 (0)31-772 1000

Cover:
Picture of one of the shock absorbers modelled in this thesis project.

Repro service / Department of Applied Mechanics
Göteborg, Sweden 2014

Shock absorber modelling

Master's Thesis in the *Master's programme Automotive Engineering*

HENRIK SKAGERSTRAND

Department of Applied Mechanics

Division of Vehicle Dynamics

Chalmers University of Technology

ABSTRACT

The automotive industry is becoming increasingly competitive. It is therefore important to keep development time cost down, while still making safe and comfortable cars. One costly part of the development process is the testing done using prototype vehicles, something that can be reduced if more of the testing were done using computer simulations.

The shock absorbers of the car play a very important role in the safety and the comfort of the vehicle. Despite this many major car manufacturers use a simple force velocity curve as a computer model of the shock absorber. The engineers at Volvo Car Company has found that there is potential for improvement when it comes to the model of the shock absorber, and Modelon AB was asked to initiate a master's thesis to develop a physical model of the shock absorber.

The model was developed in Dymola, a software based on the language Modelica. The model is a physical representation of the shock absorber with component models representing each of the damper components, such as chambers and valves. Most of the parameters in the model can be taken from physical measurements of the shock absorber, however 10 of the parameters need to be tuned against measurements.

The model was verified against tests done on the real shock absorbers in a dynamometer. It was then imported to one of Volvo's full vehicle models in Adams using FMI, and verified against four poster measurements. In the dynamometer the damper was tested for a frequency range of 0.5 Hz to 30 Hz, and in the four poster a road profile measured by Volvo was used. These tests showed that the model performed significantly better than the force velocity curve, which was the alternative before the thesis work. However due to the simple nature of the force velocity curve based model, it is questionable if the gain of the Dymola model compensates for the extra time required by the engineers to tune the parameters. Therefore the recommendation is to develop the Dymola model further to ensure that the Dymola model is an improvement compared to the force velocity curve, in both model accuracy and amount of tuning work.

Key words: Shock absorber, Damper, Dymola, FMI, Modelica

Contents

ABSTRACT	I
CONTENTS	II
PREFACE	IV
NOTATIONS	V
1 INTRODUCTION	1
1.1 Background	1
1.2 Problem statement	2
1.3 Scope	2
1.4 Limitations	3
2 THEORY AND LITERATURE STUDY	4
2.1 Shock absorber theory	4
2.2 Study of existing damper models	6
2.2.1 Overview	6
2.2.2 Modelling of the different components	8
2.3 Building the model	9
2.3.1 Modelling in Dymola	10
2.3.2 Functional Mock-up Interface (FMI)	10
2.4 Tests and validation	10
2.4.1 Dynamometer	10
2.4.2 Tests in a four post rig	11
3 DESIGN AND CALIBRATION OF THE DAMPER MODEL	13
3.1 Building the model structure in Dymola	13
3.2 Measurements of shock absorber A	14
3.2.1 The shim stacks	14
3.3 Modelling of the components	15
3.3.1 Modelling of the chambers	15
3.3.2 Modelling of the piston valves	16
3.3.3 Modelling of the shim stack deflection	17
3.4 Verification of the model in test bench	22
3.4.1 The test bench model in Dymola	22
3.4.2 Testing of the damper in a test bench/dynamometer	24
3.5 Shock absorber B	26
3.5.1 Dismantling and measurements of shock absorber B	26
3.6 Comparison between Dymola model and damper rig	27
3.7 Verification of the Adams vehicle model with imported Dymola shock absorber model	27

4	PARAMETERIZATION AND TUNING OF THE MODEL	28
4.1	Setting up the model	28
4.1.1	Piston valves and base valve assembly	28
4.1.2	Geometry	28
4.1.3	Chambers	29
4.1.4	Seal friction	30
4.2	Calibrating the model	30
4.3	Exporting the model by FMI	32
5	RESULTS	33
5.1	Shock absorber A	33
5.1.1	Sine input to test rig	33
5.1.2	Road input to test rig	35
5.2	Shock absorber B	38
5.2.1	Influence of the bushing on the bottom mount	38
5.2.2	Sine input to test rig	41
5.2.3	Measured road input	45
5.2.4	Four poster	50
5.3	Oil parameters and cylinder expansion	52
6	DISCUSSION	55
6.1	Validation of the model	55
6.1.1	Damper rig test	55
6.1.2	Four poster	56
7	CONCLUSION	57
8	FUTURE WORK	58
9	REFERENCES	59
10	APPENDIX	61
10.1	Equations and expressions	61
10.2	Damper A in rig with sine input	62
10.2.1	Force displacement plots	62
10.2.2	Force velocity plots	65
10.3	Damper B in rig with sine input	71
10.3.1	Force displacement plots	71
10.3.2	Force velocity plots	73

Preface

This thesis describes the development of a shock absorber model for use in Volvo Car Company's full vehicle model. The thesis was conducted as part of the Master program Automotive Engineering at Chalmers University of Technology, Gothenburg. The work was performed at Modelon AB, in their Gothenburg office.

I would like to thank Modelon AB and Volvo Car Company for the opportunity to work with this thesis, and their employees for their valuable input during the work. I would especially like to thank my supervisors Edo Drenth and Carl Sandberg. I would also like to thank my examiner at Chalmers, Bengt Jacobsson.

Göteborg October 2014

Henrik Skagerstrand

Notations

Roman upper case letters

A	Area
C	Flow coefficient
C_D	Discharge coefficient
D	Diameter
D_p	Diameter of the piston
D_v	Diameter of the valve for a shim stack
ΔV	Volume difference
$dV_{chamber}$	Infinitesimal difference of volume
E, E_c	Modulus of elasticity
L	Length
M_φ	Torque in the φ direction
M_r	Torque in the r direction
M_{r1}	Torque in the r direction for the inner part of the disc
M_{r2}	Torque in the r direction for the outer part of the disc
N	Number of elements in the vector x
Q	Volumetric flow rate
Q_c	Volumetric flow rate through a compression valve
Q_{lp}	Volumetric flow rate of the leakage
Q_v	Volumetric flow rate through a valve
SD	Standard deviation
V	Force
V_1	Force for the inner part of the disc
V_2	Force for the outer part of the disc
$V_{chamber}$	Volume of the chamber

Roman lower case letters

a_0, a_{01}, a_{02}	Constants
b, b_0, b_{01}, b_{02}	Constants
c_0, c_{01}, c_{02}	Constants
d_0, d_{01}, d_{02}	Constants
Δp	Pressure difference
Δp_c	Pressure difference over a compression valve
Δp_{valve}	Pressure difference over a valve

$dp_{chamber}$	Pressure difference between the chambers
$f, f_{1,1}, f_{1,1(ori)}$	Constants
f_{ori}, f_1, f_2	Constants
h	Thickness of a disc
l	Thickness of the piston
l_{bc}	The hydraulic perimeter of the compression valve disc
p_A	Pressure acting on the bottom of a shim stack
p_B	Pressure acting on the top of a shim stack
p_1	Pressure acting on the inner part of a disc
p_2	Pressure acting on the outer part of a disc
r	Radius
r_1	Inner contact radius
r_2	Outer contact radius
r_0	The radius where the inner and outer part of a disc meets
r_i	Inner radius
r_o	Outer radius
t	Thickness of a disc
w	Deflection of a disc
$w_{1,ori}$	Deflection of the first shim disc at the radius equal to the radius of the orifice disc
w_i	Deflection of shim disc number i
w_{ori}	Deflection of orifice shim
w^*	Particular solution to the differential equation describing w
w_1	Deflection of the inner part of a disc
w_2	Deflection of the outer part of a disc
x	The difference between the model and the measurements of the radial coordinate of the normalized force-displacement points
\dot{x}	The piston velocity
y	The deflections of the shims in a shim stack valve

Greek letters

β_{oil}	Bulk modulus of the oil
δ	The deflection of the compression valve disc
ε_θ	Strain in the θ direction
ε_A	Strain in the A direction
μ	Dynamic viscosity

ν Kinematic viscosity

ρ Density

1 Introduction

This report describes the development of a shock absorber model in Dymola. The model is developed for use in one of Volvo Car Corporation's full vehicle models. The master thesis project is carried out in cooperation with Modelon AB and Volvo Car Corporation.

1.1 Background

Volvo Car Corporation, from here on referred to as Volvo, has for a long time had a reputation of building safe and comfortable cars. To meet these expectations while keeping costs for development down, computer simulations are a very important tool. These simulations become increasingly less time demanding as the computers get faster and simulation tools better, which gives the possibility for more accurate simulation results through more detailed models. Shock absorbers in complete vehicle models are however still modelled using a vector describing the force versus the velocity, see figure 1.1. The shock absorbers are an important part of the dynamical behaviour of a vehicle and engineers at Volvo would like to replace this simple shock absorber model with a more advanced model to better describe the actual behaviour of interest of the car. A plot of the current model is shown in figure 1.1

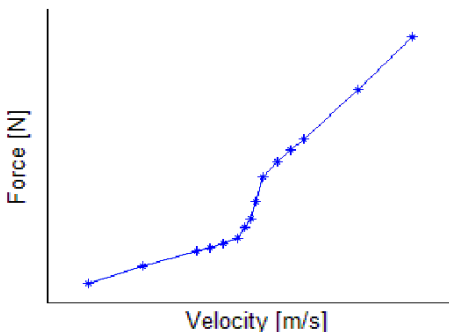


Figure 1.1 The shock absorber model currently used

The table based model in use at Volvo today consists of two vectors describing the relationship between the force and velocity. These two vectors create the piecewise linear curve that can be found in figure 1.1, with the vector pairs marked with a star. To distinguish this model from the model created in this project it will be referred to as the "force velocity curve" throughout this report.

The car damper is a very important part of the vehicle's suspension system, while at the same time being a very complicated system. When studying the behaviour of a shock absorber one quickly realizes that a linear or piecewise linear relationship between force and velocity is far from the whole truth. The force-velocity graphs are not linear, and with increased frequency a hysteresis effect is apparent. A number of attempts to model the behaviour of a shock absorber has been done, a sample of these are described further in the theory and literature section.

Modelon AB, from here on referred to as Modelon, is a global company that specializes in providing technical solutions and services within research and development of dynamic systems. Modelon is the premier provider of libraries for

Modelica, the language used in Dymola, and its employees have extensive knowledge about Dymola.

1.2 Problem statement

The engineers at Volvo experiences effects of the suspension that they can neither capture with measurements nor simulations. The shock absorber model is suspected to be one of the most important causes for this since it is a very simple model, therefore they would like a more accurate model of one of the types of shock absorbers commonly used in production vehicles.

1.3 Scope

This thesis aims at develop a Dymola model of a shock absorber that is to be used in future Volvo simulation models. The model will be developed by connecting blocks that model the different components of the shock absorber, some of which are available in libraries and some of which will be developed during the project. Since the model is to be used in Volvo's full vehicle simulations in Adams, the model needs to be compatible with Adams. It will be exported from Dymola to Adams using FMI technology, a technology for import and export of models between different software.

The model should show significant improvement compared to the model used in Volvo's Adams model today. The verification of this will be done in a full vehicle test in a four post rig, using a test cycle that is close to what is experienced in actual road conditions. Thus a road like cycle will be tested on the real vehicle in a rig and then the same test will be simulated in Adams using both the old and new damper model, the result from these three tests will be compared to validate the improvement accomplished with the new model.

A number of deliverables were formulated to define the desired outcome of the project.

- A Dymola model of the shock absorber with the possibility to modify the model in order to simulate a different damper setup
- A user's manual for using and modifying the Dymola model
- An Adams model of the shock absorber exported via FMI from the Dymola model, compatible for use in Volvo's full vehicle model.
- A user's manual for using the shock absorber model in Adams
- Validation results comparing the model to dynamometer tests and full vehicle test in a four poster

The objectives for the model were also defined. The shock absorber model should

- Have a short simulation time
- Be a good match to reality verified by comparison to shock absorber rig tests and four post shake rig tests
- Capture complicated phenomena within the vehicle's dynamics caused by the shock absorber

To verify the model's ability to successfully model different twin-tube dampers two different shock absorbers, hereon denoted shock absorber A and shock absorber B,

were modelled. The model will be built based on, and verified for, shock absorber A. Then the model will be changed to model shock absorber B, and verified for that damper.

1.4 Limitations

The shock absorber model will not be a general model but only represent the shock absorbers given by Volvo. However the model shall be created to be easy to change in order to get a representation of a similar shock absorber.

2 Theory and literature study

To be able to understand the problem and how others have approached it, a literature study was carried out during the first weeks of the project. The basics of shock absorbers, earlier models of shock absorbers, modelling in Dymola and validation and testing of earlier models were researched.

2.1 Shock absorber theory

The dampers that will be modelled in this project are twin-tube dampers. Twin-tube means that the shock absorber consists of two chambers as can be seen in figure 2.1. The outer chamber contains, in addition to the oil, pressurized gas on top. This gas is pressurized to keep the pressure of the oil from dropping too much, which would result in cavitation. (Dixon, 2007)

The layout of the different parts of a twin-tube shock absorber can be seen in figure 2.1. The valves that control the oil flow are located in the piston and in the base.

The damping during low speeds in the shock absorber is dominated by oil flow through channels in the piston and base valves that are always open. These valves are commonly known as bleed valves or low speed valves. When the speed increases a pressure difference occurs. Upon the pressure difference the secondary valves start to open and the effective coefficient of damping decreases, these valves commonly consists of shim stacks.

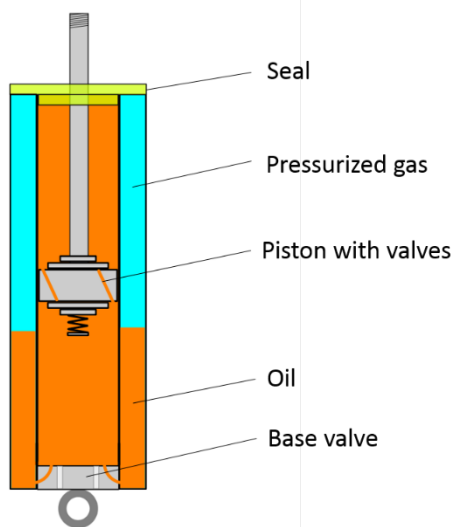


Figure 2.1 Picture showing the design of a twin-tube shock absorber, which is the type used in this project

The piston and base valve consists of valves to control the oil flow. The configuration of the valves differ between different shock absorbers, the shock absorbers modelled in this project use compression valves on both the piston and base, a rebound valve on the piston and a check valve on the rebound side of the base. The most common type of valve is the shim stack. A shim stack valve is a pile of thin discs on top of a channel, when a pressure difference occurs on the top and bottom of the shim stack the discs deflect resulting in an increased opening area. A schematic view of a shim stack can be seen in figure 2.2. To get satisfactory damping during slow movements the shim stacks are often fitted with an orifice disc in the bottom, which acts as the low speed valve. The orifice disc has cut-outs along the edge, providing a small area

that is always open independent on the pressure difference. Shim stacks may be set up in a number of different ways, with or without an orifice disc and pyramidal or cylindrical are the most common differences. Some shim stacks use a spacer and a stop disc; these are fitted on top of the stack and control the maximum deflection. The shock absorbers modelled in this project use a pre-tensioned spring on top of the shim stack that delay the opening of the valve, this is however not very common. In Figure 2.2 the compression valve on the base of one of the shock absorbers used in this project can be seen. The parts are, from the left hand side, the stop disc and spacer disc controlling the maximum deflection, the four shims, the orifice disc and the base. Note the channels on the base leading up to the shims.

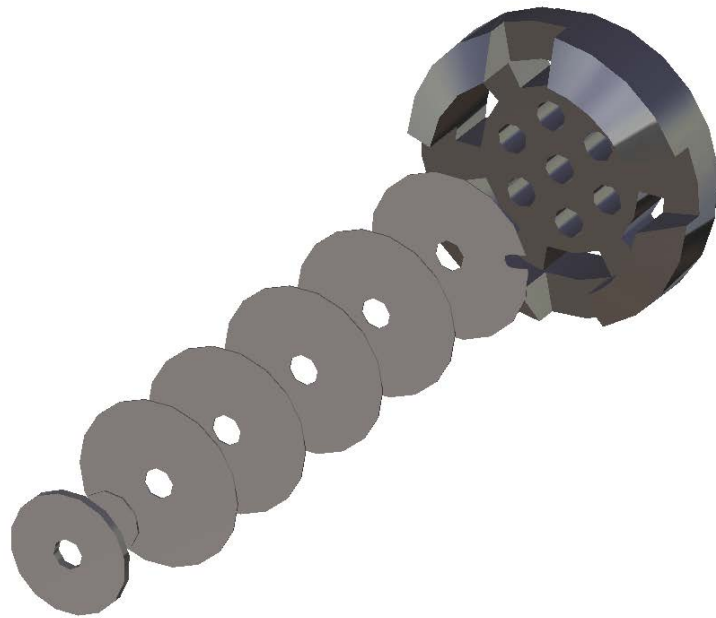


Figure 2.2 Illustration of a shim stack valve

The hysteresis phenomena that becomes obvious in the phase plot showing the force versus velocity curve during higher frequencies, seen in figure 2.3 below, is one important reason that a simple damper model may not adequately predict certain dynamic behaviour. Hysteresis is the separation of the compression and expansion lines in the force-velocity graph. The rebound part of the stroke displays as positive force and the compression part as negative force in the diagram. During a stroke the curve is followed counter clockwise.

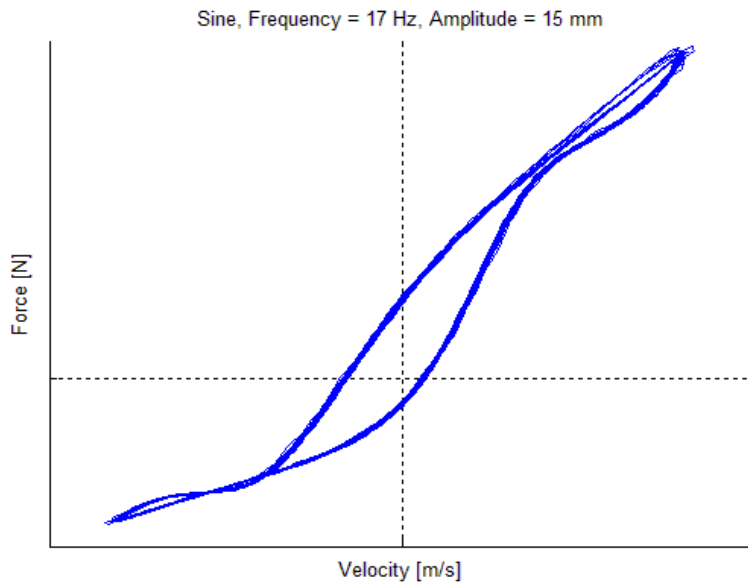


Figure 2.3 Graph demonstrating hysteresis

The main causes for hysteresis are gas compression, oil compressibility, oil inertia and the expansion of the cylinders. (Cossalter, Doria, Pegoraro, & Trombetta, 2010) Claesson contradicts this and states that the expansion of the cylinders doesn't have a significant effect. (Claesson, 2012)

2.2 Study of existing damper models

In this chapter the existing models that were studied in the literature study phase will be presented. Chapter 2.2.1 provides a summary of the models, and chapter 2.2.2 describes how a selection of components of the shock absorbers was modelled in the researched models.

2.2.1 Overview

One very early model is described in H.H. Lang's doctoral dissertation. (Lang, 1977) Lang developed a model of a twin-tube damper, and validated it over the frequency range of 1-10 Hz. The simulations were made on an analogue computer with custom-made circuits representing each component.

In 2002 Talbott and Starkey developed a model of an Öhlins WCJ 22/6 mono-tube damper, designed for stock car racing. One very interesting finding of their work is the shim stack modelling, they modelled the shim stack as a pile of circular thin plates and found that it was a very accurate model. Areas of improvement that were pointed out in this paper were to include fluid compressibility and temperature difference effects. However their model is validated to be quite accurate when compared to the real damper. (Talbott & Starkey, 2002)

Chahine developed a model of the Öhlins TPX damper in his master's thesis using Simulink. (Chahine, 2011) The model was very detailed but didn't match the performance of the real damper very well. Even though Chahine's model turned out to not be valid his modelling procedure seemed to be good and will probably be useful when creating the model. It is suggested to include temperature and pressure dependence in the bulk modulus for the oil, which has not been done on Chahine's model.

An Öhlins damper with variable damping using a CES (Continuously controlled Electronic Suspension) system was modelled in (Gällsjö & Johansson, 2012). Öhlins CES system uses an electrically controlled valve to adjust the damper's stiffness dependent on the need. Even if the CES system differs from the damper modelled in this thesis there are several similar components. The CES model was validated to be good. Areas identified to have room for improvement are the check valves and the model for mechanical friction. It was also concluded that the viscous friction might need to be different for compression and expansion.

In (Hou, Li, He, Zhang, & Chen, 2011) the authors develop a modular model that can be used for both mono- and twin-tube dampers. They get good results when comparing to their test bench results of runs from several shock absorbers. The most useful result from this report is probably the tests done to find the influence of different parameters of the shock absorber. The influence is plotted for variations of, amongst others, fluid compressibility.

Hou et al. developed a model of a shock absorber using the modelling language Modelica, which is the base for Dymola. The shock absorber modelled was a twin-tube damper. Even if their model is probably over simplified and is not validated against a real shock absorber it might be useful to look at, especially since the modelling was done in Modelica. (Hou, Li, He, Zhang, & Chen, 2011)

In his master's thesis Claesson developed a physical model of the Öhlins TTR damper, which is an adjustable shock absorber used in motor cycle racing applications. The shock absorber has large number of adjustments that can be done, both externally and internally by disassembling the damper. The model was created in Dymola using components from Modelon's hydraulics library. The model is one of the most complete models found using a bulk modulus varying with pressure, temperature differences and heating of the damper. (Claesson, 2012)

A detailed damper model can be found in the Dymola library AutomotiveDemos. The model is created using the hydraulics and pneumatics libraries provided by Modelon. It is a mono-tube damper with check valves. The layout of the damper model can be seen in figure 2.4.

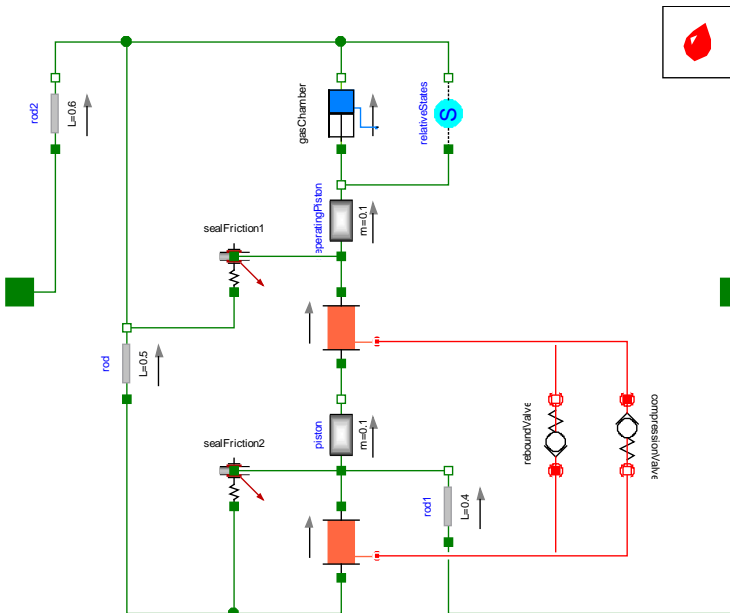


Figure 2.4 The detailed damper model from the **AutomotiveDemos** library

2.2.2 Modelling of the different components

Here different ways to model the most important components are presented.

2.2.2.1 Modelling of the valves

The valves are very important to model correctly to capture the behaviour of the damper. However, since the valves also are complicated the computational power needed to model them completely physically isn't practical for most applications. Both FEM and CFD calculations is required, which consumes a lot of computational power. Therefore it exists different ways to model them as simple as possible without compromising the result.

2.2.2.1.1 Low speed valve

The low speed valve isn't really a valve but an opening, but since its function is to control the flow of oil it will be named as a valve. An opening with a constant area is relatively easy to model using equation (1) to describe the flow.

$$Q = C_D A \sqrt{\frac{2\Delta p}{\rho}} \quad (1)$$

This is done by Claesson (Claesson, 2012) and Talbott and Starkey (Talbott & Starkey, 2002) amongst others.

2.2.2.1.2 Shim stack

Talbott and Starkey uses equation (2) to describe the flow through the shim stack. (Talbott & Starkey, 2002) They get that by combining equations for the flow area and the unsteady flow through a constant area.

$$Q_v = \frac{1}{2} \pi D_v y C_D \sqrt{\frac{2\Delta p_{valve}}{\rho}} \quad (2)$$

Where y denotes the deflection of the shims. The variable y is calculated using an equation system where the effect of the different pressures are added for each of the shims.

Sorniotti, D'Alfio and Morgando (Sorniotti, D'Alfio, & Morgando, 2007) use essentially the same equation as Talbott and Starkey but the deflection of the shims is approximated as the compression of the spring for simplicity.

Hou et al. use the following equations to model their compression valve, see equations (3) and (4).

$$Q_c = \begin{cases} 0 & \text{if } \Delta p_c \leq \Delta p_{c0} \\ Cl_{bc} \delta \sqrt{\frac{2\Delta p_c}{\rho}} & \text{if } \Delta p_c > \Delta p_{c0} \end{cases} \quad (3)$$

$$\delta = \frac{\Delta p_c}{E_c h^3} \left(\frac{9r_1^4 + 8r_1^3 r_2 - 18r_1^2 r_2^2 + r_2^4}{6} - 4r_1^3 r_2 \ln \frac{r_1}{r_2} \right) \quad (4)$$

2.2.2.2 Leakage past the piston

The piston has a rubber seal to keep from leaking along the walls, however some leakage will still be present. Talbott and Starkey (Talbott & Starkey, 2002) model this using equation (5), derived from Navier-Stokes.

$$Q_{lp} = \left(\frac{\Delta p b^3}{12\mu l} + \frac{\dot{x}b}{2} \right) \pi D_p \quad (5)$$

Where D_p is the diameter of the piston, \dot{x} is the piston velocity and b is the length of the gap between the piston and the cylinder wall.

2.2.2.3 Oil

Since oil compressibility makes the calculations substantially harder it is often excluded, but those models that do include it shows that it might be of importance to the fidelity of the model. In Modelon's tutorial for their hydraulics library oil compressibility is considered a requirement for sound physical models. They argue that a little gas in the fluid will have a significant effect on bulk modulus at low pressures. (Modelon AB, 2011)

Chahine includes it in the equation for pressure change in the chambers, see equation (6). (Chahine, 2011)

$$dp_{chamber} = -\frac{dV_{chamber}}{\beta_{oil} * V_{chamber}} \quad (6)$$

2.2.2.4 Cylinder expansion

Claesson uses the equations for cylinder stress together with Hooke's law to form an equation for the change in volume, see equation (7). The equation is simplified by assuming that the square of the deformations is negligible. (Claesson, 2012)

$$\Delta V = (2\epsilon_\theta + \epsilon_A) \frac{D^2 \pi}{4} L \quad (7)$$

2.2.2.5 Thermodynamic influence

Claesson uses enthalpy and entropy flows in his model to account for changes in heat and the effect on density and this causes. The calculations for this are extensive and can be read in his thesis. (Claesson, 2012)

2.3 Building the model

The model will be created in Dymola using estimated damper parameters from measurements on the real damper.

2.3.1 Modelling in Dymola

Dymola is a simulation programme based on the modelling language Modelica. Modelica is an object-oriented, equation based modelling language developed by the Modelica Association. (Modelica home page, 2015) Dymola's multi-engineering capabilities make it possible to create a model consisting of components from different engineering domains. (Dymola for physical modeling and simulation, 2014) It comes with extensive documentation, the user manual is divided into two parts for a total of more than 1000 pages. The first part of the manual (Dassault Systèmes AB, Dymola User Manual Volume 1, 2013) is for those relatively new to Dymola and the second is for the advanced user (Dassault Systèmes AB, Dymola User Manual Volume 2, 2013). Modelon offers an introduction course to Dymola that will be taken a few weeks into this project.

Modelling in Dymola is often done by using components from the many libraries available. In this project the hydraulics library provided by Modelon will be the most used, however a number of other libraries will also be utilised.

In the demo library “AutomotiveDemos” a detailed model of a shock absorber can be found, this model is very useful when trying to understand how to model a damper in Dymola. A more detailed description of this model can be found in chapter 2.2 above.

2.3.2 Functional Mock-up Interface (FMI)

When creating an extensive product consisting of many parts, for example a vehicle, these parts are often modelled in different software. Modelling software is often specialized on a specific type of problem and not suitable for all products, but the manufacturer of the full product wants to create a full product model. This is what motivated the ITEA MODELISAR project to be started 2008 with the task to create a solution for this problem. FMI version 1.0 was released in January 2010.

Using the FMI toolbox one can create a FMU (Functional Mock-up Unit) from a component in a supported software. The result is a separation of the description of the interface data and the functionality into an XML file and C code or binary respectively. The separated files are zipped into a FMU file (*.fmu) to be imported into another program. (FMI [Start], 2014)

2.4 Tests and validation

After building a model of a complex dynamic system it's very important to test the model to verify that all the important characteristics of the system is modelled correctly. To verify all possible scenarios of the real system is of course very time consuming, it's therefore needed to plan the testing thoroughly to get good results with as few tests as possible.

2.4.1 Dynamometer

The simplest validation test that's used is a test bench run with sinus wave input. The damper is mounted in a test bench and excited with a sinus wave input for the displacement, the test is run with different frequencies and amplitude. This test might not show many important dynamic effects, especially those that show when the damper is subject to accelerations, and is also very different from when the dampers are mounted in a vehicle. In (Kowalski, Rao, Blough, Gruenberg, & Griffiths, 2001) the authors combines two sine wave inputs and establish that the result is quite different from tests done with the two sine inputs individually. However a test with

simple inputs can be very useful when examining a model to find areas of improvement.



Figure 2.5 Picture showing a dynamometer of the same model as the one at Volvo from
<https://www.mts.com/en/products/producttype/test-systems/load-frames-uniaxial/servohydraulic/damper/index.htm>, downloaded 2014-05-26

The most accurate excitation model is of course one measured on a real vehicle in use, but these are hard to find and time consuming to make. In (Akutain, Viñolas, Savall, & Biera, 2006) the changes in force on the damper mounted in a vehicle is plotted, it's easily seen that simple sine waves doesn't capture this at all. Li, Lu and Li use a random input of the displacement to run their validation. (Li, Lu, & Li, 2012) In (Boggs & Ahmadian, 2007) a random selection of sine waves over a predefined amplitude and frequency spectrum are summed to get a road like input. There are also examples when a white noise signal is used as an input.

2.4.2 Tests in a four post rig

When testing is done using some kind of simplified environment, such as a damper in a dynamometer, the risk that the results doesn't show small but important and interesting effects is always apparent. Due to this it is a good idea to do some of the tests in an environment that is closer to the real conditions. However it's important to not lose control of the results, for example it's important to be able to replicate the test to verify the measured results. A four post rig consists of four posts with actuators on which the vehicle's wheels are mounted. The actuators are given drive signals to excite the suspension. To give the vehicle a relevant input and to get interesting results, the inputs are often recorded data from roads or test tracks. (French, 2000) In (Akutain, Viñolas, Savall, & Biera, 2006) examples of outputs from road tests can be seen.



Figure 2.6 Picture of the four poster at Volvo

In figure 2.6 above a picture of the four post rig at Volvo can be seen. The posts and actuators are located under the floor.

3 Design and calibration of the damper model

This chapter describes the method that was used to develop and calibrate the damper model.

3.1 Building the model structure in Dymola

The top structure of the Dymola model can be seen below in figure 3.1. The model structure is based upon the components in the real shock absorber, the Dymola view in figure 3.1 may be compared to the schematic shock absorber in figure 2.1.

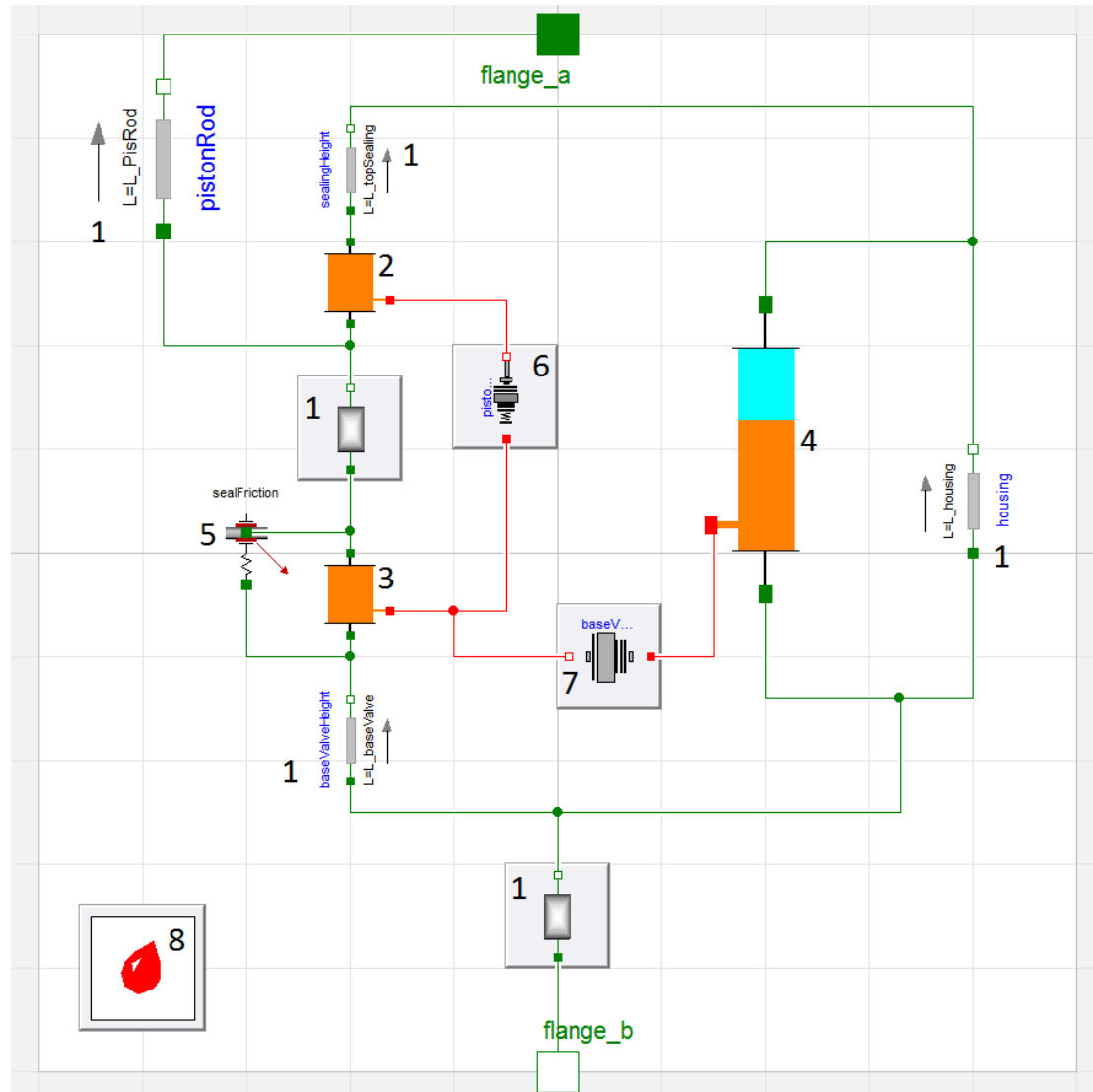


Figure 3.1 The top structure of the Dymola model

The components denoted with the number 1 describe the geometry of the components. Component 2 to 4 is the model of the upper, lower and outer chambers. The friction between the piston and cylinder wall and between the piston rod and the sealing is described by component 5. The valve models can be found inside component 6, the piston valves, and component 7, the base valves. The components found in the hydraulics library uses a fluid model placed in the top level at the model, in this case that is the oil denoted by 8. The components surrounded by grey square are replaceable, which means that the user can choose to change the class and get a list of appropriate components. The replaceable components marked with 1 are the upper

and lower mass. When the model is exported to Adams the masses are to be placed in Adams, so the replaceable masses are changed to massless rods in Dymola before exporting.

3.2 Measurements of shock absorber A

To measure the components the shock absorber needed to be dismantled, this was done in the workshop at Chalmers. To take the damper apart it needed to be cut apart and drained of oil. The outer cylinder was cut and the components separated, see figure 3.2.

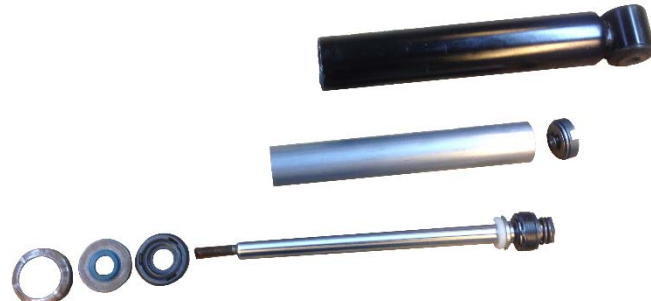


Figure 3.2 Shock absorber A disassembled

3.2.1 The shim stacks

The compression shim stack valve on the piston is a simple cylindrical shim stack with three shims, a spacer and a stop disc, see figure 3.3.



Figure 3.3 View of the compression valve on the piston

The expansion valve on the piston is a cylindrical valve with five shims and an orifice disc that are pre-tensioned by a spring, see figure 3.4.



Figure 3.4 View of the rebound valve on the piston

The compression valve on the base is a cylindrical valve with four shims, an orifice disc, a spacer and a stop disc, see figure 3.5.

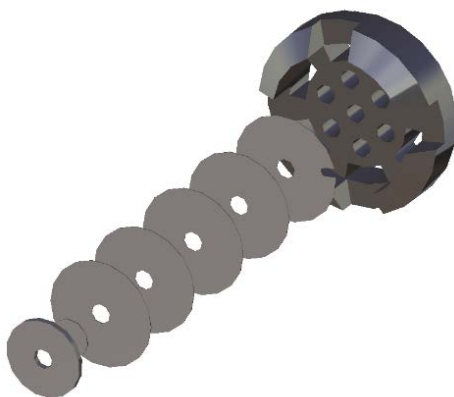


Figure 3.5 View of the compression valve on the base

The rebound valve on the base consists of one single shim that acts as a check valve, see figure 3.6.



Figure 3.6 View of the rebound valve on the base

3.3 Modelling of the components

Below the development of the models of the different components is presented.

3.3.1 Modelling of the chambers

All of the chambers are modelled using existing components in a shell. This shell makes it possible to rename the input parameters and give them a relevant description.

The inner chambers use the component `Hydraulics.Volumes.Chamber`. The outer chamber consist of a model for the oil filled part, which is the same as for the inner chambers, and model for the gas filled part, which uses the component `Hydraulics.Volumes.PistonGasAccumulator`.

3.3.2 Modelling of the piston valves

The piston model contains models for the leakage past the piston, the rebound valve and the compression valves; see figure 3.7. The red and white squares on the left and right in the picture below are the ports where the oil flows in to the components. The red lines from the ports denotes the oil flow leading to the valve and leakage models. The leakage model is at the centre of the picture and the valve models are above and below that. The valve models consists of an orifice model with variable area, an area calculation model, a gain model for calibration and two pressure sensors. The area calculation model calculates the opening area of the shim stack using the pressure on each side of the valve, and equations described below in chapter 3.3.3. The gain model is used since the flow is impossible to calculate without the use of CFD, which is outside the scope of this thesis, and needs to be found empirically.

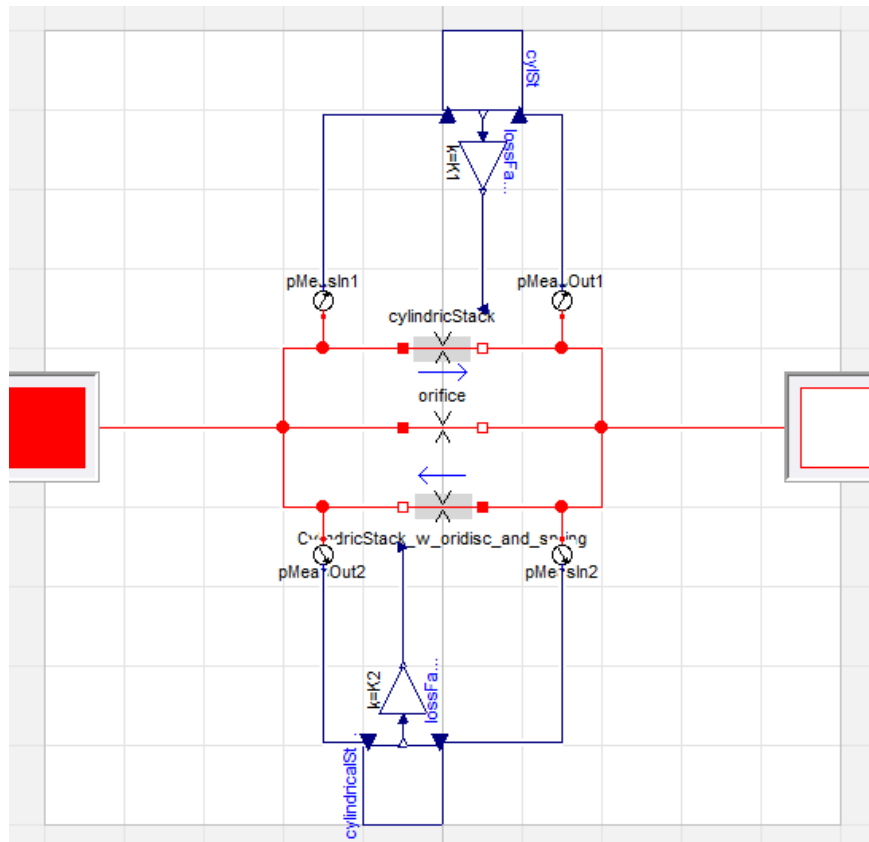


Figure 3.7 The layout of the piston valves

The base valve consists of components for the rebound and compression valve. The layout of the base valves are identical to the piston valves except for the leakage model, see figure 3.8.

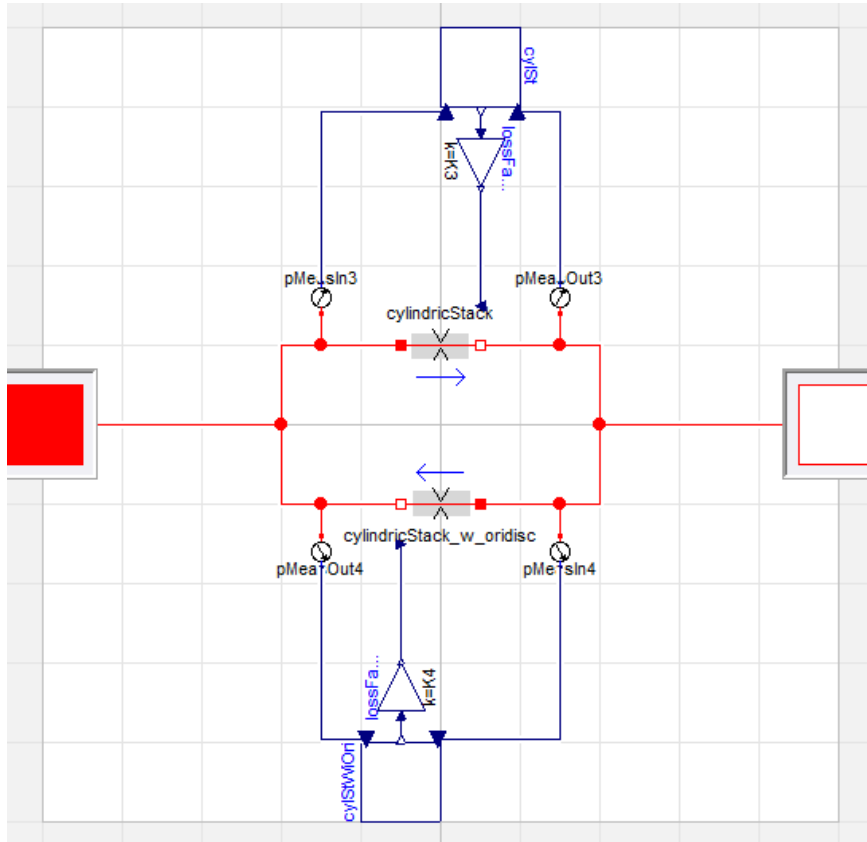


Figure 3.8 The layout of the base valves

3.3.3 Modelling of the shim stack deflection

The shock absorbers consists of three different types of shim stacks. On the base valve a shim stack that acts on the compression side consists of an orifice disk and a number of shims. On the end the spacer and washer limits the maximum deflection. The compression shim stack on the piston has essentially the same construction, but no orifice disk. The shim stack on the expansion side of the piston has an orifice disk and is preloaded with a coil spring.

The deflections are calculated using formulas for axisymmetric Kirchhoff plates from (Sundström, 2008), see equation (8) and (9).

$$w = w^* + a_0 \ln r + b_0 r^2 + c_0 r^2 \ln r + d_0 \quad (8)$$

$$w^* = \frac{1}{D} \int \frac{1}{r} \int r \int \frac{1}{r} \int p(r) r dr dr dr dr dr \quad (9)$$

Where

$$D = \frac{E t^3}{12 * (1 - \nu)} \quad (10)$$

All of the pressures are assumed to be constant for the whole radius, the reaction between the plates are approximated as a pressure over the contact radii. For a constant pressure:

$$w^* = \frac{pr^4}{64D} \quad (11)$$

The inner edge of the shims are mounted by an approximately stiff disc, which is interpreted as a fixed inner edge at the outer edge of the stiff disc. The outer edges are free. This gives the boundary conditions, where r_i is the inner edge and r_o is the outer edge, see equation (12).

$$\begin{cases} \mathbf{w}(\mathbf{r}_o) = \mathbf{0} \\ \mathbf{w}'(\mathbf{r}_o) = \mathbf{0} \\ \mathbf{M}_r(\mathbf{r}_i) = \mathbf{0} \\ \mathbf{V}(\mathbf{r}_i) = \mathbf{0} \end{cases} \quad (12)$$

Where (Ekh, 2013)

$$\begin{cases} \mathbf{M}_r(\mathbf{r}) = \mathbf{D} \left(-\mathbf{w}''(\mathbf{r}) - \frac{\nu \mathbf{w}'(\mathbf{r})}{\mathbf{r}} \right) \\ \mathbf{V}(\mathbf{r}) = \frac{\mathbf{M}_r(\mathbf{r})}{\mathbf{r}} + \mathbf{M}'_r(\mathbf{r}) - \frac{\mathbf{M}_\varphi(\mathbf{r})}{\mathbf{r}} \\ \mathbf{M}_\varphi(\mathbf{r}) = \mathbf{D} \left(-\nu \mathbf{w}''(\mathbf{r}) - \frac{\mathbf{w}'(\mathbf{r})}{\mathbf{r}} \right) \end{cases} \quad (13)$$

Using these boundary conditions the constants a_0, b_0, c_0 and d_0 in equation (8) can be calculated. The constants are calculated using Mathematica and the expression is simplified to get the following.

$$\mathbf{w}(\mathbf{r}) = \mathbf{f} * \mathbf{p} \quad (14)$$

Where f is a constant describing the stiffness in meters per Pascal, dependent on the geometry, Young's modulus and the Poisson number of the disc. The full expression can be found in Appendix 10.1.

Even if the pressures can be assumed to be constant over all radii, some of them do not act on the whole plate. This means that two equations have to be calculated and connected:

$$w_1 = \frac{p_1 r^4}{64D} + a_{01} \ln r + b_{01} r^2 + c_{01} r^2 \ln r + d_{01} \quad (15)$$

$$w_2 = \frac{p_2 r^4}{64D} + a_{02} \ln r + b_{02} r^2 + c_{02} r^2 \ln r + d_{02} \quad (16)$$

Here w_1 is valid for $r \leq r_0$ and w_2 is valid for $r \geq r_0$, where r_0 is the radius of the change of the load. Since the deflection of the plate is continuous the four variables w , w' , M_r and V has to be the same for both functions at r_0 , see equation (17).

$$\begin{cases} w_1(r_0) = w_2(r_0) \\ w'_1(r_0) = w'_2(r_0) \\ M_{r1}(r_0) = M_{r2}(r_0) \\ V_1(r_0) = V_2(r_0) \end{cases} \quad (17)$$

The boundary conditions in equation (12) together with (17) gives the constants in equation (15) and (16). Since only the deflection at $r \geq r_0$ is of interest, it is enough to describe the deflection with w_2 . The constants were derived using Mathematica to create the expression in equation (18).

$$w_2 = f_1 * p_1 + f_2 * p_2 \quad (18)$$

With equations for the deflection of each shim the interaction between the shims of the shim stack has to be described to create an equation system. The interaction between the shims is assumed to be a constant pressure over the contact area. This gives an equation system with $2n - 1$ unknowns and n equations. The equations missing to create a solvable equation system will be connecting the deflections of shims in contact, and therefore different for each type of shim stack. These will be described further below for the shim stacks present in the damper in question.

The orifice disc is modelled as the first shim but as an ordinary circular plate, with a modified diameter to give it the same area as it actually has, see figure 3.9.

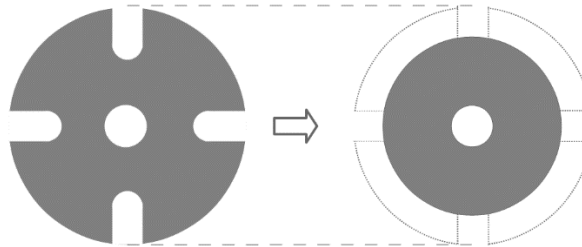


Figure 3.9 Showing the approximation of the orifice geometry into ordinary circular plate

Since the shim stack deflection is restricted from being negative a condition has to be introduced that sets the minimum deflection to zero.

3.3.3.1 Cylindrical stack

The equation system with i shims and without an orifice disc is as follows.

$$\begin{cases} w_1 = f_1(p_A - p_{1,2}) \\ w_2 = f_2(p_{1,2} - p_{2,3}) \\ \dots \\ w_i = f_i(p_{i-1,i} - p_B) \end{cases} \quad (19)$$

The equations are made on the edge of each shim disc. The different pressures used in equation (19) can be seen in figure 3.10.

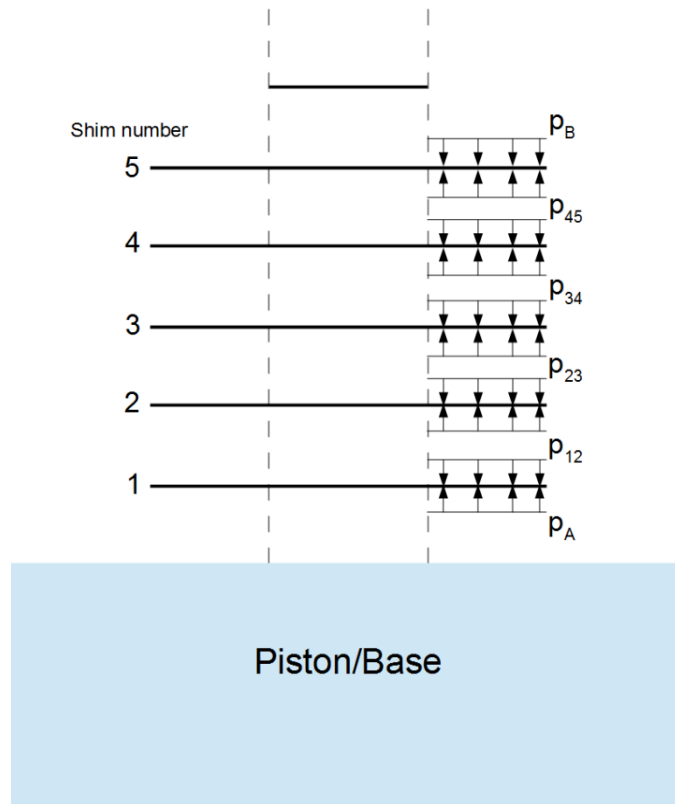


Figure 3.10 Figure showing the different pressures used in equation (19)

It's seen that the deflection on the edge must be the same for all shims, see equation (20).

$$w_1 = w_2 = \dots = w_i \quad (20)$$

3.3.3.2 Cylindrical shim stack with an orifice disc

When looking at a shim stack with i shims and an orifice disc the equation system becomes, see equation (21).

$$\left\{ \begin{array}{l} w_{ori} = f_{ori}(p_A - p_{ori,1}) \\ w_{1,ori} = f_{1,1(ori)}(p_{ori,1} - p_{1,2}) + f_{2,1(ori)}(p_a - p_{1,2}) \\ w_1 = f_{1,1}(p_{ori,1} - p_{1,2}) + f_{2,1}(p_a - p_{1,2}) \\ w_2 = f_2(p_{1,2} - p_{2,3}) \\ \dots \\ w_i = f_i(p_{i-1,i} - p_B) \end{array} \right. \quad (21)$$

Where $f_{1,1(ori)}$ and $f_{2,1(ori)}$ are calculated for the first shim disc's geometry at the radius equal to the radius of the orifice disc. The pressures in equation (21) are demonstrated in figure 3.11.

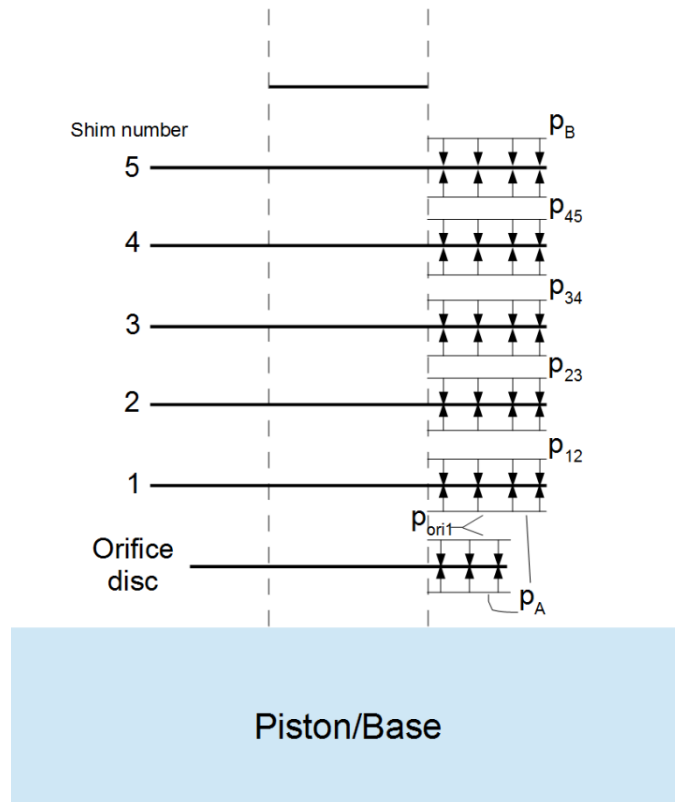


Figure 3.11 Figure showing the different pressures used in equation (21)

From figure 3.11 the relationship between the deflections can be derived to be.

$$\begin{cases} w_{ori} = w_{1,ori} \\ w_1 = w_2 = \dots = w_i \end{cases} \quad (22)$$

3.3.3.3 Shim stack with pre-loaded spring

If the shim stack has a pre-loaded shim the pressure p_B is simply replaced by the pressure caused by the spring added to p_B so that $p_B = (p_B + p_{spring})$.

3.3.3.4 Other shim stack configurations

Any other shim stack configuration can be modelled in the same fashion using equations (14) and (18) describing the deflection and inserting it in equilibrium equations.

3.4 Verification of the model in test bench

The first part of the validation and improvement of the model is done in Dymola since it's a comparison against tests done in a test bench, which makes an export to Adams redundant.

3.4.1 The test bench model in Dymola

A model for the test bench can be found in the Hydraulics library (Hydraulics.Examples.DamperModel.damperTestModel). To the right in figure 3.12 the bottom of the damper is fixed and to the left the sine input of the displacement can be seen. The component that looks like a damper contains the whole damper model.

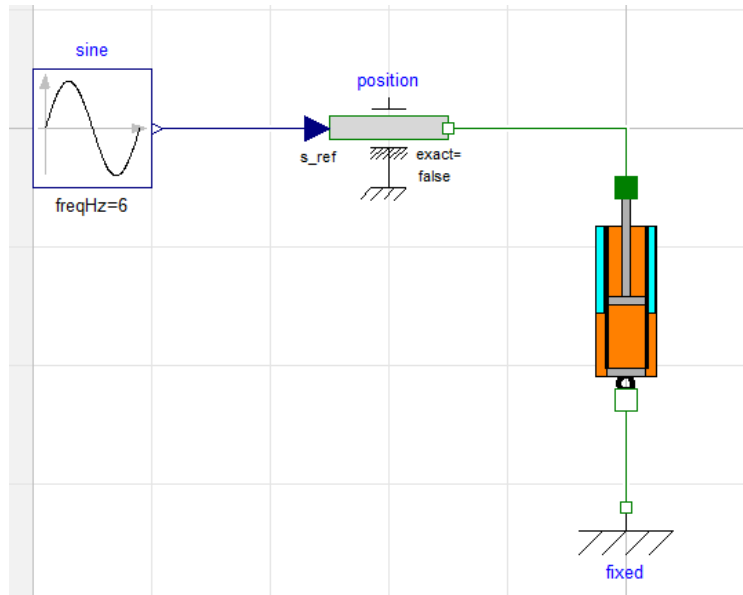


Figure 3.12 Hydraulics library damper test bench model

The sine input is only a number and needs to be defined as a position, this is done by the block position. If the input type is for example force the position block is simply changed to the corresponding block for force. The sine input is defined by amplitude, frequency, phase and offset. The sine block may off course be changed if another input type is desired. In this project a number of sine inputs and an input based on measurements on a test track is used.

For shock absorber B a force velocity curve exists and so the model is extended to include a calculation of the results of that model, see Figure 3.13. The force velocity curve model consists of a speed sensor, a gain model and a look up table. The look up table interpolates the force from the velocity and outputs that, the gain converts the velocity from metres per second to millimetres per second which is used in the table look up.

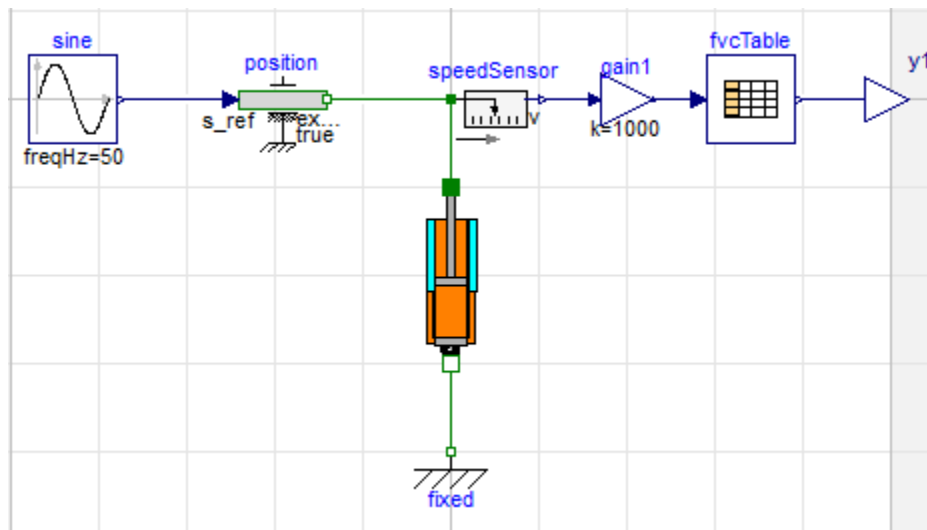


Figure 3.13 Damper rig model for shock absorber B

The measured road input is modelled replacing the sine block with a CombiTimeTable block, which takes a .mat file and uses that matrix as input. Since the displacement input was a measurement, it is suitable to do the differentiation to

velocity and acceleration as pre-processing. For this reason, the displacement was differentiated twice in Matlab to create a velocity and an acceleration input, this can be seen to the left in figure 3.14.

For shock absorber B the force velocity table model was included, see the right hand side of figure 3.14. An add block was included to simulate the preload caused by the gas pressure. When the damper is simulated in a vehicle the vehicle's mass will compress the spring and damper to an equilibrium, and when driving forces is applied causing compression and rebound. In the damper rig case the start position is shifted from the equilibrium, which is in fully expanded position since no mass is put on the shock absorber. Since the preload isn't included in the table model from the start, it is added with the add and constant blocks.

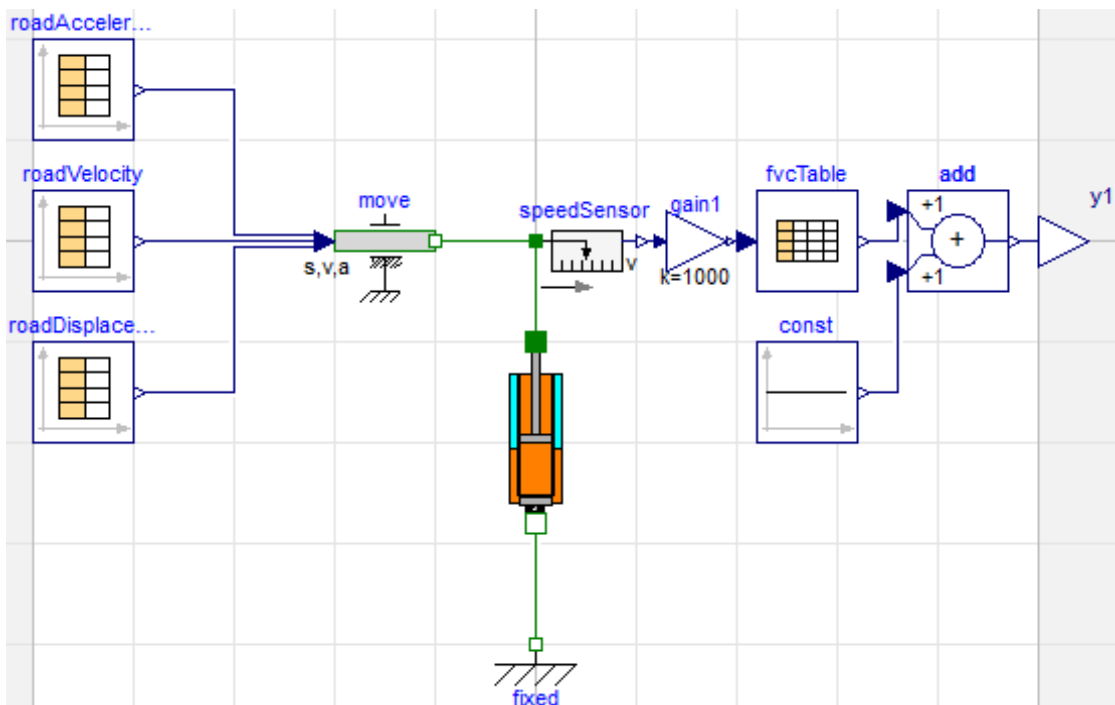


Figure 3.14 Damper rig model for shock absorber B with measured road input

3.4.2 Testing of the damper in a test bench/dynamometer

From the articles and reports presented in the literature study section it's clear that the sine wave input on the displacement is the most common, the reason is that the output from this is a clean signal with few uncertainties. This clean result is very useful in the first stage of model verification, where a few parameters that are difficult to estimate are adjusted to get good agreement between the simulations and the tests. Using such simple inputs will however result in a too large simplification of the reality, with probable loss of important effects from accelerations etc. Therefore a more realistic test is needed to capture the performance of the model, i.e. measurements of a road. The chosen road is used by Volvo for assessments of comfort and the chassis position relative to the wheel is measured.

The inputs given to the damper test bench in the sine wave test are presented in table 1 and in figure 3.15. Since the results may vary with the same amplitude and frequency with different initial displacements the last four are done with initial point in fully compressed and expanded position. In table 1 the sine wave inputs are displayed.

Table 1 Sine wave inputs for the damper rig

Run	Amplitude [mm]	Frequency [Hz]	Maximal speed [m/s]
1	2	30	0.38
2	4	30	0.75
3	8	30	1.5
4	8	15	0.75
5	8	5	0.25
6	15	1	0.094
7	15	6	0.57
8	15	10	0.94
9	15	17	1.6
10	45	0.5	0.14
11	45	3	0.85
12	45	6	1.7
13	15, as high in the stroke as possible	6	0.57
14	15, as low in the stroke as possible	6	0.57
15	30, as high in the stroke as possible	6	1.1
16	30, as low in the stroke as possible	6	1.1

The inputs given to the damper test bench from the measured road tests are presented in figure 3.15 below, showing the displacement of the damper.

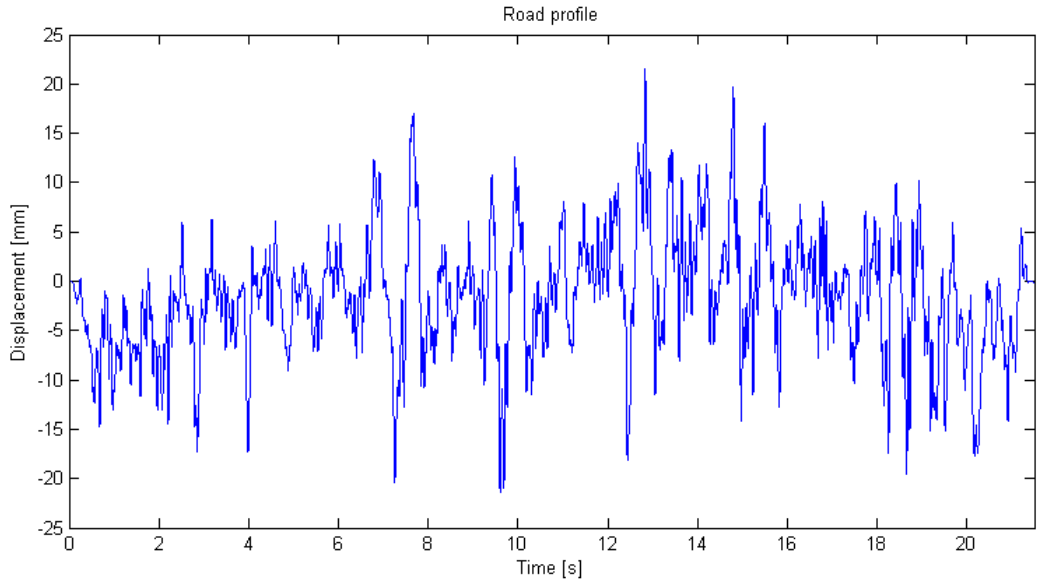


Figure 3.15 Road imitating damper bench tests

3.5 Shock absorber B

The model's ability to describe different shock absorbers had to be verified, and therefore this project included modelling of two twin-tube dampers with different tuning setups. The second damper went through the same procedure as the first one, dismantling and measurements of parts, modelling of components that differed from shock absorber A and calibration by comparison to tests in a dynamometer.

3.5.1 Dismantling and measurements of shock absorber B

As the first damper, the second was cut apart and measured in the workshop at Chalmers.

3.5.1.1 Differences in construction between damper A and B

The basic composition of damper B is the same as for damper A, with some small differences. The most obvious difference is the length is that the housing is 36 mm longer, and the piston rod is 23 mm longer. The piston rod also has the stop 19 mm further up on the rod, see figure 3.16.



Figure 3.16 Picture of the piston and valve

The valves are of the same type on the two dampers, but the configurations are a bit different. The compression valve on the piston has 5 shims instead of 3 in the case of damper A, the shims also differ in thickness. The rebound valve on the piston has a different stiffness on the spring, damper A's spring is almost twice as stiff. It has the same number of shims, but with a different thickness. The rebound valve on the base is essentially the same, but the compression valve has five instead of three shims and another thickness. However, the most obvious difference on the valves are the channels leading up to the shim stacks, these are significantly smaller on damper B.

3.6 Comparison between Dymola model and damper rig

Some of the parameters of the model are very hard to measure, these parameters were determined by comparison of sine input damper rig tests. The parameters used to calibrate the model are listed in table 2.

Table 2 Calibration variables

Variable	Comment
$K1, K2, K3$ and $K4$	The gain of the opening areas of the valves
$ScaleAch1, ScaleAch2, ScaleAch3$ and $ScaleAch4$	Scaling of the channel area used in the effective opening area of the valves
$leakageGap$	The gap between the piston and chamber wall, causing leakage
s_{rel}	Oil level in the outer chamber at equilibrium

The calibration variables are described further in chapter 4.2.

When the results were satisfactory for the sine input tests the model was tested for the road imitating input. Those results were compared to the force velocity curve and the measurements using four different types of error. The mean absolute error, the mean square error and the standard deviation were calculated and the error of each sample point were plotted.

3.7 Verification of the Adams vehicle model with imported Dymola shock absorber model

When the model is verified against results from tests done in a four post rig the shock absorber model is already exported to Adams and implemented into Volvo's full vehicle model. This means that any adjustments of the model in this stage will be time consuming and are therefore avoided if possible.

The tests in the four poster only includes excitation of the rear axle of the vehicle, since only the rear dampers are investigated.

To get a simple measurement to compare to simulation results and to be able to analyse which frequencies are better modelled by which model a frequency sweep was used as an input of the displacement on the posts of the rig. The frequency sweep spanned frequencies from 1 to 25 Hz with a constant maximum velocity. The second test performed on the four post rig was created by using the measured road as an input.

The measured road profile that was used in the damper rig measurements was also used in the four poster rig to excite the rear axle of the vehicle. The displacement of the left rear damper was exported from the Adams results and the measurements and compared.

4 Parameterization and tuning of the model

This chapter describes how the model is used to enable usage with another twin tube shock absorber.

4.1 Setting up the model

The model uses the geometrical properties of the damper, which means that either a detailed drawing of the shock absorber or a workshop to take the shock absorber apart is needed.

It is a good idea to base new models on one of the existing models where the parameters are propagated to the top level and to change the default value of the parameters to the correct values. This will save the developer of the new model a lot of time, and is done by choosing duplicate model in Dymola.

4.1.1 Piston valves and base valve assembly

The valves on both the piston and on the base are probable to be the components that need to be modified the most when modelling another shock absorber. To model a different type of shim stack a new area block needs to be created. However, by studying chapter 3.3.3 and by basing the new block on one of the existing area blocks this ought to be a simple task.

The valves are numbered to avoid too long names, the numbering is described in figure 4.1.

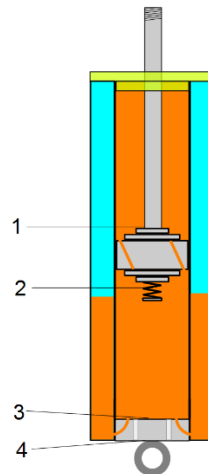


Figure 4.1 Figure showing the numbering of the valves

4.1.2 Geometry

The different geometrical properties are listed and explained below.

The length of the piston rod, L_{PisRod} , is measured from the mounting point to the first stop. The length of the piston, L_{piston} , is the full length from the stop to the bottom of the piston. How the piston rod and piston length are measured can be seen in figure 4.2.

The length of the housing is measured from the bottom to the top of the chambers, i.e. not including the thickness of the material in the bottom and on the top.

The length of the base valve is simply the length difference between the inner and outer cylinder.

The length of the top sealing, $L_{topSealing}$, is not the actual length of the sealing but the difference in length between the inner and outer chamber caused by the sealing.

The length of the lower mount, $L_{lowerMount}$, is the measurement between the bottom of the outer chamber and the middle of the hole for the mount.

The upper mass, m_{upper} , is the mass of the piston and piston rod. The lower mass, m_{lower} , is the mass of all the other parts including the oil.

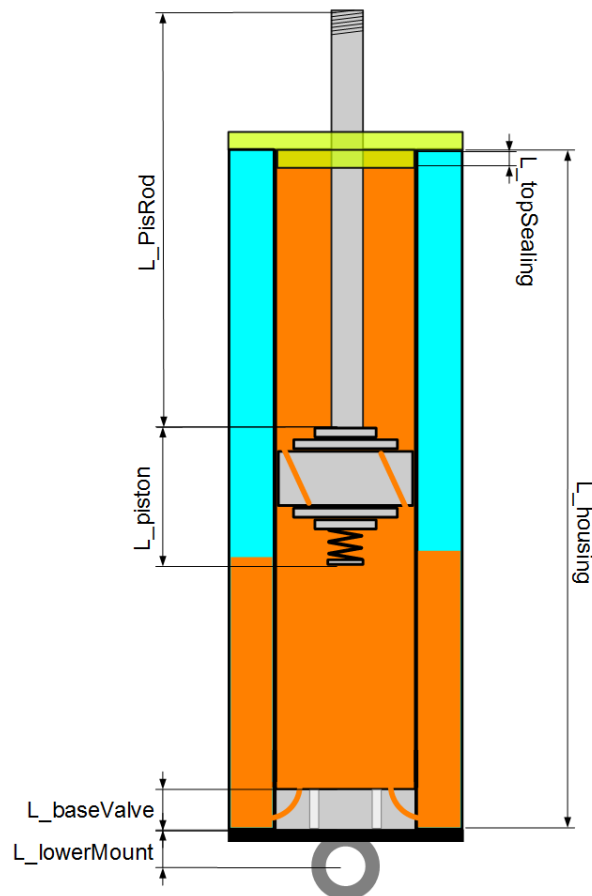


Figure 4.2 Picture demonstrating the placement of the geometrical variables

4.1.3 Chambers

The dead volumes in the inner chambers represent the volume between the piston and the chamber wall on the upper and lower part of the piston, see figure 4.3.

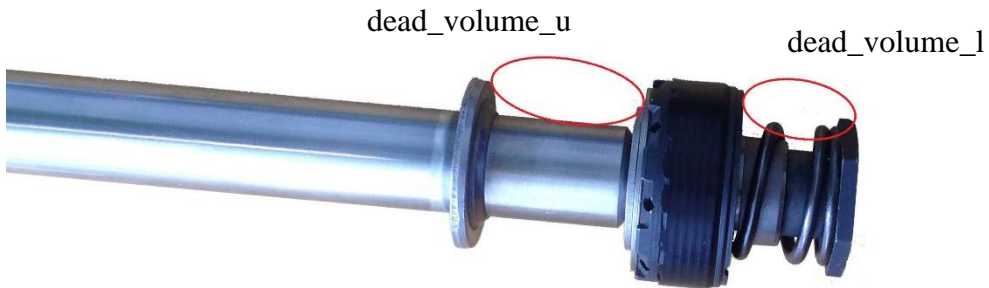


Figure 4.3 Figure illustrating the location of the dead volume of the inner chambers

The dead volume in the outer chamber, `dead_volume_outer_lower`, represents the volume caused by the complicated geometry of the base valve, see figure 4.4. If the geometry on the top of the base valve is complicated, that geometry might need to be added as dead volume. This is added to the dead volume of the lower inner chamber.



Figure 4.4 Demonstrating the dead volume in the outer chamber on the base valve

The preload pressure that is put on the gas in the outer chamber is represented by the variable `p_preload`.

4.1.4 Seal friction

The seal friction in the model is characterized by three parameters for elasticity spring rate, elasticity damping rate and the Coulomb friction.

4.2 Calibrating the model

Some of the parameters are hard or impossible to measure and needs to be determined by comparison to measured data for the modelled shock absorber. It is found that the calibration parameters are easiest to be determined when looking at the force versus displacement plot, the effects caused by each of the parameters are more distinguishable.

All of the four valves in the shock absorbers used in this project are calibrated in the same manner, using two constants. The first constant, K_i , is the gain of the area fed to the orifice model and acts as a scaling of the resistance through the valve, see figure 4.5. The second constant, $ScaleAchi$, is a scaling of the channel area and controls how much influence the channel area has on the area fed to the orifice model. The gain of the area is the variable with the most influence on the results, with a low gain the resistance of the flow is increased which leads to a higher required force for a given displacement, and vice versa. The scaling of the area controls the top and bottom of the force versus displacement plot, a representation of the scaling's influence on the result is shown in figure 4.6.

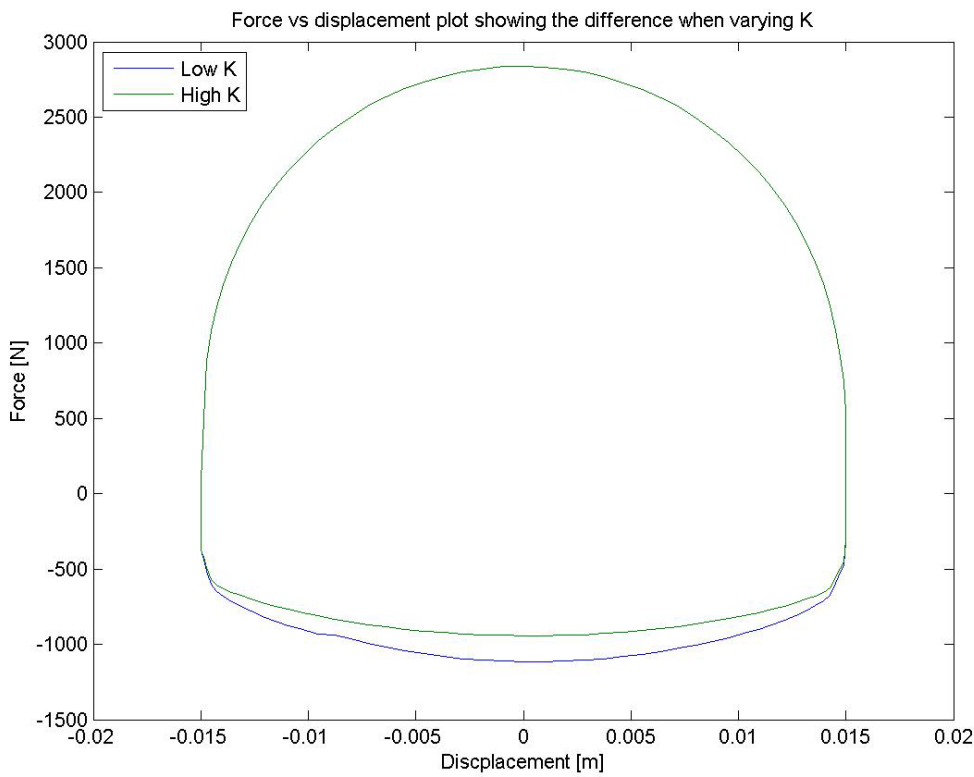


Figure 4.5 Plot showing the difference caused by changing K. It can be seen that the force decreases evenly on the compression side.

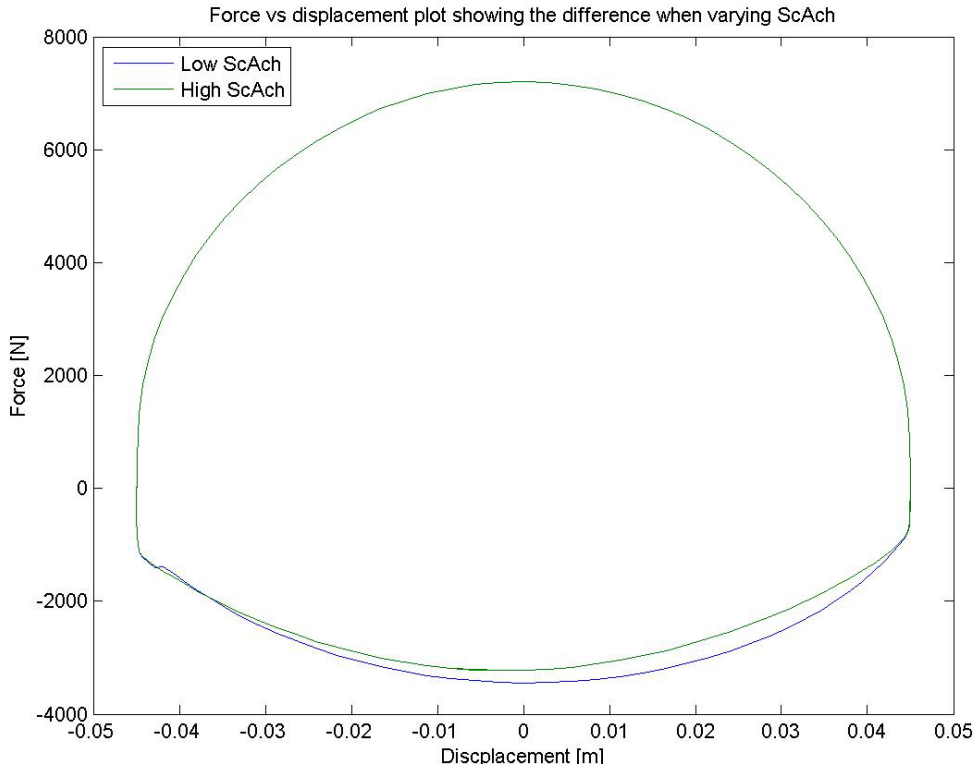


Figure 4.6 Plot showing the difference caused by changing ScaleAch. It can be seen that the force is decreased on the compression side, with a larger effect to the right in the picture.

The remaining calibration variables are the gap between the piston and the inner chamber walls, leakageGap, and the start value for the oil level in the outer chamber. The gap between the piston and the walls controls the model for the leakage past the

piston. When lowering the length of the gap the force needed increases both for rebound and compression, with more influence when the piston's speed is low. The oil level in the outer chamber is immensely difficult to measure, therefore it is easier to estimate a value. Incorrect oil level effects mostly slow moment with low frequencies, for which it distorts the bottom of the force versus displacement plot, see figure 4.7

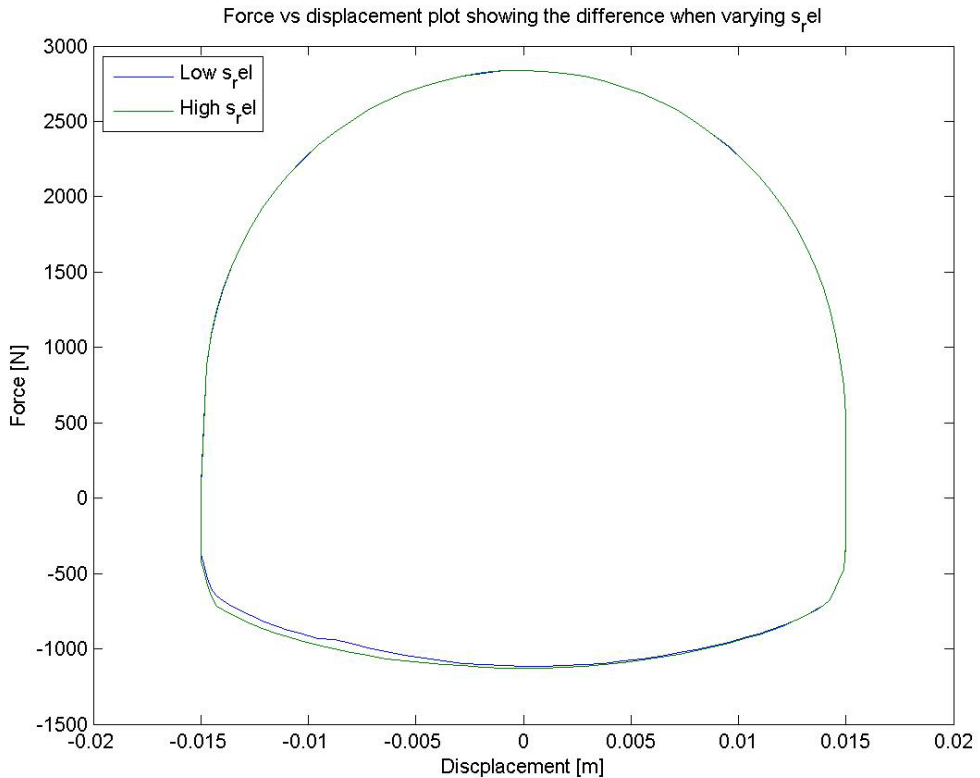


Figure 4.7 Plot showing the influence of the calibration variable s_{rel}

One should be aware that the model doesn't represent negative pressures in a satisfactory way, which could result in distortions in the force displacement plot.

4.3 Exporting the model by FMI

When exporting FMU:s from Dymola there are a few options that needs to be considered. Firstly, the requirements of the software that the FMU will be imported into needs to be met. The FMU can be created using 32-bit or 64-bit binaries, or both which means that the receiving software chooses the correct one. Note that the compiler used by Dymola has to be able to create 64-bit binaries and that Dymola has to be started in 64-bit or a flag has to be set. The flag is set in the command window using the command line *Advanced.CompileWith64=2*. The version also has to be set, the default is version 1.0 which is the most common but version 2.0 is also available for export. There are two types of FMU files used for co-simulation or model exchange. In Dymola a third option is available to export both types, making it possible to use the same FMU for both co-simulations and model exchange. There is a fourth option that uses Dymola's solver in co-simulations. To enable this option a specific export flag has to be activated. The command for setting the flag that allows export with Dymola solvers is *Advanced.FMI.EnableCoSimSolvers=true*.

5 Results

In this project it is found that the differences between the measurements are clearer when using force displacement plots, for sine wave movement. Therefore those graphs are used in the results sections, and the force velocity plots can be found in appendix.

During translational movement up and down the force-displacement curve rotates clockwise and the force velocity curve rotates anticlockwise, see figure 5.1 and figure 5.2. During a sine wave displacement, or similar, the maximum velocity occurs when the damper is at the centre position. This means that the centre on the horizontal axis in the force displacement plot corresponds to the minimum and maximum on the horizontal axis in the force velocity plot, and vice versa.

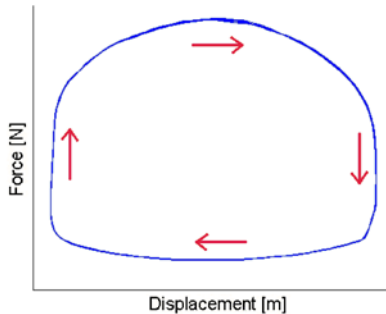


Figure 5.1 Force-displacement plot showing the rotation during a stroke

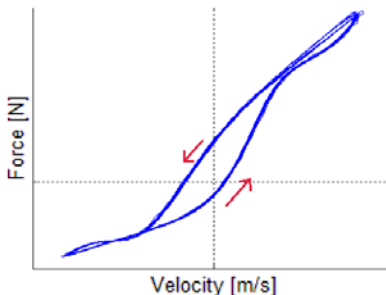


Figure 5.2 Force-velocity plot showing the rotation during a stroke

5.1 Shock absorber A

Since the first shock absorber only was used to develop the model more data is given for shock absorber B. However a few graphs are included to show that the model can be used for different shock absorbers.

5.1.1 Sine input to test rig

Not all of the test results are shown in this chapter but all plots, including the force velocity plots, can be found in appendix chapter 10.2.

In the figure below the 0.5 Hz test is shown, observe the edges in the corners of the model's results.

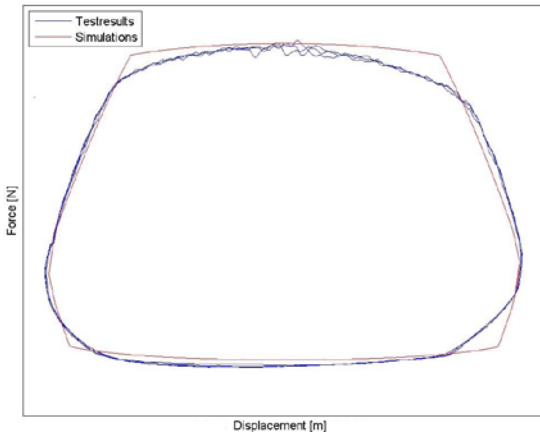


Figure 5.3 Frequency = 0.5 Hz, amplitude = 45 mm, maximum velocity = 0.14 m/s

In the figure below the 3 Hz test is shown. It shows very good correlation between the model and measurements, except for the lower right corner.

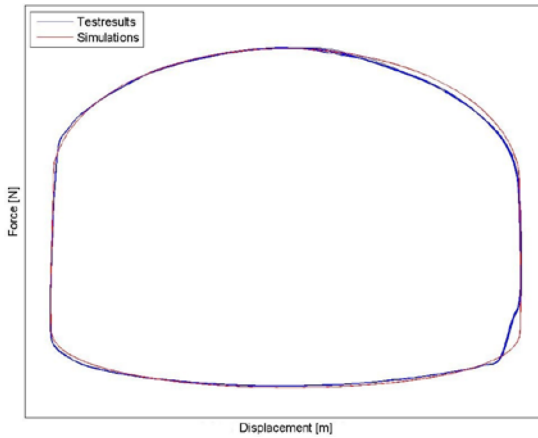


Figure 5.4 Frequency = 3 Hz, amplitude = 45 mm, maximum velocity = 0.85 m/s

In the figure below the 6 Hz test is shown, as for the 3 Hz test it shows a good correlation everywhere but the lower right corner.

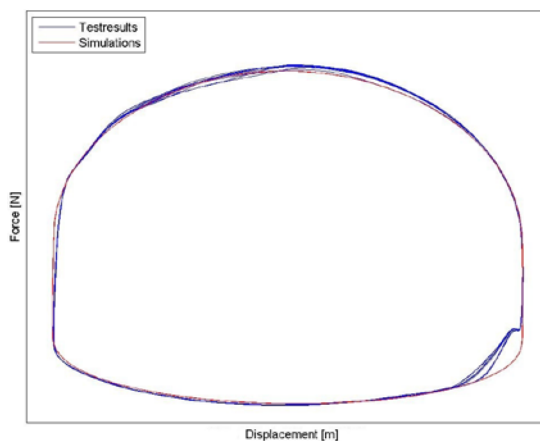


Figure 5.5 Frequency = 6 Hz, amplitude = 45 mm, maximum velocity = 1.70 m/s

Below the 10 Hz test can be seen. Observe the distortions on the measured results, which is not represented by the model.

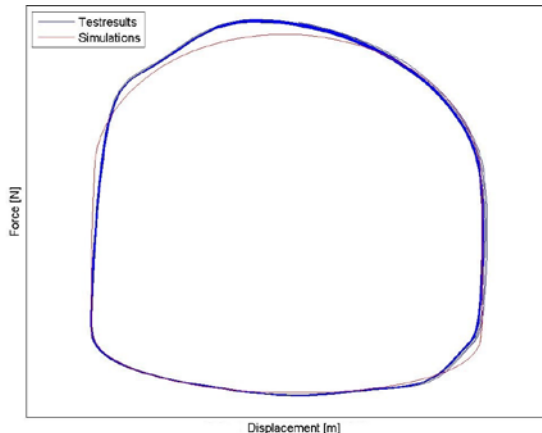


Figure 5.6 Frequency = 10 Hz, amplitude = 15 mm, maximum velocity = 0.94 m/s

In the figure below the 30 Hz test with the largest amplitude is displayed. One can see that the measurements show a tilt towards right, which the model is not representing.

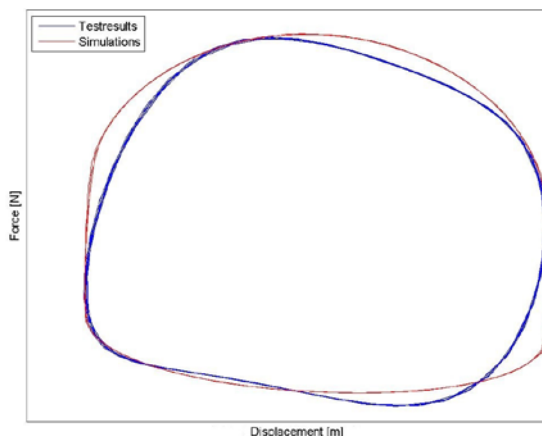


Figure 5.7 Frequency = 30 Hz, amplitude = 8 mm, maximum velocity = 1.51 m/s

5.1.2 Road input to test rig

Since damper B is the most important one for Volvo at the moment damper A was used to develop the model and to get an understanding of the influence of different parameters, and the parameters have only been roughly tuned. However a few graphs are created to verify that the model shows decent results.

The force velocity plot is shown in figure 5.8 below. The blue line represents the measurements and the red line represents the results from the Dymola model. It can be seen that the Dymola model shows more hysteresis than displayed by a force velocity curve, but the measurements show a significantly higher level of hysteresis.

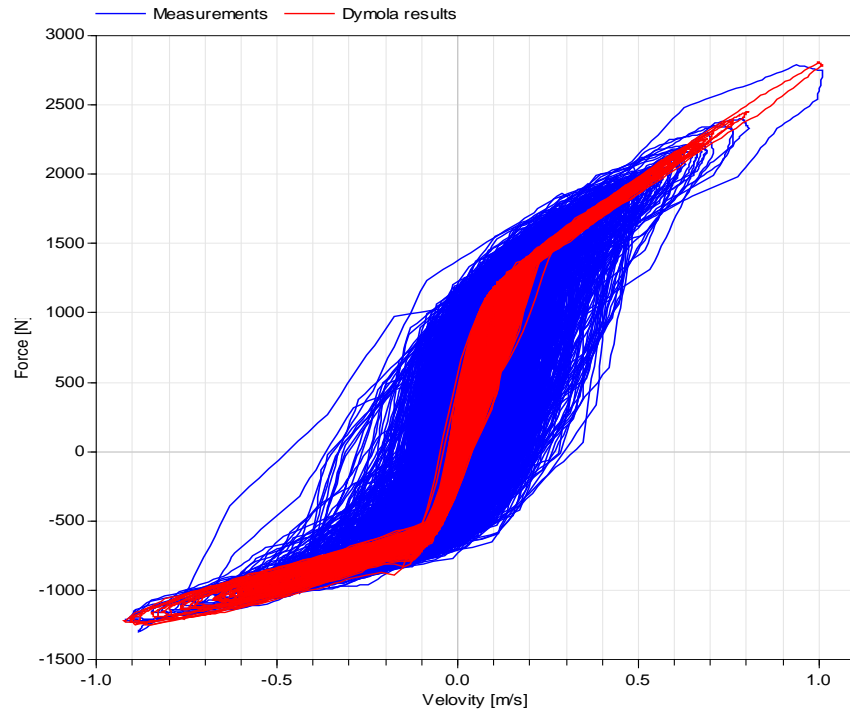


Figure 5.8 Force velocity plot, the blue line is the measurements and the red line is the Dymola results

As can be seen in figure 5.9 the force plot with respect to time doesn't show much when displaying the whole time interval of the test. Therefore two randomly chosen shorter time intervals are shown to provide results, see figure 5.10 and figure 5.11. The blue line is the measured data and the red line represents the results from the Dymola model in all plots.

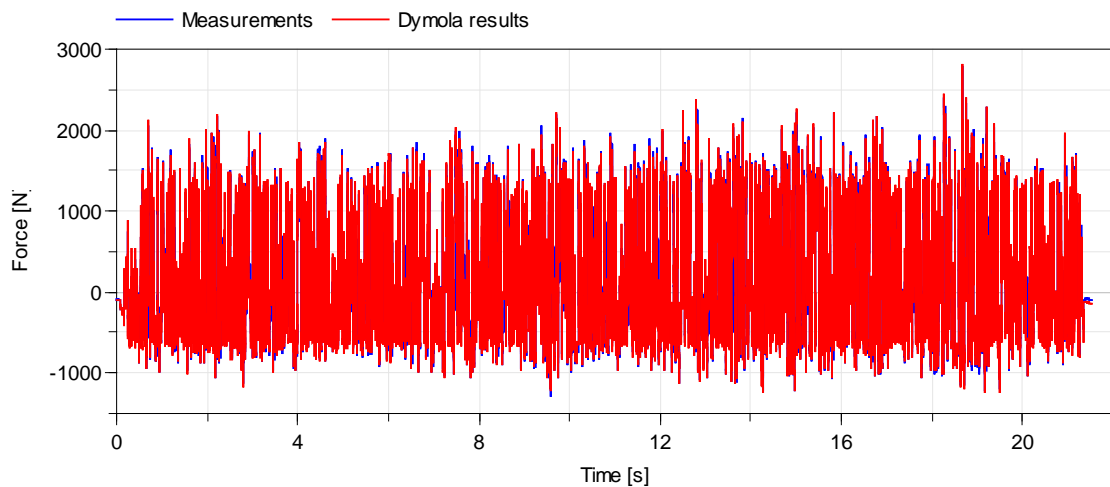


Figure 5.9 The damper rig test with road measured input on damper A

The second time interval chosen is displayed below, between 5.44 and 5.72 seconds.

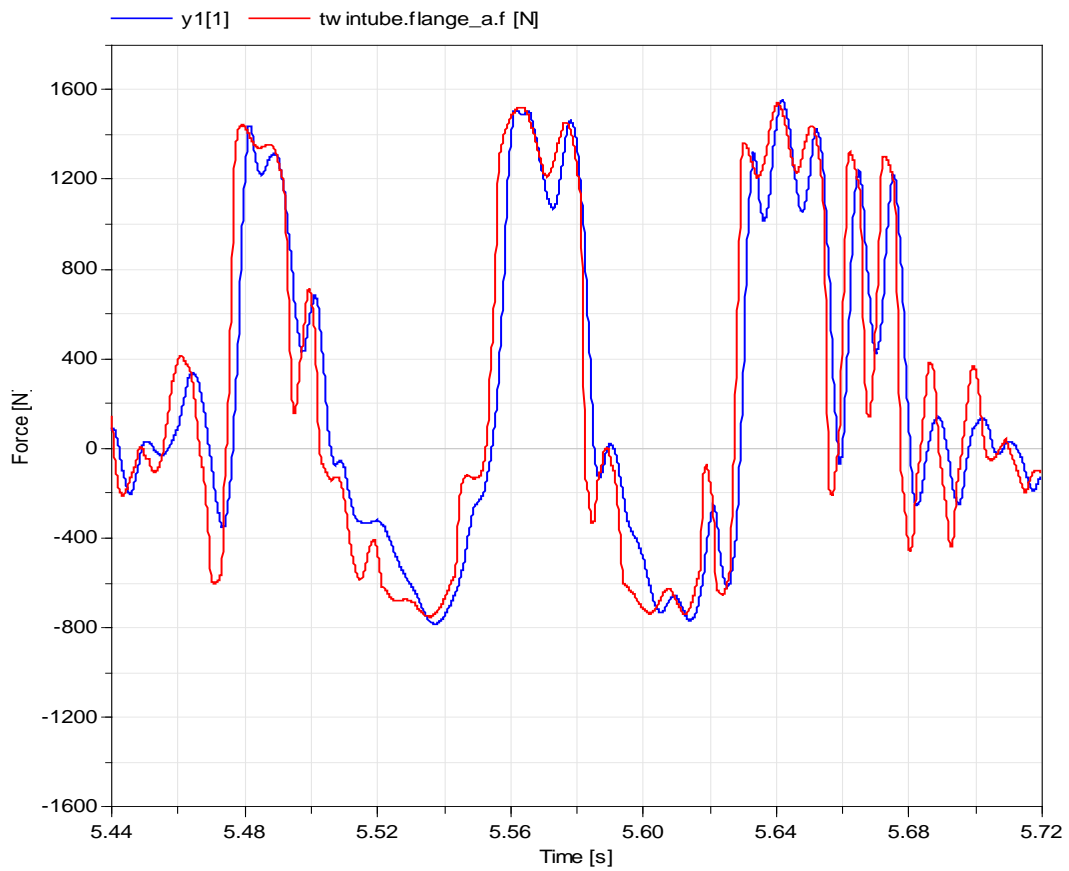


Figure 5.10 Zoomed in view of figure 5.9 for the time interval 5.44-5.72 seconds

The second time interval chosen is displayed below, between 15 and 15.3 seconds.

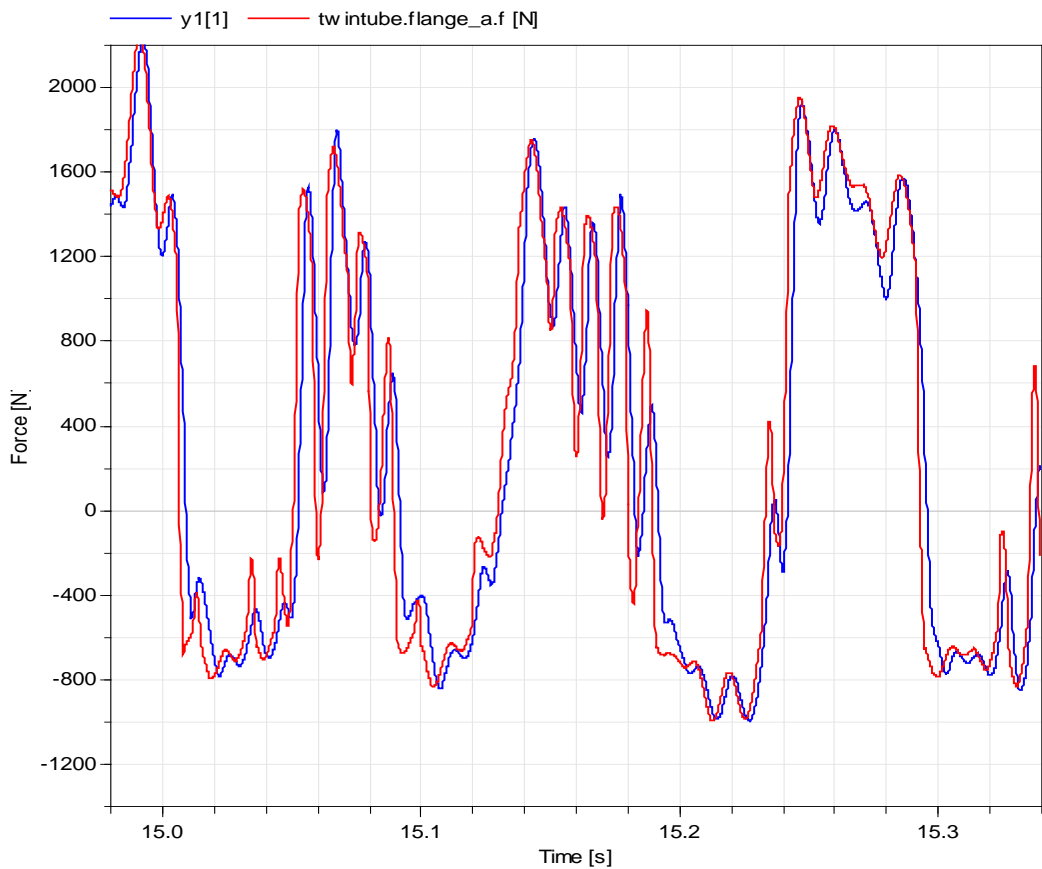


Figure 5.11 Zoomed in view of figure 5.9 for the time interval 15.0-15.3 seconds

5.2 Shock absorber B

5.2.1 Influence of the bushing on the bottom mount

When damper A was tested in the damper rig characteristics that were hard to explain were found. These were believed to be caused by the bushing in the bottom mount of the shock absorber since this is not represented in the Dymola model. Therefore shock absorber B was tested twice, once with the bushing mounted and once with the bushing removed. Below plots from some of the tests showing the influence of the bushing.

In figure 5.12 below it can be seen that the bushing doesn't have much influence on the shape of the curve but has some influence on the force levels for the 1 Hz test.

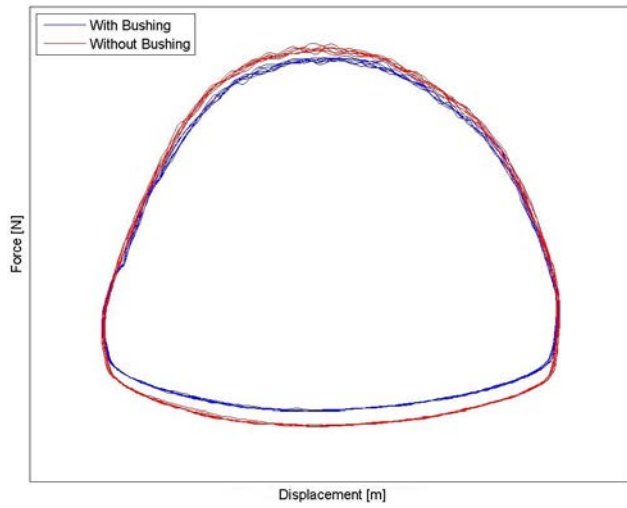


Figure 5.12 Frequency = 1 Hz, amplitude = 15 mm, maximum velocity = 0.094 m/s

In figure 5.13 below the 5 Hz test it shown, it can be seen that a number of distortions are removed with the bushing removed.

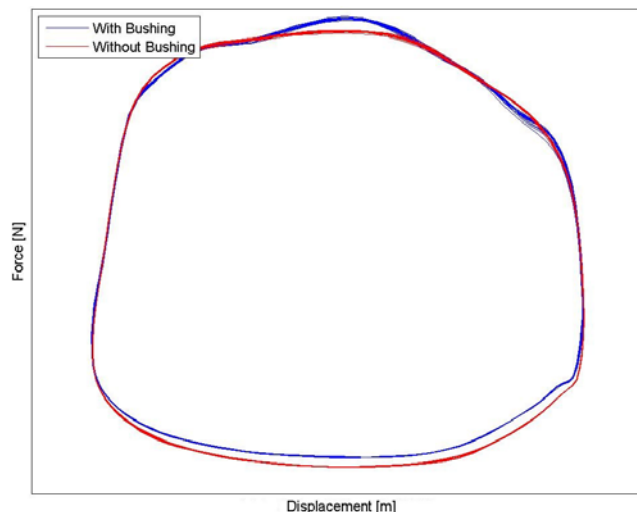


Figure 5.13 Frequency = 5 Hz, amplitude = 8 mm, maximum velocity = 0.25 m/s

In figure 5.14 below it can be seen that during the 6 Hz test with an extended starting position the bushing has almost no influence.



Figure 5.14 High position, frequency = 6 Hz, amplitude = 30 mm, maximum velocity = 1.31 m/s

Figure 5.15 below it can be seen that during the 6 Hz test with a compressed starting position removing the bushing has a significant influence on the curve shape in the bottom right corner. Compare to the extended starting position test in figure 5.14.

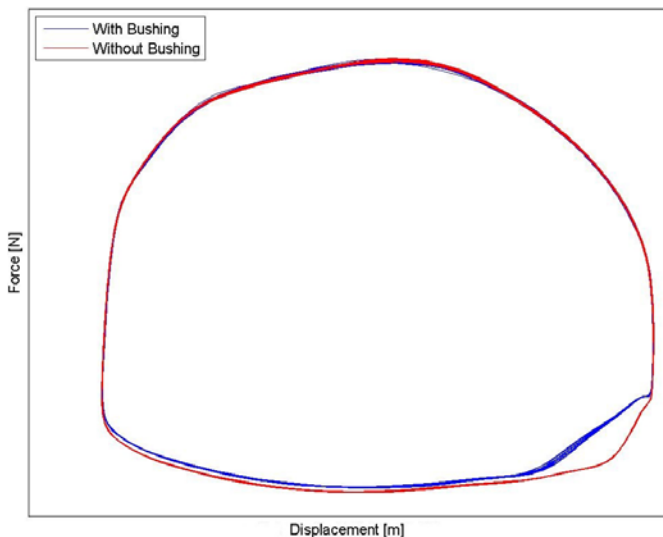


Figure 5.15 Low position, frequency = 6 Hz, amplitude = 30 mm, maximum velocity = 1.31 m/s

Figure 5.16 below the 6 Hz test with a high amplitude and a high maximum velocity is displayed. As can be seen the bushing doesn't have a relevant influence on the results.

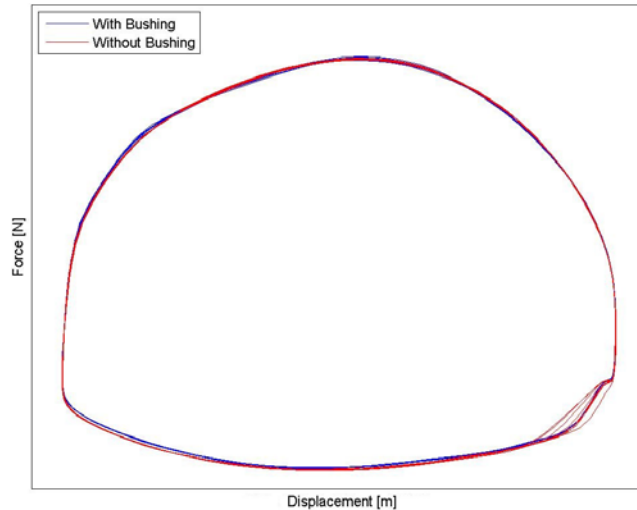


Figure 5.16 Frequency = 6 Hz, amplitude = 45 mm, maximum velocity = 1.70 m/s

Figure 5.17 below the 30 Hz test with a 2 mm amplitude is shown. It can be seen that the bushing doesn't have a significant influence on the shape of the curve but it has a significant influence on the force levels.

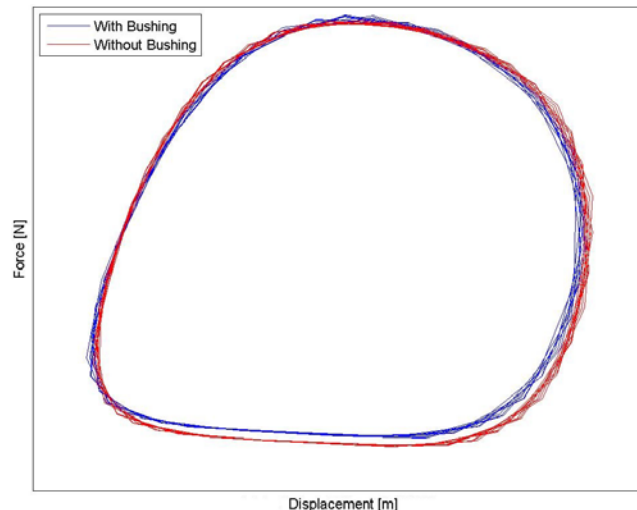


Figure 5.17 Frequency = 30 Hz, amplitude = 2 mm, maximum velocity = 0.38 m/s

It can be seen that the influence of the bushing is most significant in the tests with low maximum velocities. It can also be seen that some strange corners and peaks are removed, see figure 5.13 and figure 5.15.

5.2.2 Sine input to test rig

The force velocity curve in the figures below is calculated in Dymola using a speed sensor and a lookup table block. The force is simply interpolated from the table values for each velocity. Graphs from all of the tests can be found in appendix, chapter 10.3.

In figure 5.18 it can be seen that the force velocity curve model overestimates the value of the force during rebound a lot for the frequency 0.5 Hz. The Dymola model follows the force level satisfactory, but displays unwanted edges.

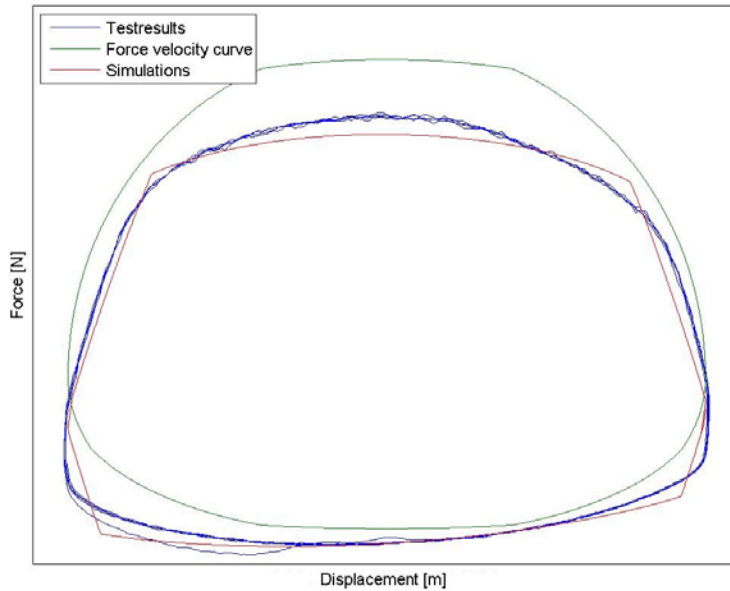


Figure 5.18 Frequency = 0.5 Hz, amplitude = 45 mm, maximum velocity = 0.14 m/s

For the frequency of 3 Hz the force velocity curve model still overestimates the rebound force, although not as much as for 0.5 Hz. The Dymola model performs well, and the edges found in the 0.5 Hz plot are gone.

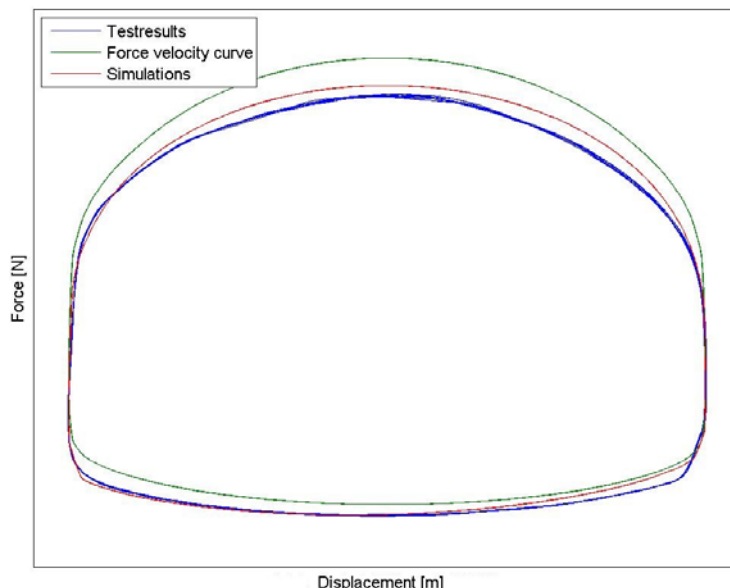


Figure 5.19 Frequency = 3 Hz, amplitude = 45 mm, maximum velocity = 0.85 m/s

As previously mentioned high means that the damper is started in an expanded position, and low means that it starts compressed. The Dymola model follows the curve well even when the starting position is changed.

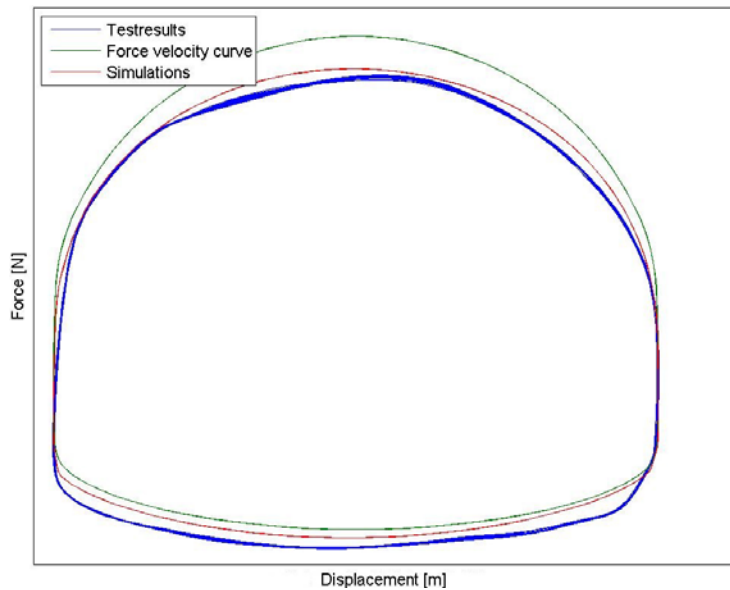


Figure 5.20 High position, frequency = 6 Hz, amplitude = 30 mm, maximum velocity = 1.31 m/s

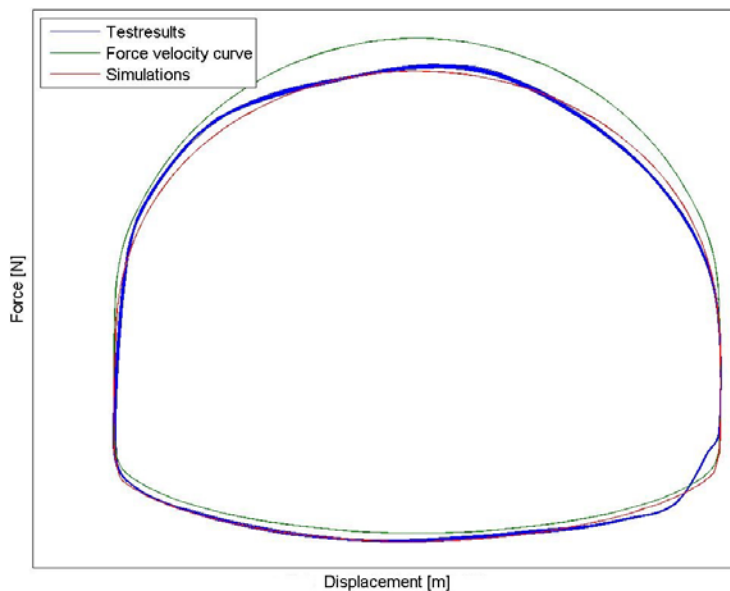


Figure 5.21 Low position, frequency = 6 Hz, amplitude = 30 mm, maximum velocity = 1.31 m/s

When the frequency is increased to 15 Hz the top left corner of the measurement curve is moved to the right. The top gets pointier and the bottom right corner gets somewhat distorted. All of which both the models fail to reconstruct

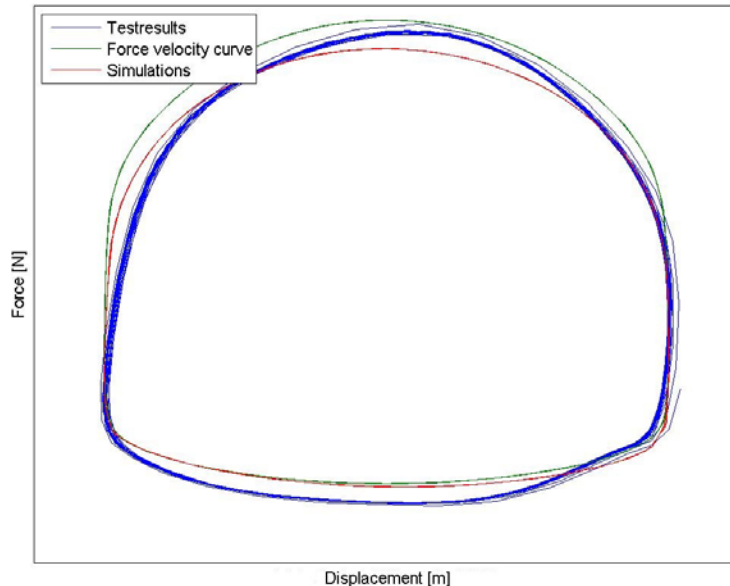


Figure 5.22 Frequency = 15 Hz, amplitude = 8 mm, maximum velocity = 0.75 m/s

When the frequency is increased a bit further to 17 Hz and the amplitude is increased the attributes of the 15 Hz becomes enhanced, and the models still fails to behave accordingly. The force levels on the rebound side is however much better represented with the Dymola model.

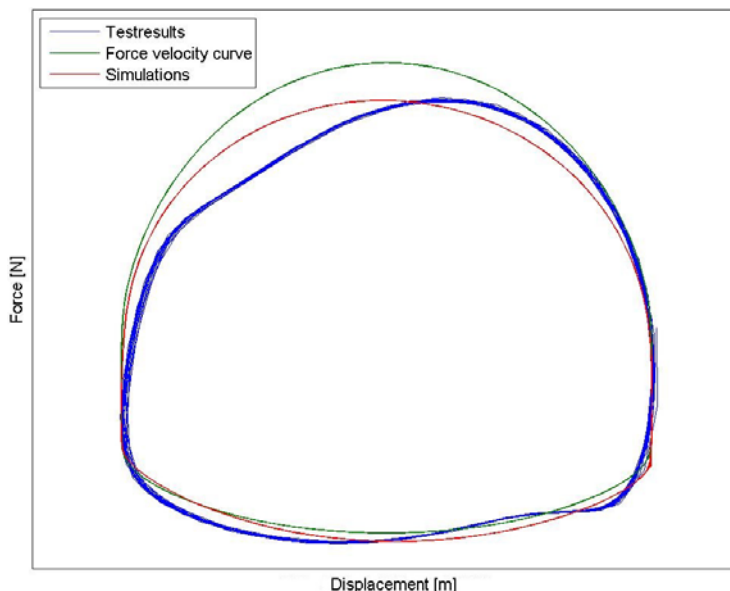


Figure 5.23 Frequency = 17 Hz, amplitude = 15 mm, maximum velocity = 1.60 m/s

With the frequency increased further to 30 Hz the measurement curve is tilted to the right, especially on the left hand side in figure 5.24 and figure 5.25. Neither the Dymola nor the force velocity curve model replicates this in a good way, but the Dymola model shows tendencies towards this behaviour. As for the low frequency and the 15 Hz frequency tests, the force velocity curve model overestimates the force levels on the rebound side.

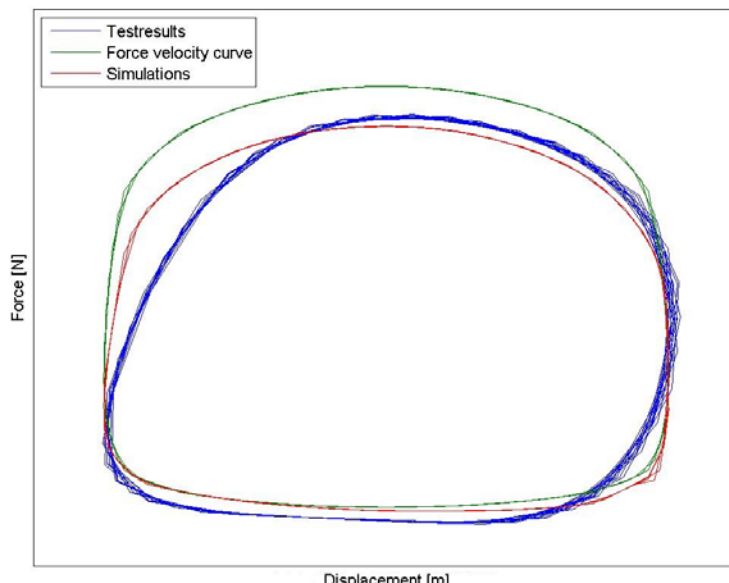


Figure 5.24 Frequency = 30 Hz, amplitude = 2 mm, maximum velocity = 0.38 m/s

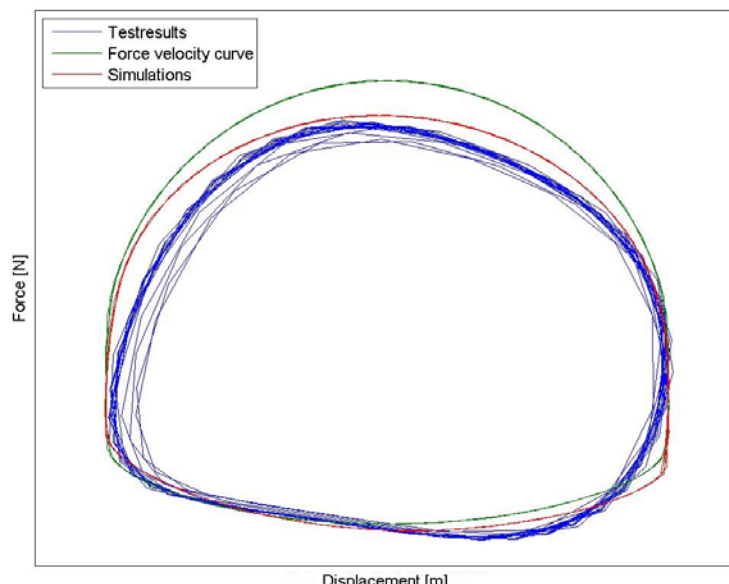


Figure 5.25 Frequency = 30 Hz, amplitude = 8 mm, maximum velocity = 1.51 m/s

5.2.3 Measured road input

Figure 5.26 shows the force-velocity plot for the road input to the damper rig. The blue line represents the measured force level, the red line the Dymola model results and the green line the force velocity curve results. It can be seen that the Dymola model replicates the force level during high positive velocities, and the hysteresis during low velocities a lot better than the force velocity curve. This was expected from the results of the sine inputs to the damper rig. During large negative velocities

the Dymola model overestimates the hysteresis while the force velocity curve underestimates the hysteresis.

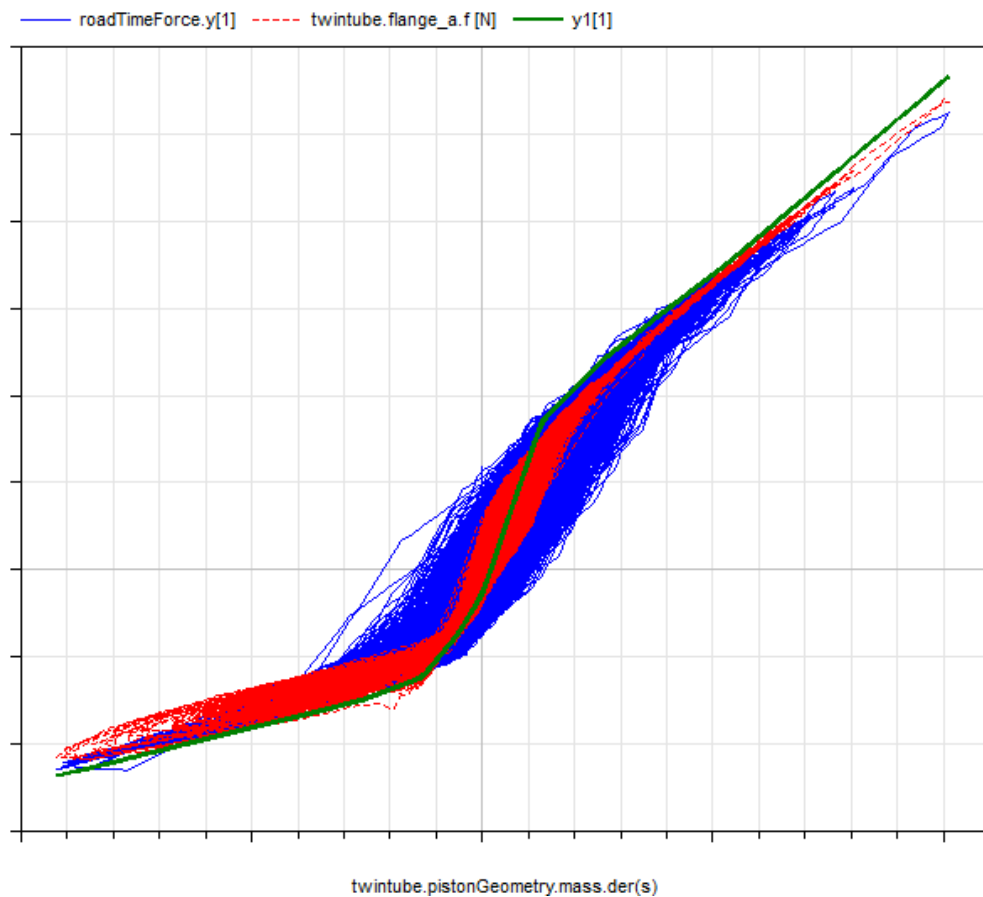


Figure 5.26 Force velocity plot, the blue line is the measurements, the red dashed line is the Dymola results and the green line is the force velocity curve model

Figure 5.27 shows the force for the measurement, Dymola simulation and the force velocity curve result for the road input. Since nothing can be said looking at that picture some small time intervals are chosen by random to show the results. The blue line represents the measurements, the green line the Dymola results and the red line is the results from the force velocity curve.

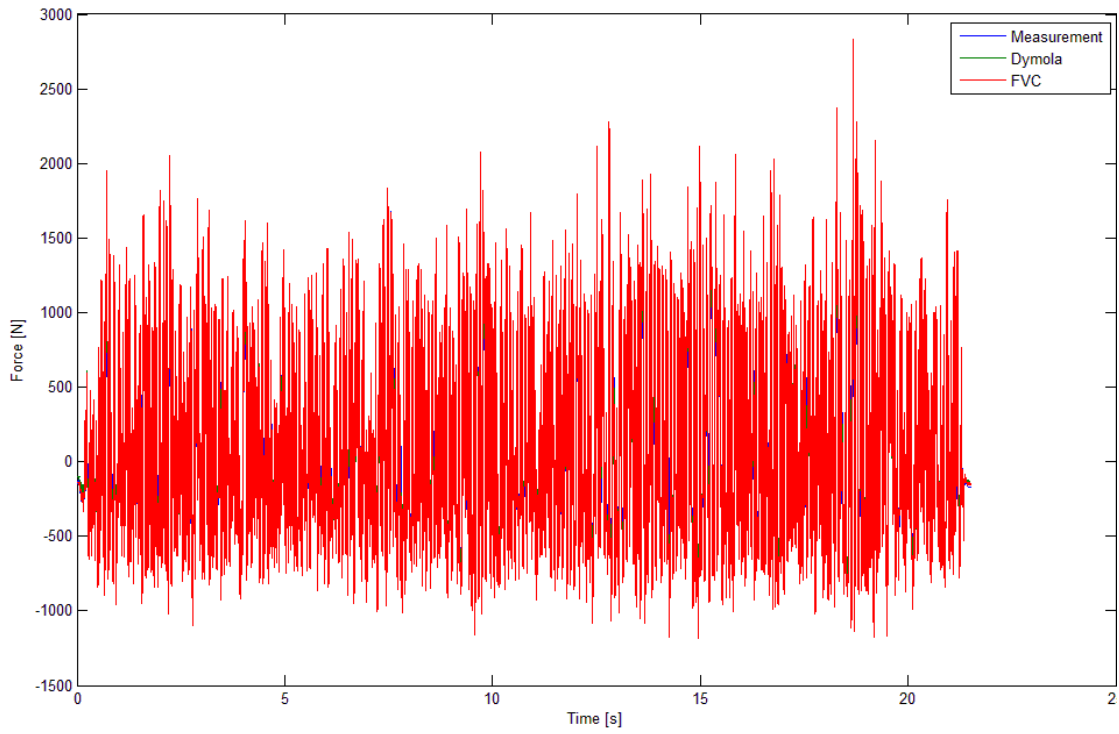


Figure 5.27 Force plot in the time domain

In figure 5.28 to figure 5.31 zoomed in views of figure 5.27 is shown to display the performance of the models during the road measured input tests.

During the interval 2.2-2.32 seconds it can be seen that both the models perform good, the Dymola model has a slight advantage after 2.26 seconds.

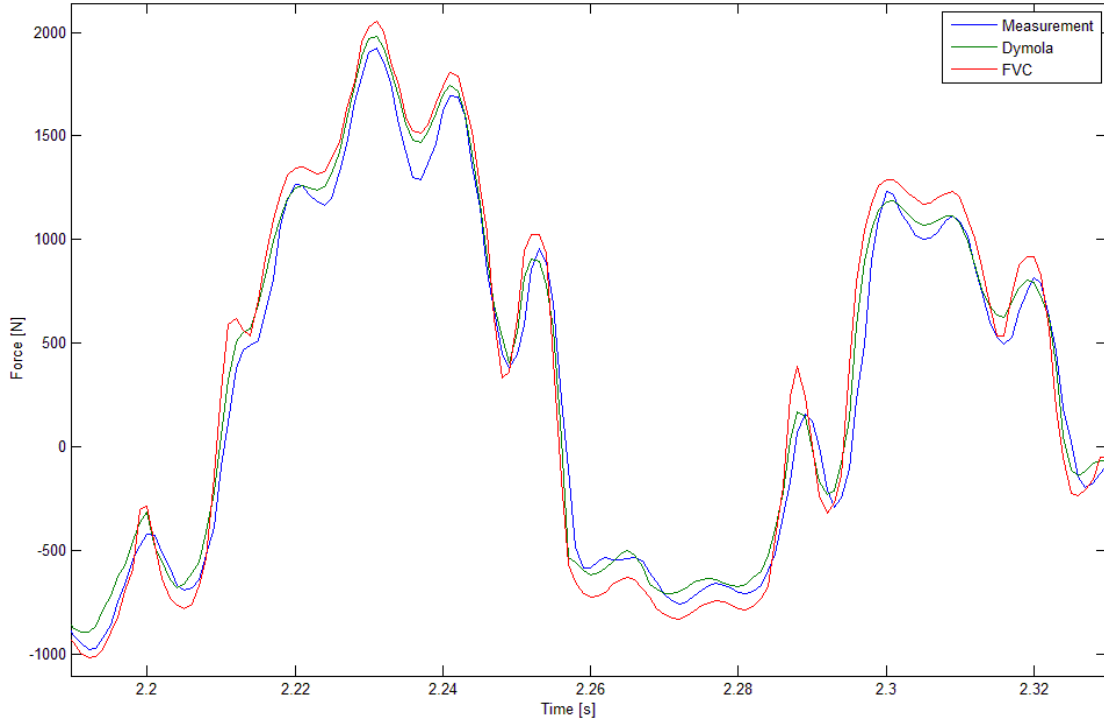


Figure 5.28 Zoomed in view of figure 5.27 for the time interval 2.2 - 2.32 seconds

During the interval 8.36-8.45 seconds the Dymola model displays significantly better force levels, but both the models show to follow the shape of the measurement curve well.

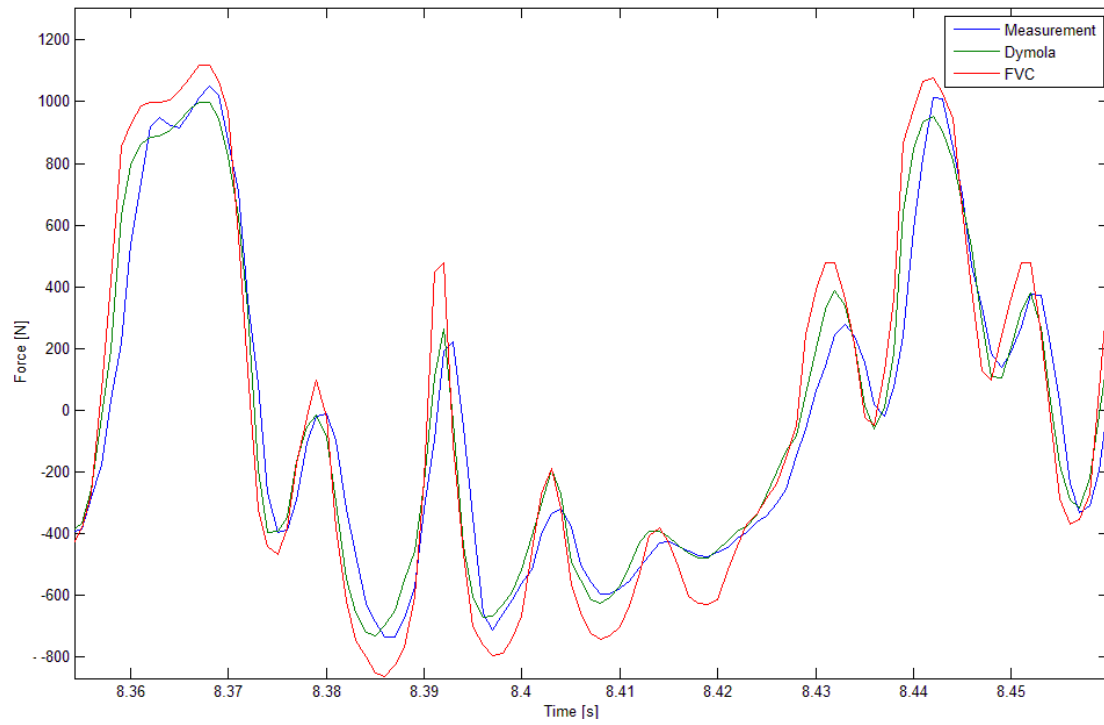


Figure 5.29 Zoomed in view of figure 5.27 for the time interval 8.36 – 8.45 seconds

In the interval 15.44-15.6 seconds it can be seen that the difference between the performance of the models are less significant than between 8.36-8.45 seconds.

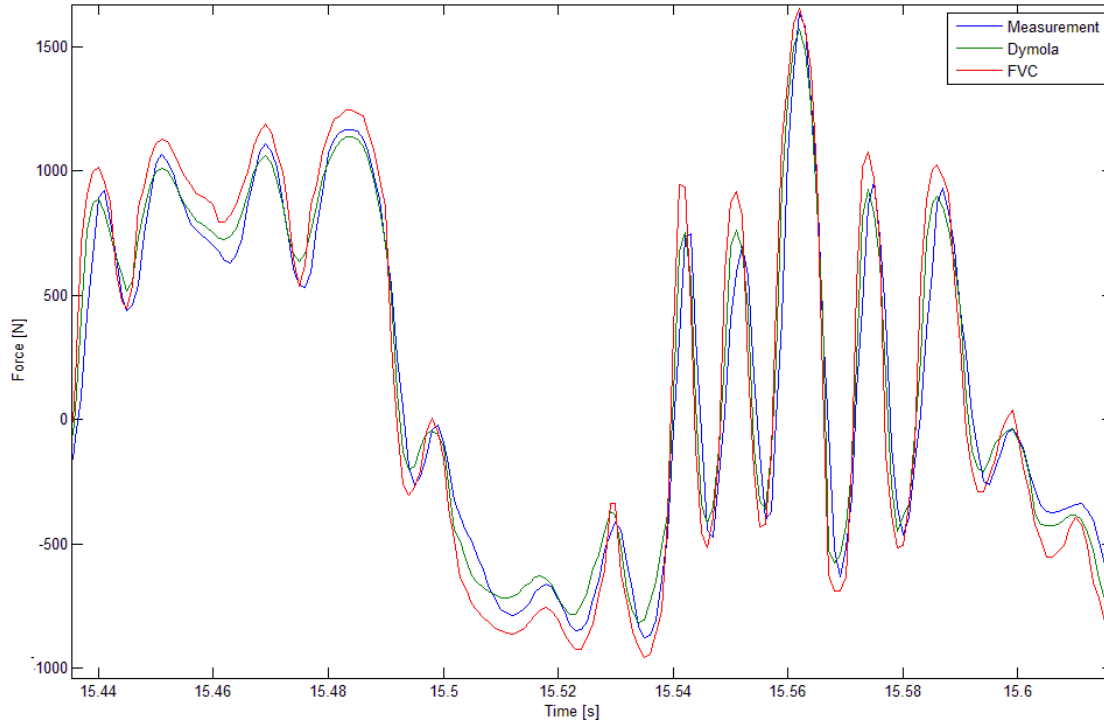


Figure 5.30 Zoomed in view of figure 5.27 for the time interval 15.44 – 15.6 seconds

During the interval 20.56-20.74 seconds it can be seen that the Dymola model performs better than the force velocity curve model. However it can also be seen that

the Dymola model performs significantly worse than before towards the end of the interval.

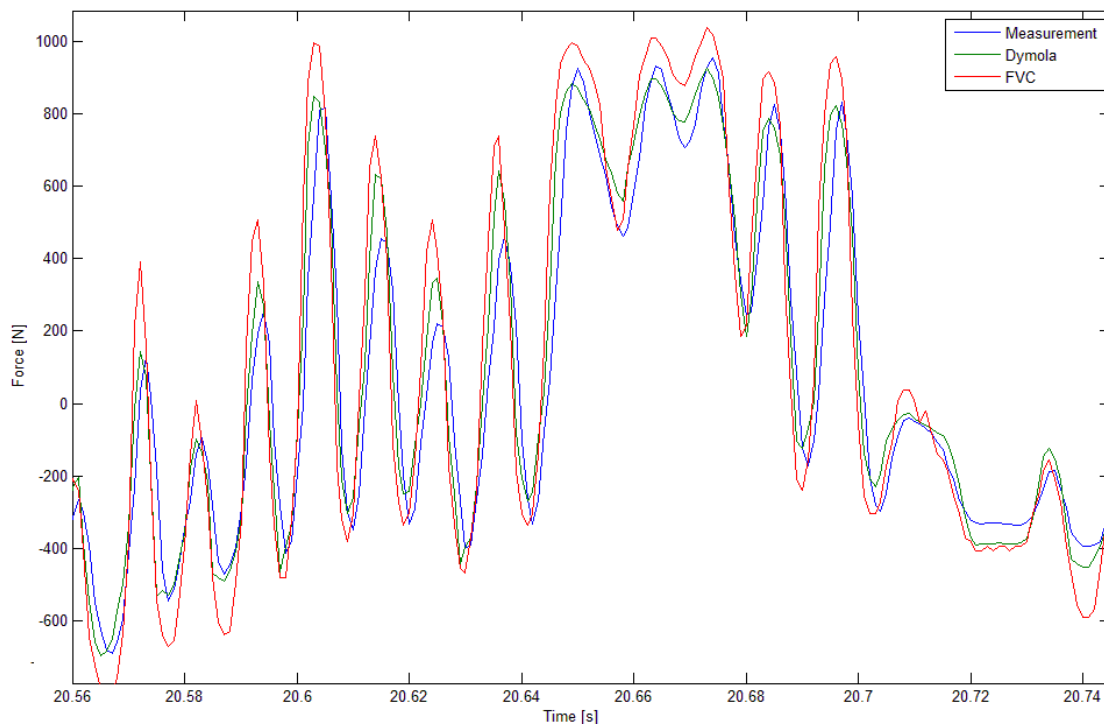


Figure 5.31 Zoomed in view of figure 5.27 for the time interval 20.56 - 20.74 seconds

Overall it can be observed that the Dymola model performs better when it comes to phase and high frequency content.

To get a measure of the error a type of standard deviation is calculated. However, the results should only be seen as an indication since the results show a slight time delay of the measurement compared to the simulations.

$$SD = \sqrt{\left(\sum x - \frac{\sum x}{N} \right)^2 \frac{1}{N}} \quad (23)$$

Where x is the difference between the model and the measurements of the radial coordinate of the normalized force-displacement points and N is the number of elements in the vector x .

Model	Standard deviation
Dymola model	116
Table based model	198

5.2.4 Four poster

The results from simulations in Adams were imported to Matlab together with the results from the measurements. The displacements of all three results were plotted and can be found in figure 5.32 - figure 5.34.

The blue line represents the potentiometer measurements, the green line the results from the force velocity curve in Adams and the red results from the FMU imported to Adams.

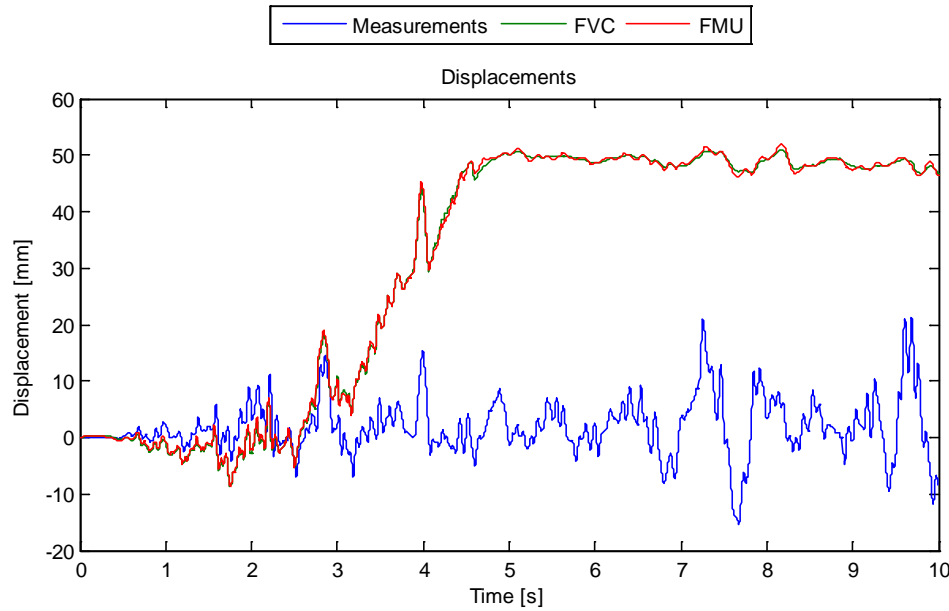


Figure 5.32 The displacement during the road measured input to the four poster

As can be seen the simulations have trouble stabilizing around the start position and at around 3 seconds in to the test the displacement increases rapidly. It is likely because of faults with the integration done in the simulations, but there was not enough time to confirm and fix that. To show what happens before this increase the first three seconds of the test are displayed in figure 5.33.

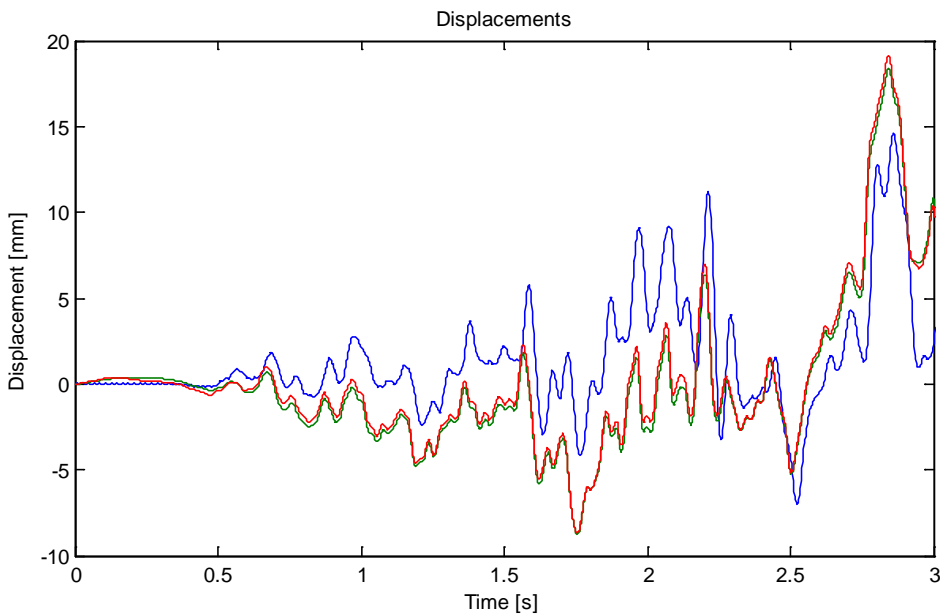


Figure 5.33 View of figure 5.32 for the time interval 0-3 seconds.

It can be seen that the Adams simulation has troubles with the displacement position during this time as well, there seems to be a built-in wave form in the simulation results. During the first 0.5 seconds there is an initialization period where the displacement is zero, this time interval is removed in figure 5.34, also the results after 2 seconds are removed.

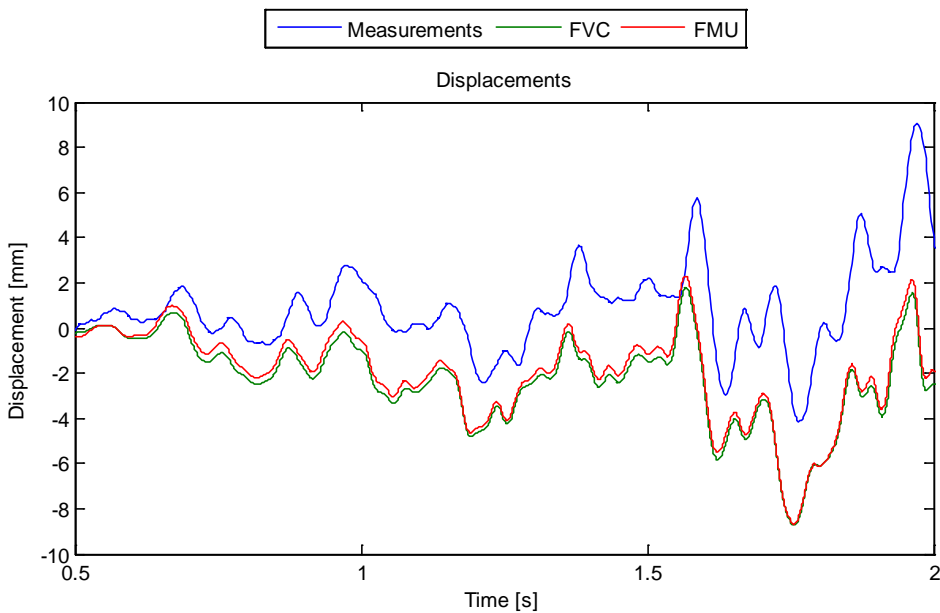


Figure 5.34 View of figure 5.32 for the time interval 0.5-2 seconds.

Even if the actual displacement levels for the simulations are wrong it can be seen that both the models follow the shape of the measured curve well. The FMU model doesn't show the expected improvements compared to the FVC model, however it should be kept in mind that the inputs to the rig are filtered at 30 Hz and that the tires dampen the high frequencies. It should also be noted that the potentiometer has trouble picking up frequencies above 10 Hz satisfactory.

5.3 Oil parameters and cylinder expansion

The bulk modulus and the volume fraction of gas where examined in the pursuit of better results during higher frequencies. In figure 5.35 and figure 5.36 the influence of decreasing the bulk modulus and increasing the amount of gas in the oil are displayed during a 30 Hz test with amplitude of 8 mm. The parameters are changed more than would be realistic to show the influence properly. It can be seen that both these parameters shows potential for improving the results for high frequencies.

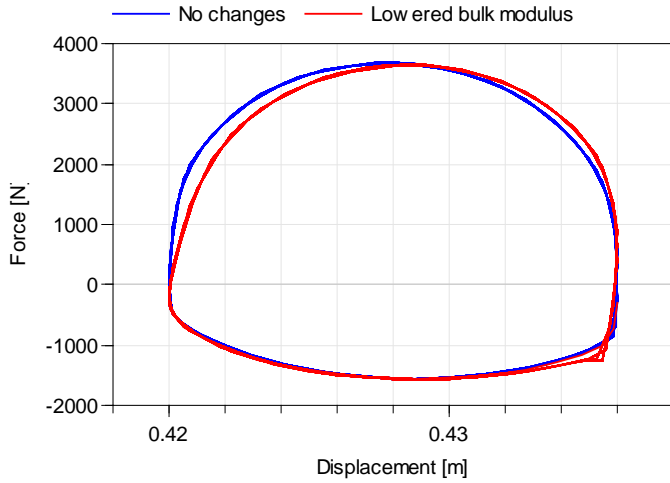


Figure 5.35 Plot showing the influence of the bulk modulus

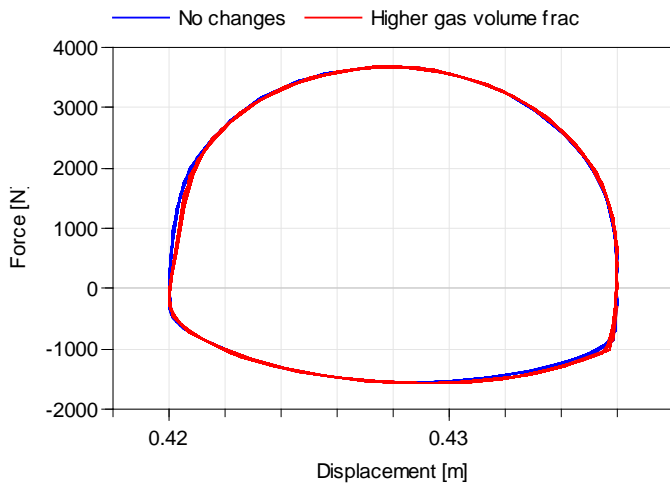


Figure 5.36 Plot showing the influence of the gas volume fraction

To model the expansion and compression of the chambers would require a significant amount of work which is outside of the time frame of the project at this stage. Therefore an approximation of the influence of the chamber expansions was introduced. This was achieved by mounting a spring to the mass that represents the movement of the piston. This should give a good indication of the influence of introducing expansion of the chambers.

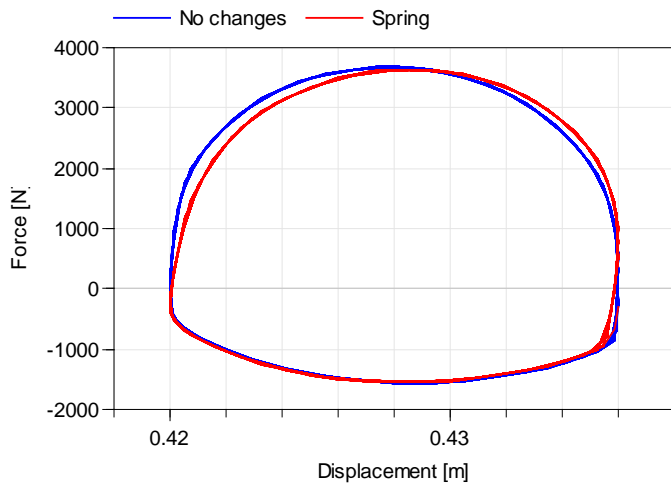


Figure 5.37 Plot showing the influence of the spring that imitates cylinder expansion

To get an indication of what these changes would mean for the road measured input test in the damper rig the spring that imitates cylinder expansion were introduced and the volume fraction of gas in the oil were increased. The results are shown in figure 5.38, for the time interval 2-2.3 seconds, and in figure 5.39 for the time interval 2-2.12 seconds.

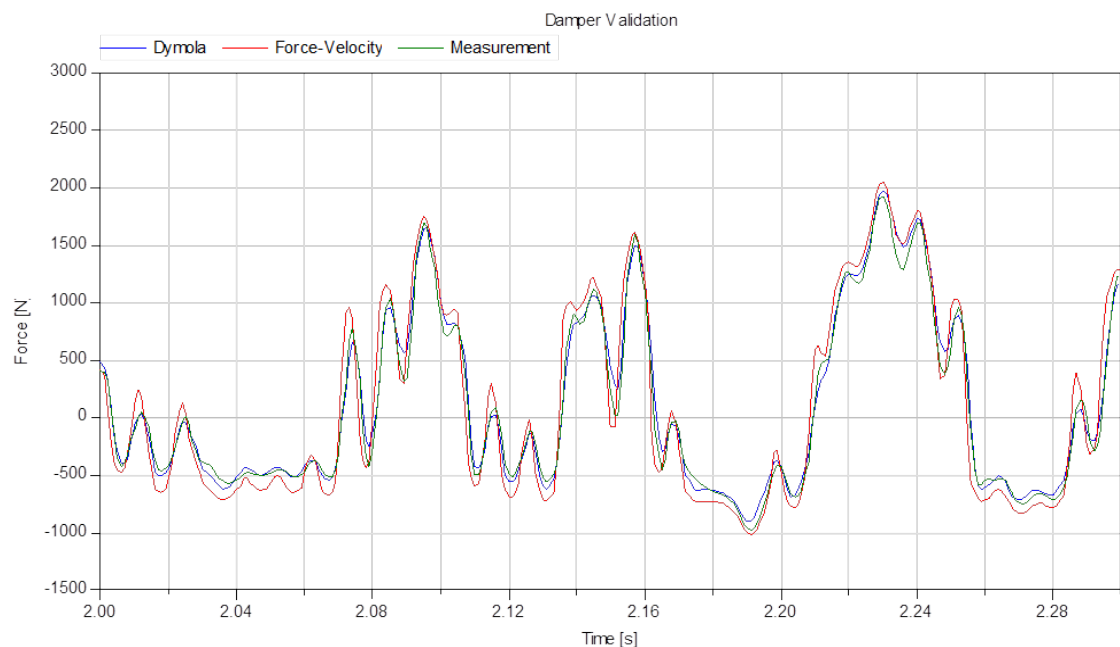


Figure 5.38 Force plot with a higher gas volume fraction and a spring acting as cylinder expansion

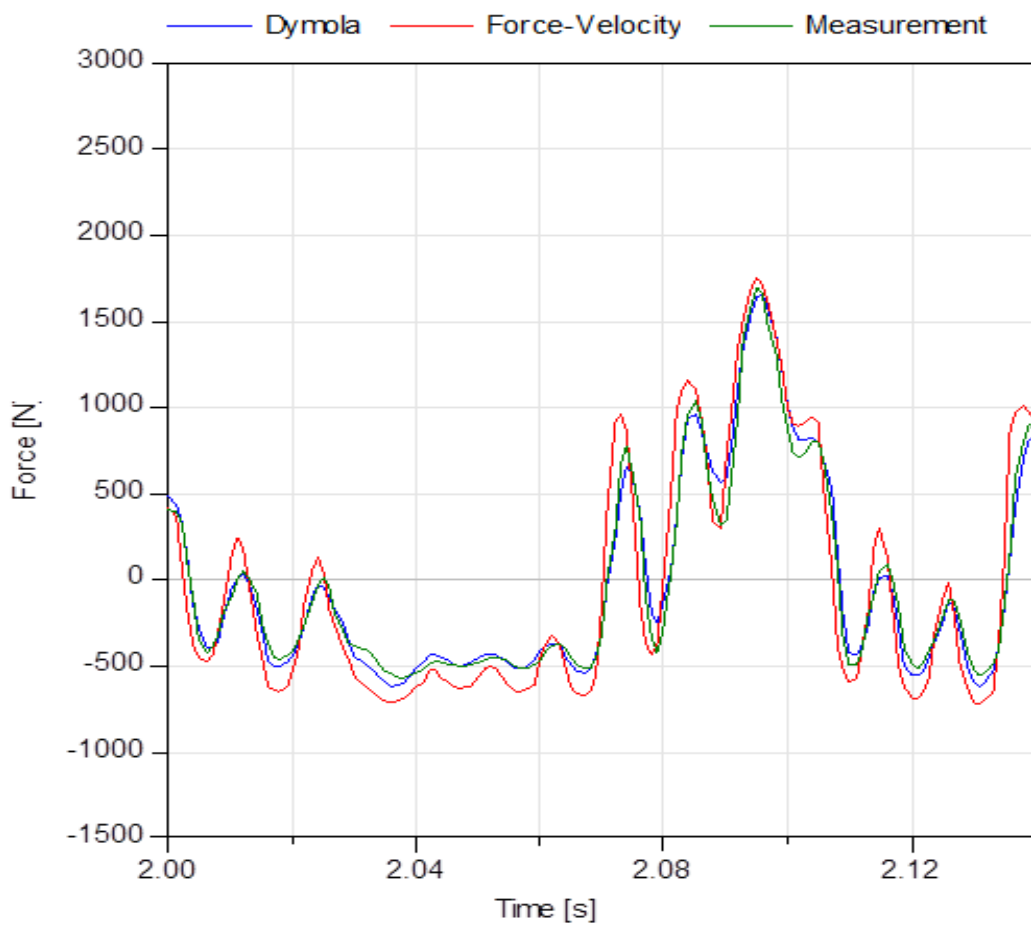


Figure 5.39 Force plot with a higher gas volume fraction and a spring acting as cylinder expansion

It seems as the force levels are better with these changes, it can also be seen that the time delay shown by the models are decreased for the improved Dymola model.

The standard deviation of the normalized results were calculated for the improved models.

Table 3 Standard deviation of the normalized results

Model	Standard deviation
FVC	198
Dymola model	116
Improved Dymola model	75

6 Discussion

This chapter attempts to analyse the results presented in the previous chapter.

6.1 Validation of the model

It should be said that all the tests have only been run once, to get conclusive results it would be good to do run some of the tests again to confirm the results.

6.1.1 Damper rig test

It is clear when observing the figures in chapter 5.2.1 that the removing the bushing in the bottom mount of the damper has a significant influence on the results. This should be taken into consideration when studying the results of the validation of shock absorber A, since this was only tested in the damper rig with the bushing mounted.

6.1.1.1 Sine

When studying the figures in chapter 5.1.1 and 5.2.2 it is clear that the model replicates the behaviour of the damper quite good. It should also be said that the measurements shows some distortions that the model doesn't capture, such as in figure 5.23.

It can also be seen that during higher frequencies the curve is tilted to the right. The left hand side towards the top of the figures are most effected, i.e. where at the most compressed position where it turns. At the lowest position when rebound starts the compression valves closes and the rebound valves opens, it is possible that the spring in the rebound valve on the piston is the source of this linear characteristic.

For the tests with low frequencies the force displacement plots show some unwanted edges. During the calibration it was found that the calibration of the friction model is probable to be the cause for this, however due to the limited time for this project this was not investigated further.

6.1.1.2 Road

Observing the figures in chapter 5.2.2, it seems like the Dymola model doesn't quite follow the measurements up and down the smaller/faster peaks. This could indicate that some of the fast dynamics of the shock absorber aren't modelled sufficiently. However it follows the measurements better than the force velocity curve model during these faster dynamics.

As previously mentioned in chapter 5.2.3 the measurements show a slight time delay compared to the results from the simulations, see figure 6.1. The cause for this delay is unknown, but it is likely that it, in part, stems from the filtering done during the measurements. The characteristics of these filters are unknown to a large extent. Another likely cause of the delay is the post processing of the results, where the velocity and acceleration inputs were differentiated from the displacement using Matlab.

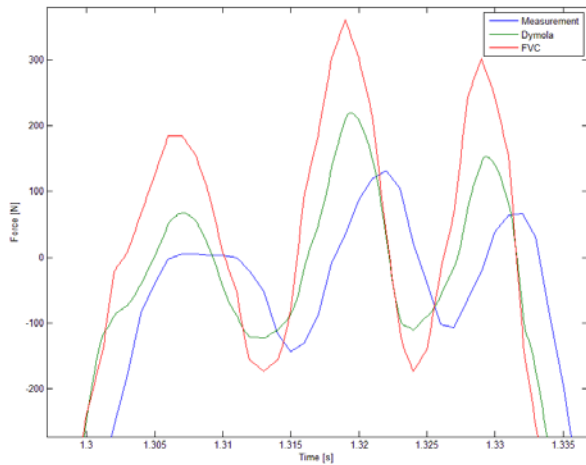


Figure 6.1 Displaying the time delay found between the measurements and the simulations

6.1.2 Four poster

Due to limitations of the four poster rig the inputs was filtered at 30 Hz. This means that the high frequencies where the Dymola model is expected to improve the results most is removed and dampened in the test. Another source of filtering during the full vehicle tests are the tires that filter the movement of the stands before transferring it to the vehicle body. It was seen that the models performed in a similar manner throughout the test. It should be said that the Adams simulations where run with an acceleration signal as the input for the virtual rig, this is believed to be the cause of the built in wave and the rapid increase in displacement 3-5 seconds in to the test.

7 Conclusion

When the damper rig receives a sine wave as input for the displacement the Dymola model showed a significant improvement compared to the force velocity curve model. The Dymola model displays better results than the force velocity curve throughout the frequency span that was studied. There are a few phenomenon that neither the Dymola nor the force velocity curve model replicates properly, these may be possible to replicate with an even more advanced Dymola model. The Dymola model shows potential to replicate these events, especially for the tilted curve that occurs for the highest frequencies. However, a more advanced Dymola model may be too complicated for the applications this model was designed for, resulting in too long simulation times. It would also require further measurements to determine which of the phenomenon is caused by the damper and which are caused by the measurement equipment or the post processing. Some adjustments to the model were investigated and showed promising results when it comes to model the tilt shown during high frequencies. These are adjustments that won't increase the simulation time very much, a description of these can be found in chapter 5.3.

As for the road input to the damper rig, the results from the Dymola model are clearly better than the force velocity curve model. This is also indicated by the calculated standard deviation, even though the values are unreliable due to the phase difference between the simulations and the measurement. The results also show that there is room for improvement on the fast dynamics, as indicated by the results from the sine wave input to the damper rig. The phase difference was shown to decrease for the Dymola model when some of the improvements described in chapter 5.3 were implemented. This would indicate that the phase difference is a result of some dynamics that the model doesn't fully capture without these improvements. These results should however be more investigated before any real conclusions can be drawn from this.

The results from Adams on the other hand are not quite as good. It is believed that the Dymola model could perform better than it currently does if the input to the virtual rig were less filtered, i.e. contained more fast dynamics. The results should also be improved by using the displacement, velocity and acceleration as inputs instead of only the acceleration, this is believed to remove the distortion of the simulation's displacement values.

In the more controlled environment of the damper rig tests the Dymola model proves to be a significant improvement compared to the force velocity curve model. In the full vehicle tests the model doesn't show the same improvements compared to the force velocity curve model. To get the full potential shown in the damper rig in the full vehicle scenario from the model, more investigation is needed of the export and import from Dymola to Adams, the simulations in Adams and the measurements done in the four-poster.

8 Future work

When the model is imported to Adams it is installed between bushings. These bushings may cause high frequency interactions between Adams and the FMU. Since the FMU and Adams exchange information at a fixed time interval, information on high frequency interactions might be lost if the sampling frequency isn't high enough. This could be avoided by increasing the sampling frequency, but that would cause very slow simulations. Another way to avoid this would be to have the bushings modelled in Dymola as a part of the damper model. However rubber is very hard to model, and it was not within the scope of this project.

When the model was developed very little time was spent at calibrating the parameters of the oil model. These parameters shows potential when it comes to the tilting of the force-displacement curves at high frequencies, especially at 30 Hz. This should be investigated further. Further discussion of this can be found in chapter 5.3.

When the model was developed the expansion of the cylinders was excluded since the results of (Claesson, 2012) shows that it doesn't have a large effect on the results. However, the damper modelled in Claesson's thesis was a mono-tube damper, which means that it consists of only one cylinder. When looking at the dampers in this project, the outer cylinder is very thick compared to the inner cylinder. This could mean that the inner cylinder of the dampers in this project may experience expansion that would affect the results. Therefore the model may benefit largely from modelling of cylinder expansion. Further discussion of this can be found in chapter 5.3.

The measurement methods that were used in this project were developed to assess the performance of a shock absorber and to create a force velocity curve model. These methods are not necessarily the optimal for the calibration of a physical model such as the Dymola model. Hence the measurement methods should be revised with the calibration of the Dymola model in focus, if the model is to be used for other dampers.

9 References

- Akutain, X. C., Viñolas, J., Savall, J., & Biera, J. (2006). A Parametric damper model validated on a track. *Int. J. Heavy Vehicle Systems*, 13(3), 145-162.
- Boggs, C. M., & Ahmadian, M. (2007). Efficient Empirical Modeling of a High-Performance Shock Absorber for Vehicle Dynamics Studies. *Steering & Suspension Technology Symposium*. Detroit: SAE International.
- Chahine, R. (2011). *Modeling of a World Rally Championship Car Damper and Experimental Testing of Its Components*. Stockholm.
- Claesson, J. (2012). *Fysikalisk modellering av avancerad racingstötdämpare*. Lund: Lunds Tekniska Högskola.
- Cossalter, V., Doria, A., Pegoraro, R., & Trombetta, L. (2010). On the non-linear behaviour of motorcycle shock absorbers. *Journal of Automobile Engineering*, 15-27.
- Dassault Systèmes AB. (2013). *Dymola User Manual Volume 1*.
- Dassault Systèmes AB. (2013). *Dymola User Manual Volume 2*.
- Dixon, J. C. (2007). *The Shock Absorber Handbook*.
- Dymola for physical modeling and simulation*. (2014, 02 07). Retrieved from Modelon web site: <http://www.modelon.com/products/dymola/>
- Ekh, M. (2013). *Formulas in Mechanics of Solids*. Applied Mechanics, Chalmers.
- FMI [Start]*. (2014, 02 07). Retrieved from FMI [Start]: https://trac.fmi-standard.org/export/700/branches/public/docs/Modelica2011/The_Functional_Mockup_Interface.pdf
- French, M. (2000). Shaker Tables and Four-Posters. *Experimental Techniques*.
- Gällsjö, A., & Johansson, M. (2012). *Physical Modelling and Automatic Configuration of CES Valve*. Linköping: Linköping University.
- Hou, Y., Li, L., He, P., Zhang, Y., & Chen, L. (2011). Shock Absorber Modelling and Simulation Based on Modelica. *8th Modelica Conference*, (pp. 843-846). Dresden.
- Kowalski, D., Rao, M. D., Blough, J., Gruenberg, S., & Griffiths, D. (2001). The Effects of Different Input Excitation on the Dynamic Characterization of an Automotive Shock Absorber. *Proceedings of the 2001 Noise and Vibration Conference*. Traverse City: SAE International.
- Lang, H. H. (1977). *A Study of the Characteristics of Automotive Hydraulic Dampers at High Stroking Frequencies*.
- Li, S., Lu, Y., & Li, L. (2012). Dynamical Test and Modeling for Hydraulic Shock Absorber on Heavy Vehicle under Harmonic and Random Loadings. *Research Journal of Applied Sciences, Engineering and Technology*, 1903-1910.
- Lundh, H. (2008). *Grundläggande hållfasthetsslära*. Stockholm.
- Modelica home page*. (2015, January 05). Retrieved from Modelica and the Modelica Association: modelica.org

- Modelon AB. (2011). *Modeling of Hydraulic Systems - Tutorial for the Hydraulics Library*. Lund, Sweden.
- Sorniotti, A., D'Alfio, N., & Morgando, A. (2007). Shock Absorber Modeling and Experimental Testing. *Steering & Suspension Technology Symposium*. Detroit.
- Sundström, B. (2008). *Handbok och formelsamling i hållfasthetsslära*. Stockholm.
- Talbott, M. S., & Starkey, J. (2002). An experimentally validated physical model of a Hi-Per Mono-Tube Damper. *Proceedings of the 2002 SAE Motorsports Engineering Conference and Exhibition*. Indianapolis: SAE International.
- Young, W., Budynas, R., & Sadegh, A. (2012). *Roark's Formulas for Stress and Strain* (8th Edition ed.). The McGraw-Hill Companies, Inc.

10 Appendix

10.1 Equations and expressions

$$f = \left((r_o - r_i) * (r_o + r_i) * \left(2r_o^2 r_i^2 (3 - 2\nu) + r_i^4 (-1 + \nu) + r_o^4 (7 + 3\nu) \right) \right.$$

$$\quad - 4 r_o^2 r_i^2 \left(-(r_o^2 (-5 + \nu)) + r_i^2 (1 + \nu) + 4 r_o^2 (1 + \nu) \right)$$

$$\quad * (\log r_o - \log r_i) \left(\log r_o - \log r_i \right)$$

$$\quad \left. * \frac{1}{64 * D * \left(-(r_i^2 * (-1 + \nu)) + r_o^2 * (1 + \nu) \right)} \right)$$

$$f_1 = \left(-16 r_o^2 r_i^2 (1 + \nu) r_o^2 (\log r_i)^2 - (r_i - r_o) * (r_i + r_o) \right.$$

$$\quad * \left(r_o^2 (1 + \nu) * (r_i^2 + 5 r_o^2) + (-1 + \nu) \right.$$

$$\quad * \left(r_i^4 - 2r^2 r_o^2 - r_i^2 (2r^2 + 3r_o^2) \right) + 4r_o^2 (1 + \nu)$$

$$\quad * \left(r_i^2 + r_o^2 \right) \log r \left. \right) - 4r_o^2 (r_o^2 (1 + \nu) * (2r_i^2 + r_o^2) - r_i^2 (-1 + \nu))$$

$$\quad * (2r^2 + r_o^2) + 4r_o^2 r_i^2 (1 + \nu) \log r \log r_o$$

$$\quad + 4r_i^2 \log r_i \left(-((-1 + \nu)r_o^2 (2r^2 + r_o^2)) + r_o^2 (1 + \nu) * (r_i^2 + 2r_o^2) \right.$$

$$\quad \left. \left. + 4r_o^2 (1 + \nu) r_o^2 (\log r + \log r_o) \right) \right) * \frac{1}{64 D (r_o^2 + r_i^2 + r_o^2 \nu - r_i^2 \nu)}$$

$$f_2 = \left(-2r_o^4 (3 + \nu) * (r_i - r) * (r_i + r) \right.$$

$$\quad + r_o^2 \left(4r_i^4 (-1 + \nu) + 4r_i^2 \left(-((-1 + \nu)r^2) + (1 + \nu)r_o^2 \right) + (1 + \nu) \right.$$

$$\quad * (r^4 - 5r_o^4) \left. \right) - (-1 + \nu) * \left(4r_i^4 r_o^2 - 2r^2 r_o^4 + r_i^2 (r^4 - 3r_o^4) \right)$$

$$\quad + 8r_o^4 (1 + \nu) \log r_o \left(-r_i^2 + r^2 + 2r_i^2 (\log r_i - \log r) \right)$$

$$\quad + 4 \left(-4r_o^2 r_i^2 (1 + \nu) * (r_o - r_0) * (r_o + r_0) (\log r_i)^2 \right.$$

$$\quad + r_o^2 (2r_i^2 (-1 + \nu)r^2 + r_o^2 (r_i^2 (-1 + \nu) - 2(1 + \nu)r^2))$$

$$\quad - (1 + \nu)r_o^4) \log r$$

$$\quad + r_o^2 (r_o^2 (1 + \nu) * (2r_i^2 + r_o^2) - r_i^2 (-1 + \nu) * (2r^2 + r_o^2))$$

$$\quad + 4r_o^2 r_i^2 (1 + \nu) \log r \log r_o$$

$$\quad + r_i^2 \log r_i \left((r_o - r_0) * (r_o + r_0) \right.$$

$$\quad * (r_o^2 (3 + \nu) - (-1 + \nu) * (2r^2 + r_o^2) + 4r_o^2 (1 + \nu) \log r)$$

$$\quad \left. \left. - 4r_o^2 (1 + \nu) r_o^2 \log r_0 \right) \right) * \frac{1}{64 D (r_o^2 + r_i^2 + r_o^2 \nu - r_i^2 \nu)}$$

10.2 Damper A in rig with sine input

10.2.1 Force displacement plots

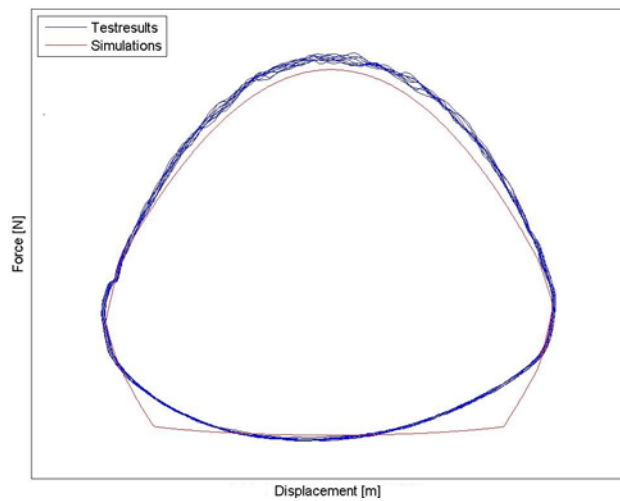


Figure 2 Frequency = 1 Hz, amplitude = 15 mm

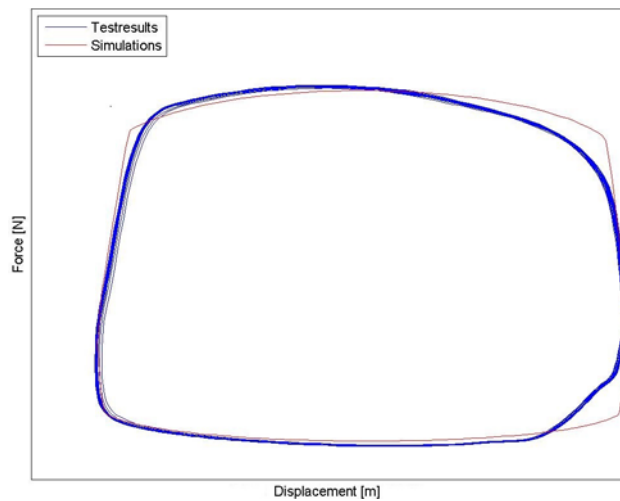


Figure 3 Frequency = 5 Hz, amplitude = 8 mm

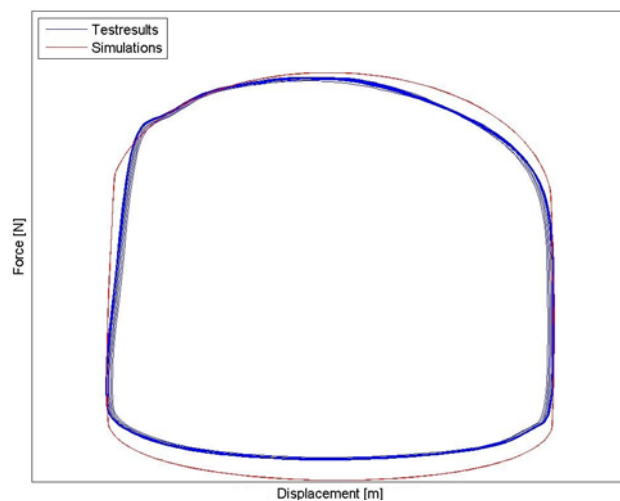


Figure 4 Frequency = 6 Hz, amplitude = 15 mm, high position

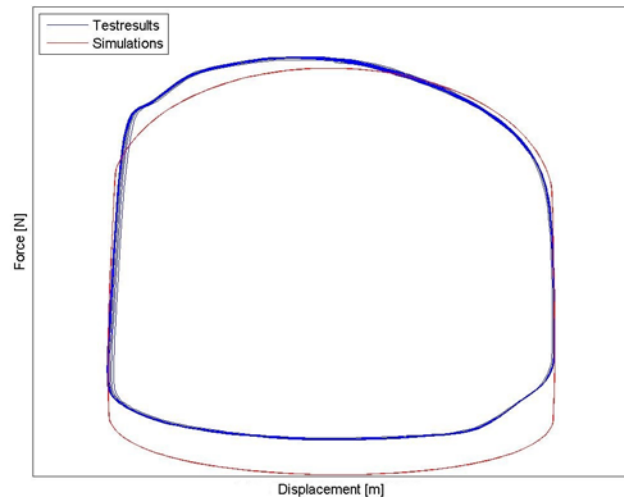


Figure 5 Frequency = 6 Hz, amplitude = 15 mm, low position

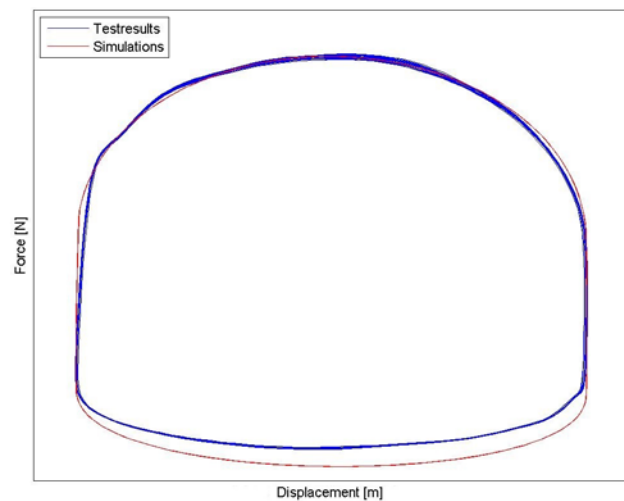


Figure 6 Frequency = 6 Hz, amplitude = 30 mm, high position

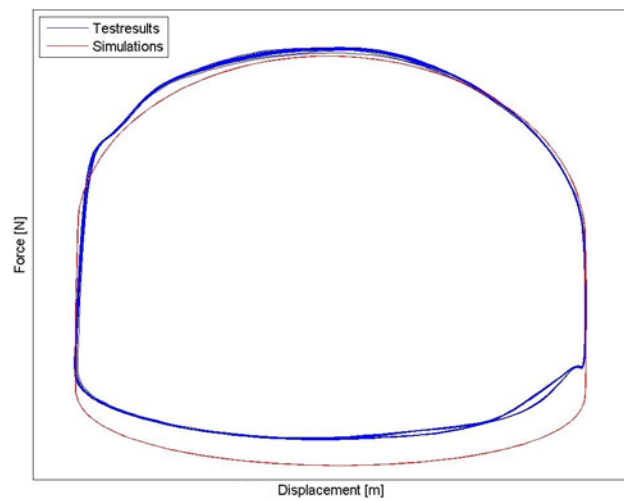


Figure 7 Frequency = 6 Hz, amplitude = 30 mm, low position

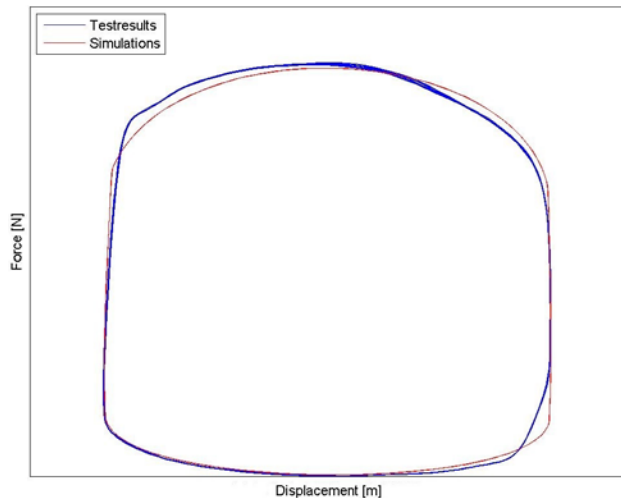


Figure 8 Frequency = 6 Hz, amplitude = 15 mm

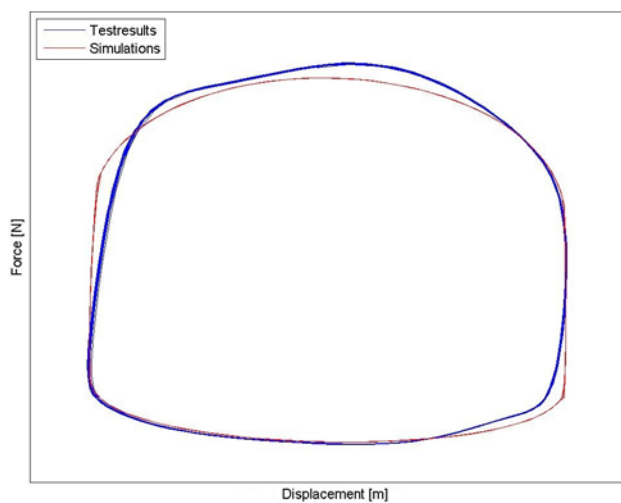


Figure 9 Frequency = 15 Hz, amplitude = 8 mm

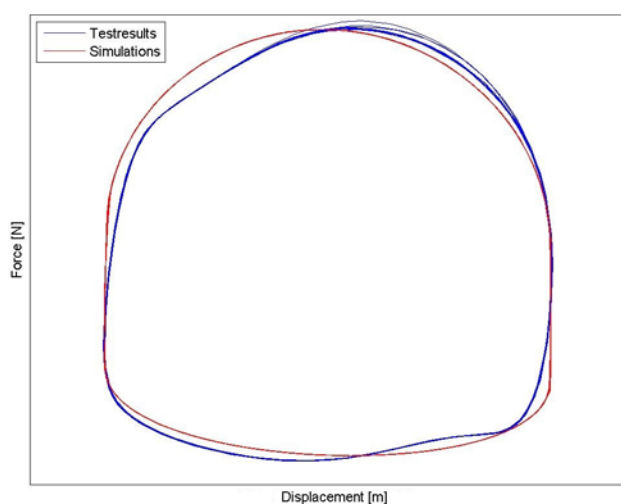


Figure 10 Frequency = 17 Hz, amplitude = 15 mm

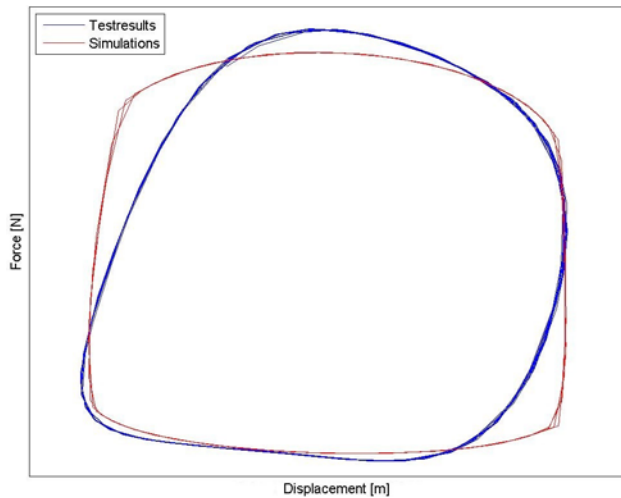


Figure 11 Frequency = 30 Hz, amplitude = 2 mm

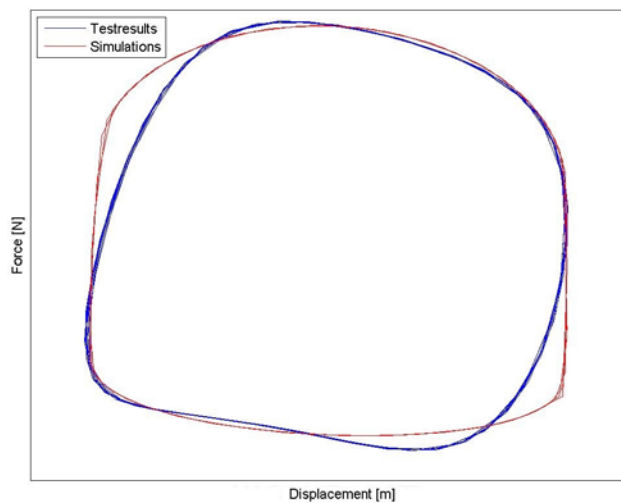


Figure 12 Frequency = 30 Hz, amplitude = 4 mm

10.2.2 Force velocity plots

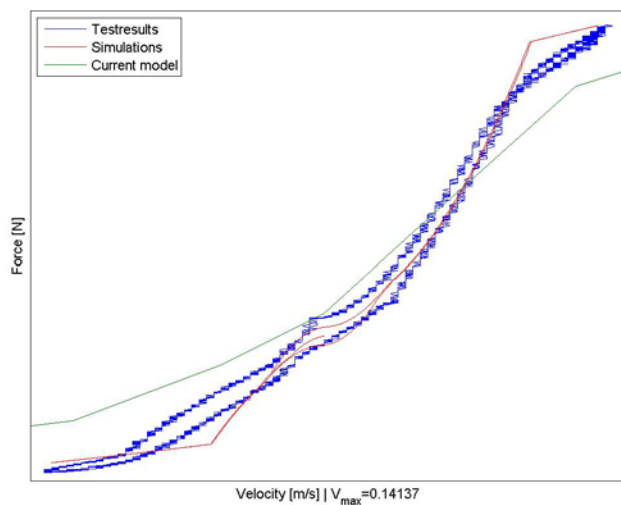


Figure 13 Frequency = 0.5 Hz, amplitude = 45 mm

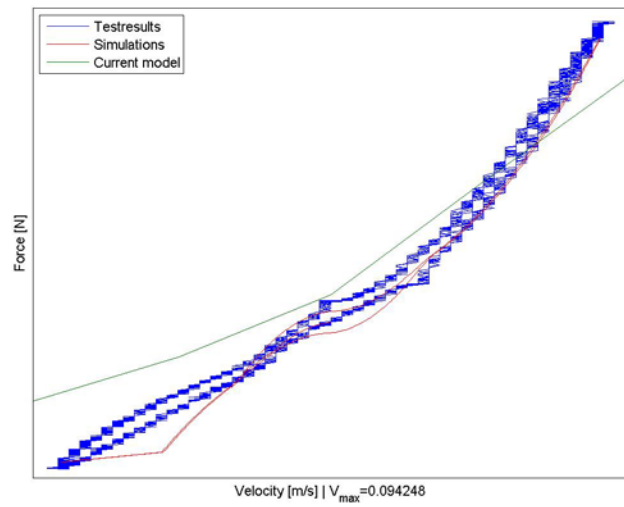


Figure 14 Frequency = 1 Hz, amplitude = 15 mm

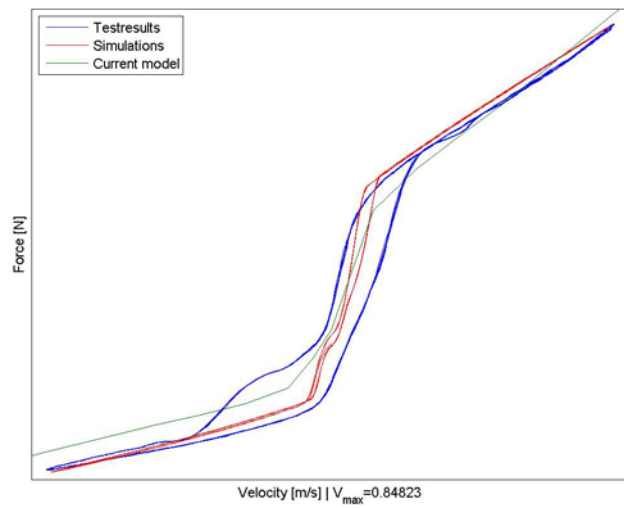


Figure 15 Frequency = 3 Hz, amplitude = 45 mm

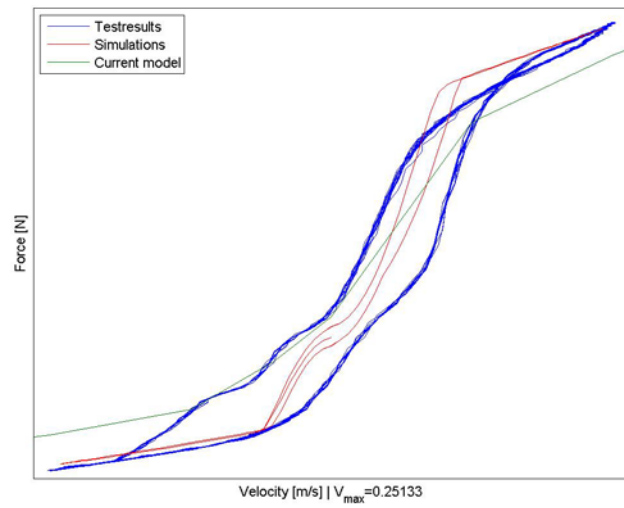


Figure 16 Frequency = 5 Hz, amplitude = 8 mm

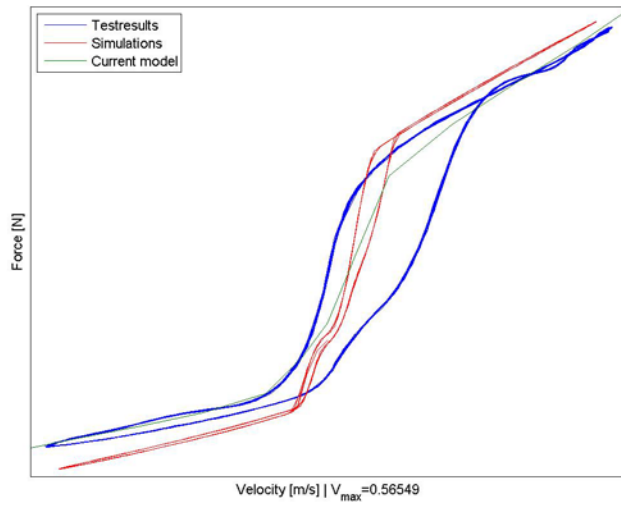


Figure 17 Frequency = 6 Hz, amplitude = 15 mm, high position

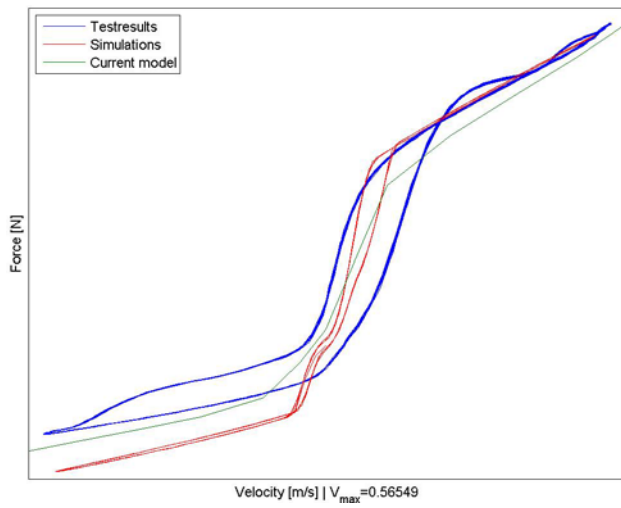


Figure 18 Frequency = 6 Hz, amplitude = 15 mm, low position

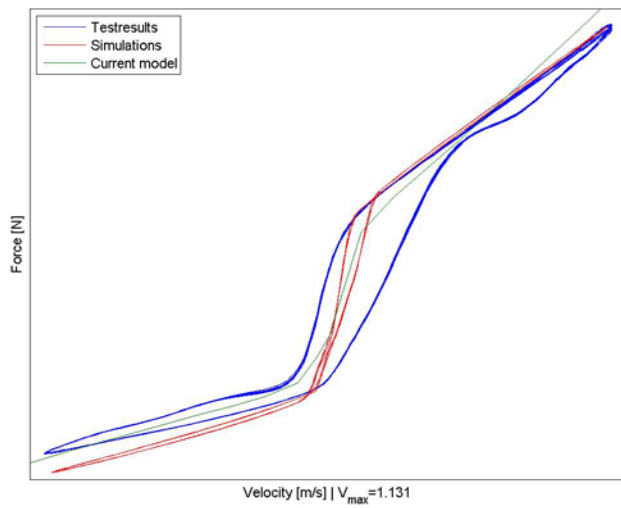


Figure 19 Frequency = 6 Hz, amplitude = 30 mm, high position

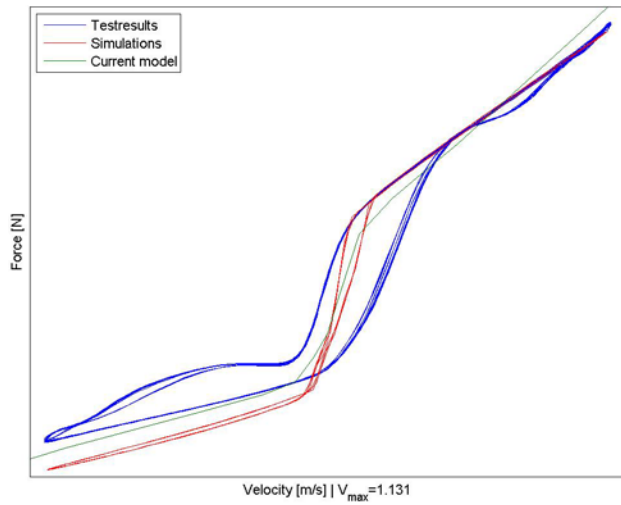


Figure 20 Frequency = 6 Hz, amplitude = 30 mm, low position

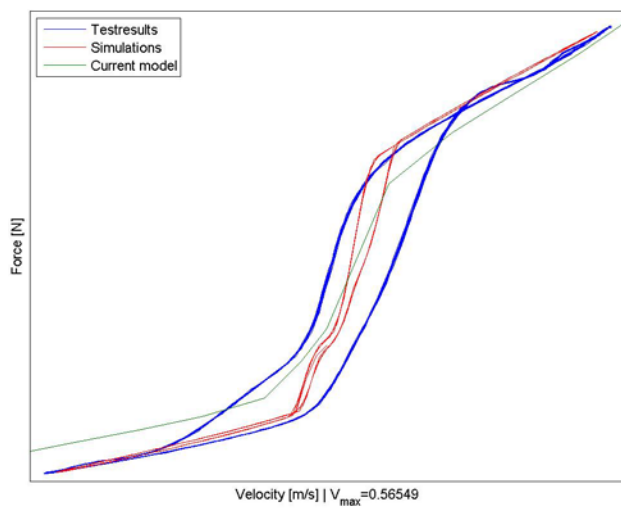


Figure 21 Frequency = 6 Hz, amplitude = 15 mm

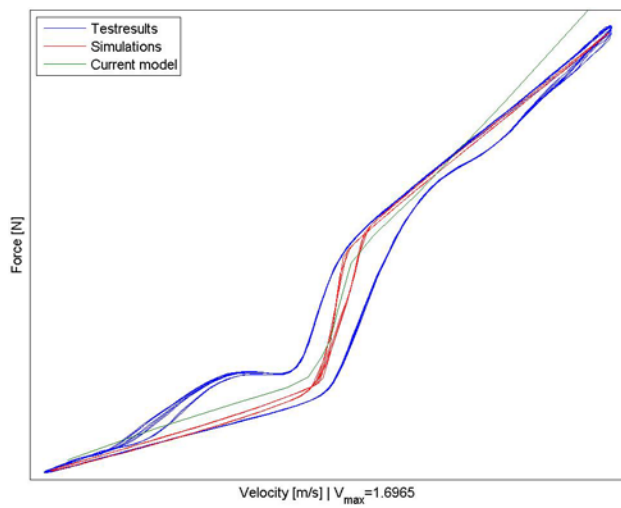


Figure 22 Frequency = 6 Hz, amplitude = 45 mm

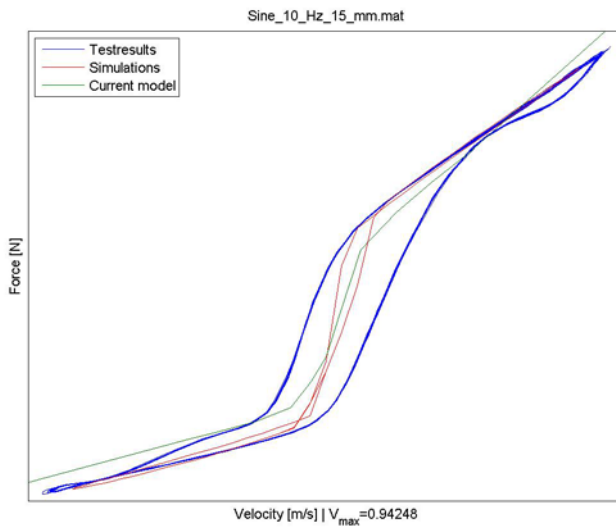


Figure 23 Frequency = 10 Hz, amplitude = 15 mm

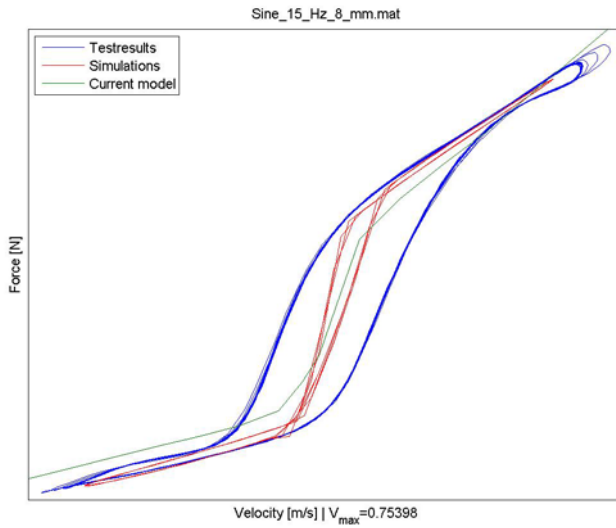


Figure 24 Frequency = 15 Hz, amplitude = 8 mm

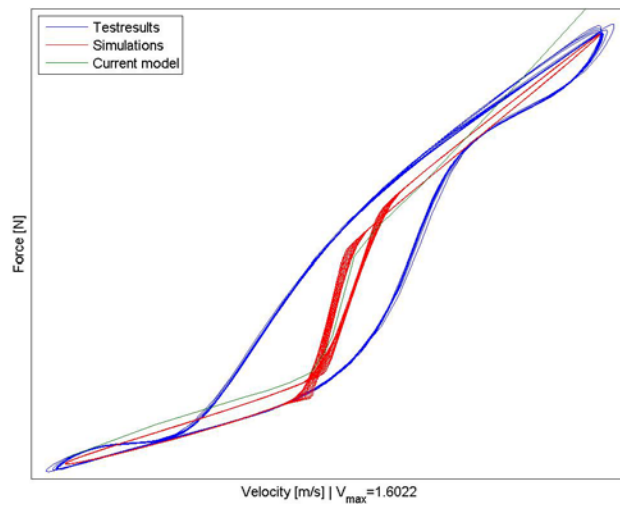


Figure 25 Frequency = 17 Hz, amplitude = 15 mm

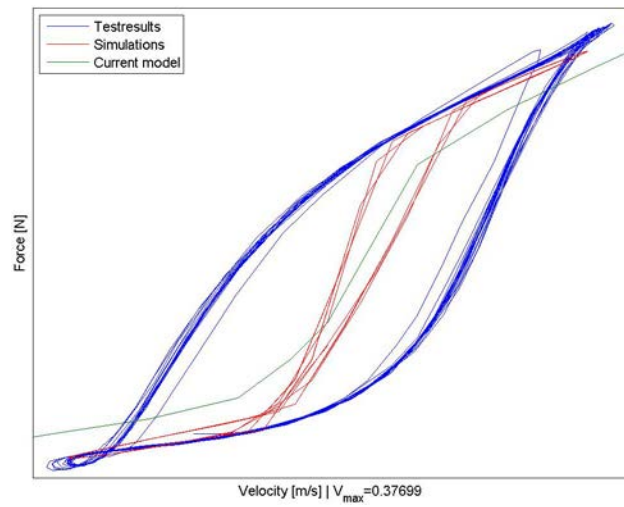


Figure 26 Frequency = 30 Hz, amplitude = 2 mm

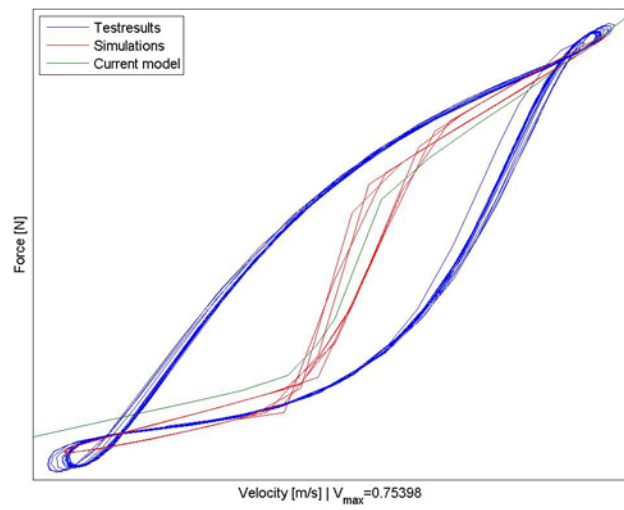


Figure 27 Frequency = 30 Hz, amplitude = 4 mm

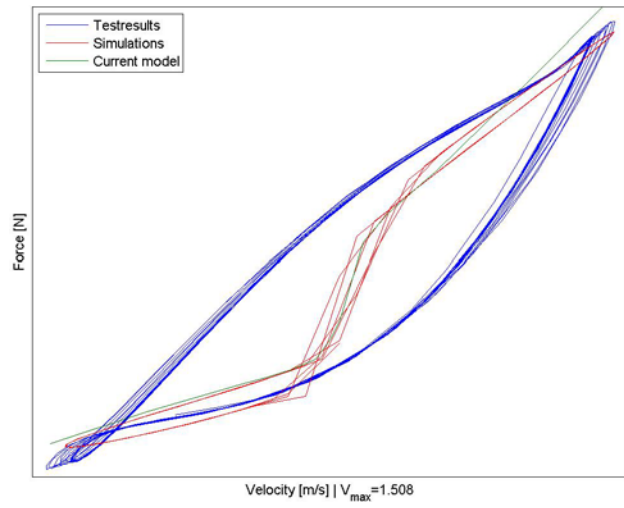


Figure 28 Frequency = 30 Hz, amplitude = 8 mm

10.3 Damper B in rig with sine input

10.3.1 Force displacement plots

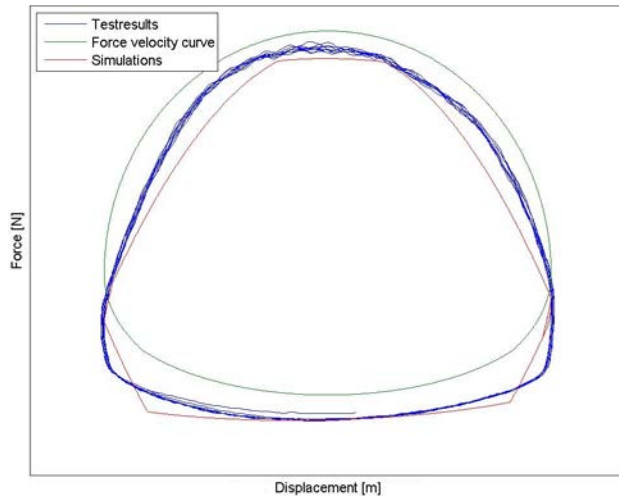


Figure 29 Frequency = 1 Hz, amplitude = 15 mm

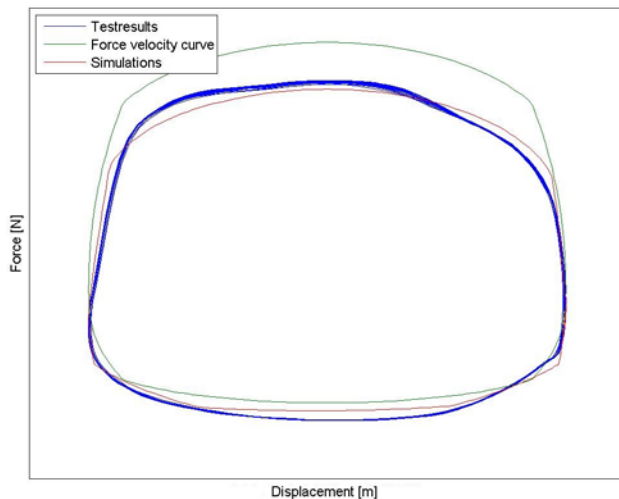


Figure 30 Frequency = 5 Hz, amplitude = 8 mm

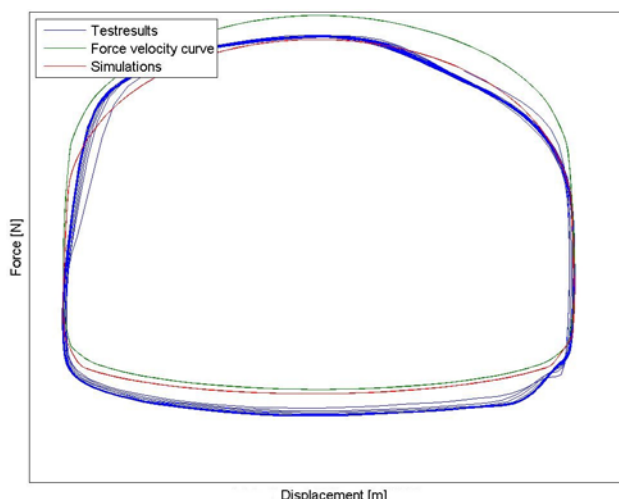


Figure 31 Frequency = 6 Hz, amplitude = 15 mm, high position

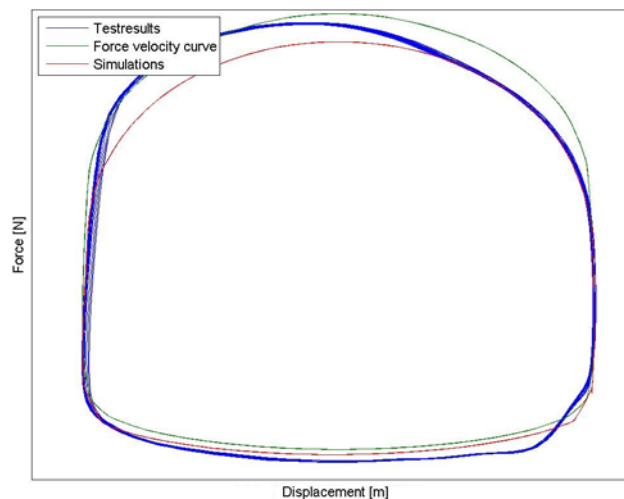


Figure 32 Frequency = 6 Hz, amplitude = 15 mm, low position

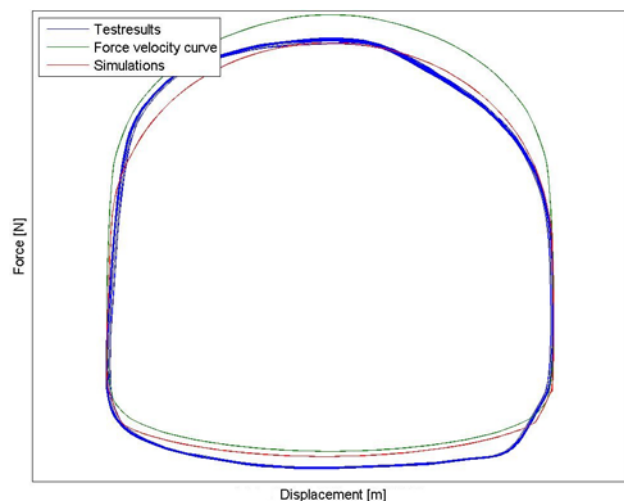


Figure 33 Frequency = 6 Hz, amplitude = 15 mm

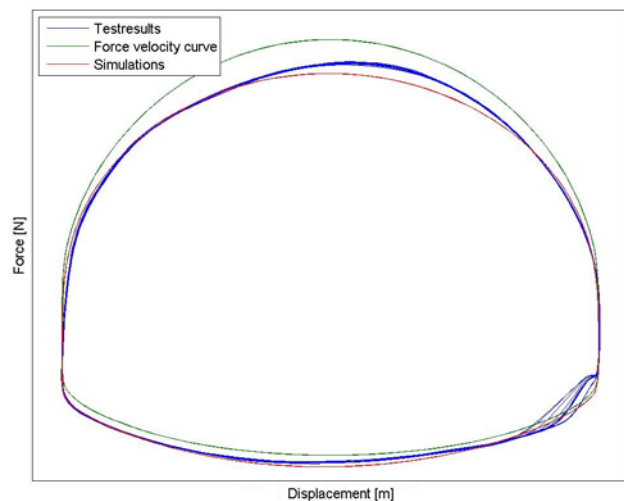


Figure 34 Frequency = 6 Hz, amplitude = 45 mm

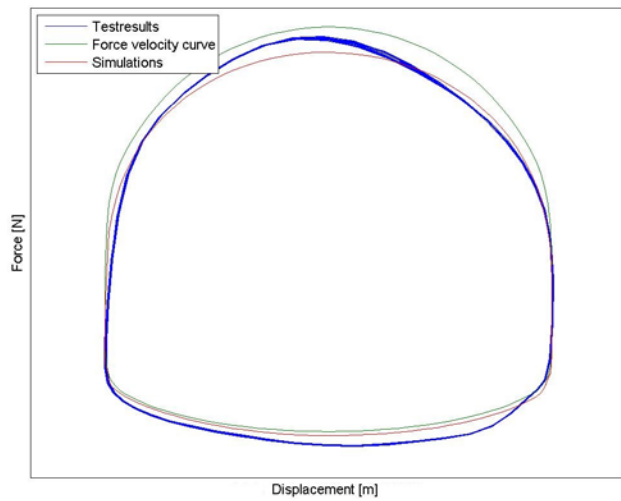


Figure 35 Frequency = 10 Hz, amplitude = 15 mm

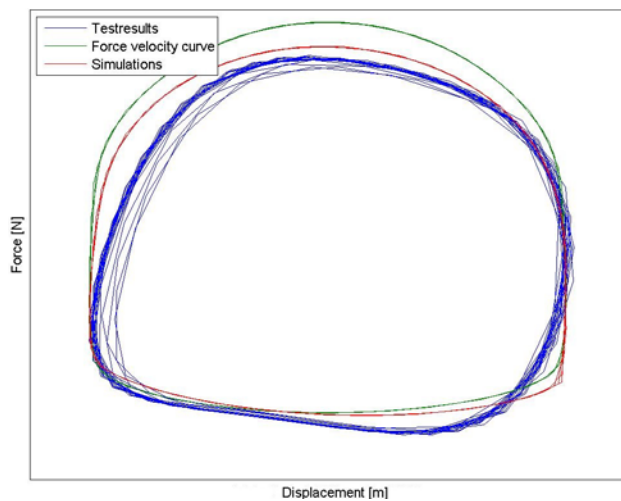


Figure 36 Frequency = 30 Hz, amplitude = 4 mm

10.3.2 Force velocity plots

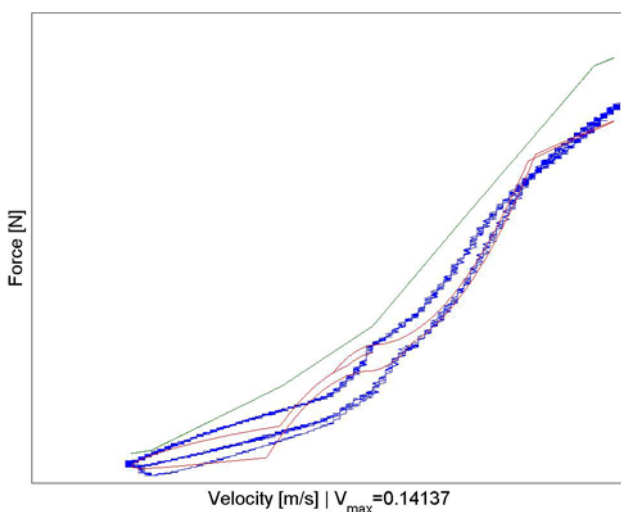


Figure 37 Frequency = 0.5 Hz, amplitude = 45 mm

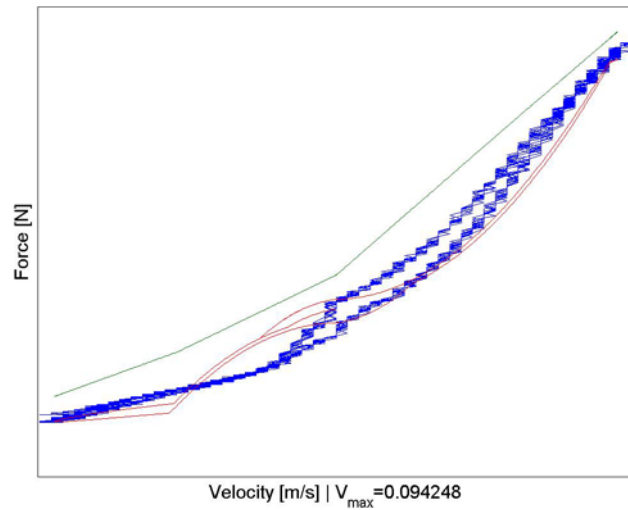


Figure 38 Frequency = 1 Hz, amplitude = 15 mm

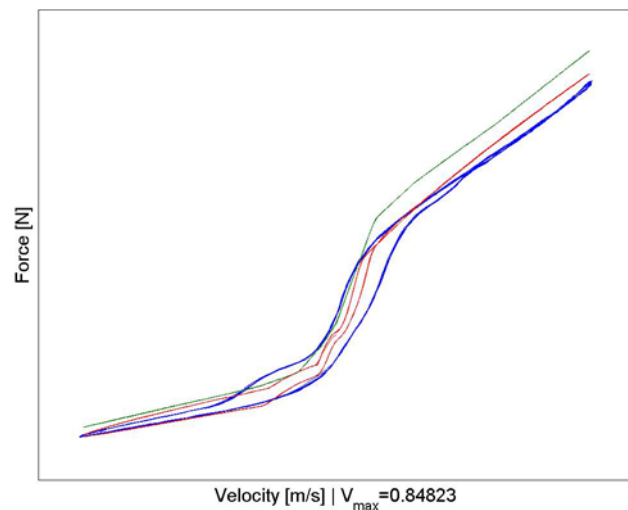


Figure 39 Frequency = 3 Hz, amplitude = 45 mm

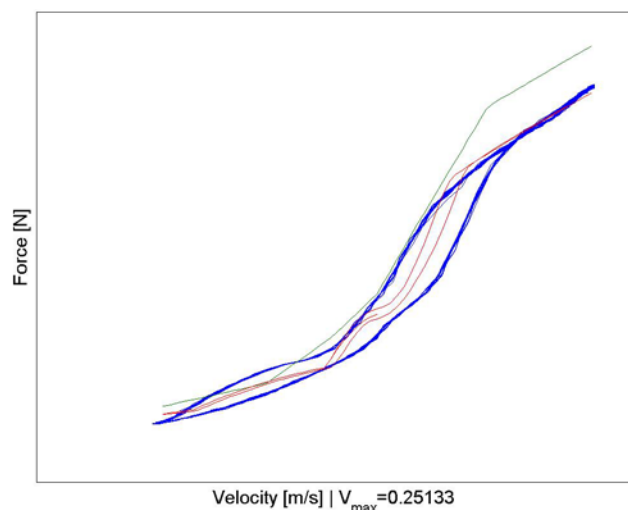


Figure 40 Frequency = 5 Hz, amplitude = 8 mm

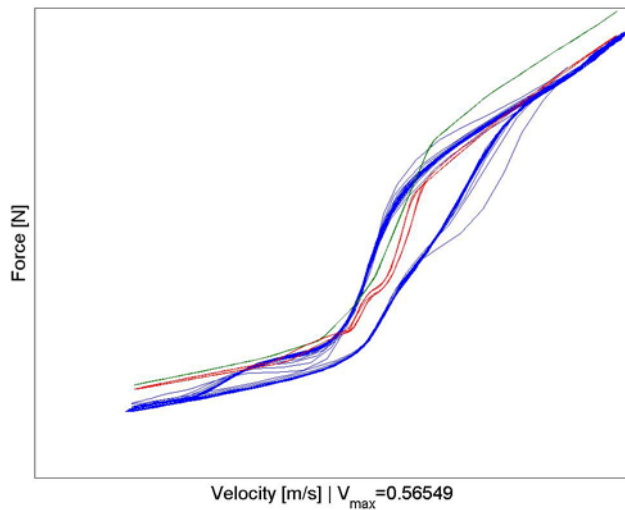


Figure 41 Frequency = 6 Hz, amplitude = 15 mm, high position

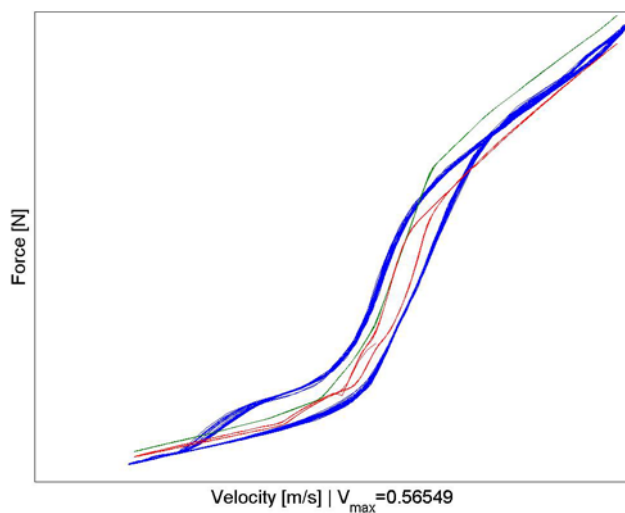


Figure 42 Frequency = 6 Hz, amplitude = 15 mm, low position

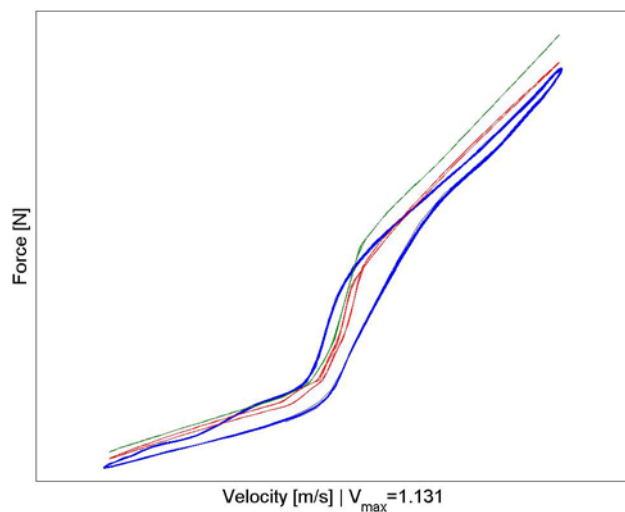


Figure 43 Frequency = 6 Hz, amplitude = 30 mm, high position

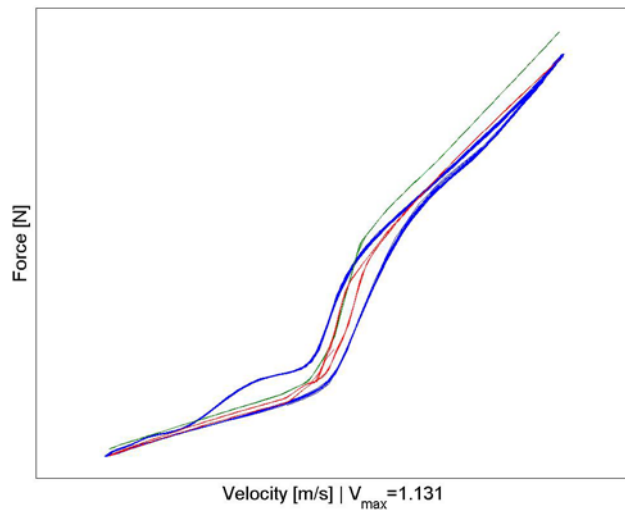


Figure 44 Frequency = 6 Hz, amplitude = 30 mm, low position

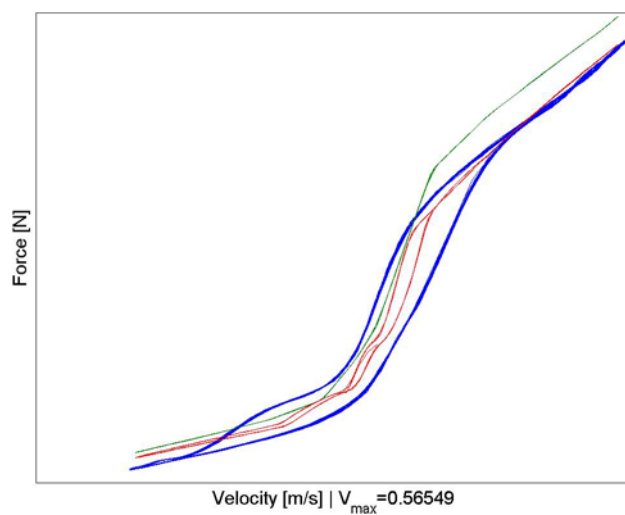


Figure 45 Frequency = 6 Hz, amplitude = 15 mm

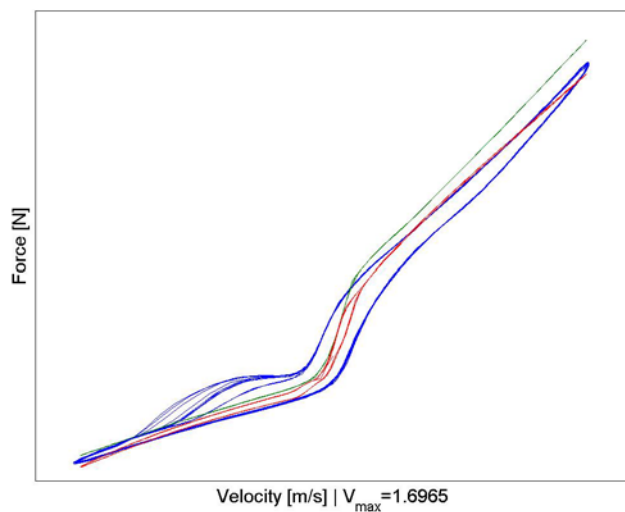


Figure 46 Frequency = 6 Hz, amplitude = 45 mm

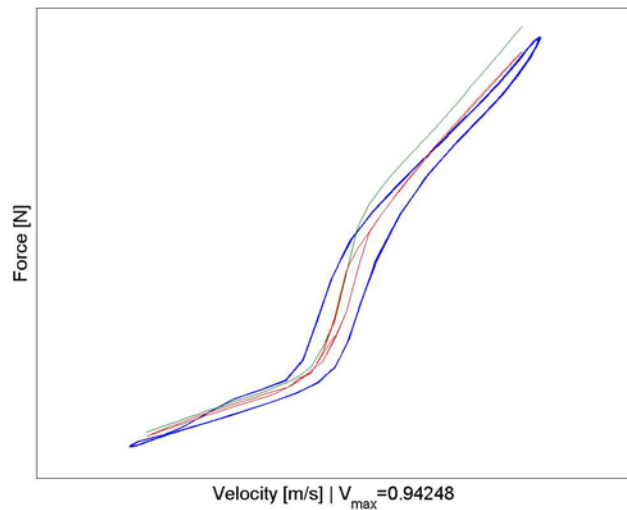


Figure 47 Frequency = 10 Hz, amplitude = 15 mm

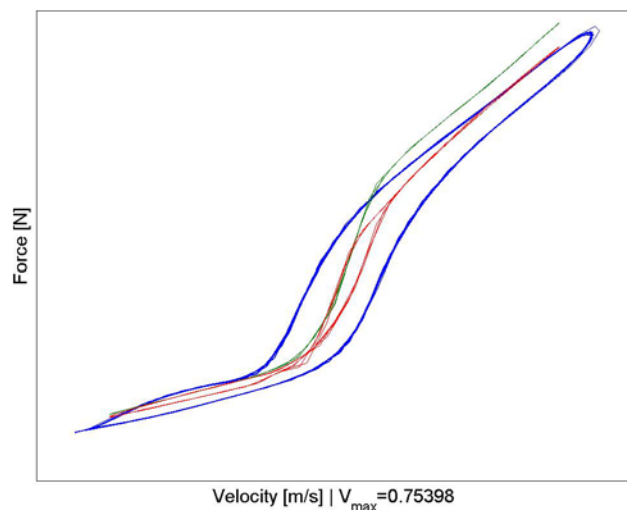


Figure 48 Frequency = 15 Hz, amplitude = 8 mm

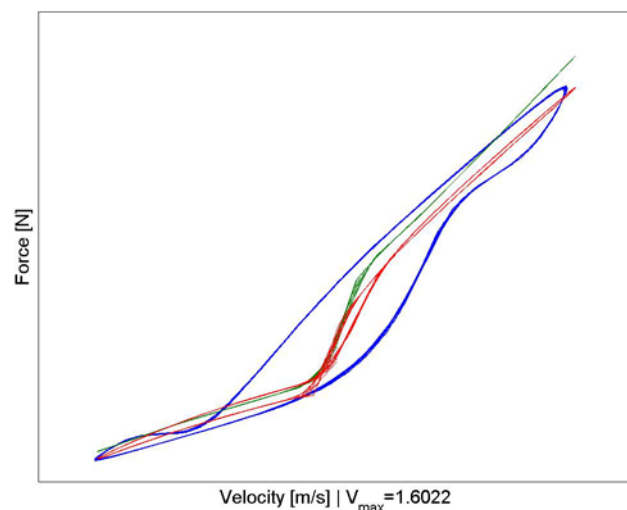


Figure 49 Frequency = 17 Hz, amplitude = 15 mm

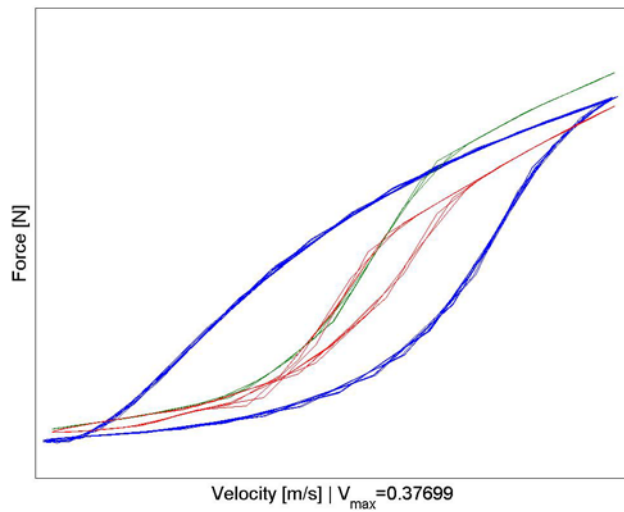


Figure 50 Frequency = 30 Hz, amplitude = 2 mm

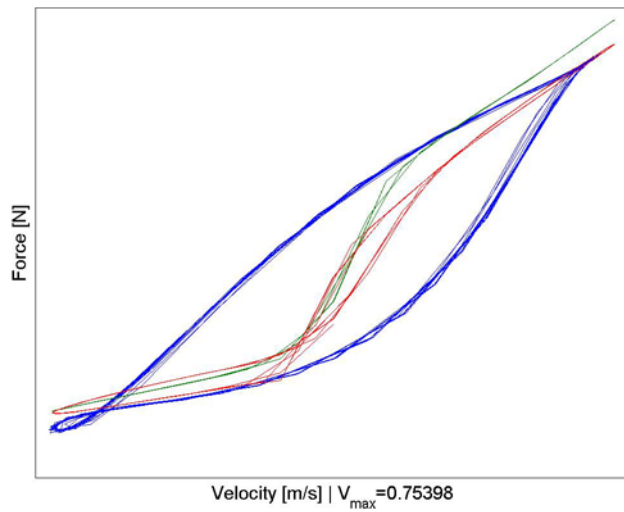


Figure 51 Frequency = 30 Hz, amplitude = 4 mm

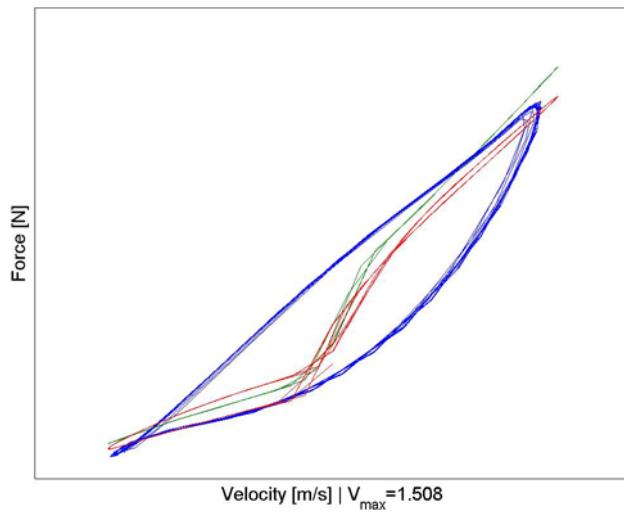


Figure 52 Frequency = 30 Hz, amplitude = 8 mm